Oral uptake of aluminum and aluminum oxide nanoparticles: particle characterization and internal dose

Inaugural-Dissertation

to obtain the academic degree

Doctor rerum naturalium (Dr. rer. nat.)

submitted to the Department of Biology, Chemistry, Pharmacy

of Freie Universität Berlin

by

Benjamin Christoph Krause

born in Berlin

year of submission: 2021

This thesis was carried out at the Federal Institute for Risk Assessment (BfR) in Berlin from May 2014 to April 2020 under the supervision of Prof. Dr. Dr. Andreas Luch.

1st Reviewer: Prof. Dr. Dr. Andreas Luch

2nd Reviewer: Prof. Dr. Daniel Klinger

Date of defense: 31.08.2021

Erklärung

Hiermit versichere ich, dass ich die vorliegende Dissertation mit dem Titel “Oral uptake of aluminum and aluminum oxide nanoparticles: particle characterization and internal dose” ohne Benutzung anderer als der zugelassenen Hilfsmittel selbstständig angefertigt zu haben. Alle angeführten Zitate sind als solche kenntlich gemacht. Die vorliegende Arbeit wurde in keinem früheren Promotionsverfahren angenommen oder als ungenügend beurteilt.

Berlin, den 16.10.2020

Benjamin Christoph Krause

Die Dissertation wurde in englischer Sprache verfasst.

Acknowledgment

First of all, I would like to thank Prof. Dr. Dr. Luch for the opportunity to do my dissertation on nanoparticles in his department. He has always motivated me to go new ways, to initiate cooperations, to think outside project boundaries and to use the manifold possibilities at the institute. The discussions with Mr. Luch have always given me important impulses and ideas for the further course of the doctoral thesis, and his hints and suggestions in the preparation of the publications have always pointed the way and been a help to me.

I would like to thank Prof. Dr. Klinger for taking over the second opinion and for the friendly discussions and stimulating comments on my doctoral thesis.

I would like to thank Dr. Laux for his support in carrying out my work by providing ideas, preparing publications and initiating collaborations within and outside the BfR.

For the close professional supervision throughout my doctoral thesis, many thanks go to Dr. Tentschert and Dr. Jungnickel, who always took a lot of time for discussions and supported me intensively in the development of project ideas and the preparation of publications.

With Dr. Giulbudagian I had many inspiring professional discussions; many thanks also for the extra portion of motivation, especially in the final section of my PhD thesis.

In addition to various internal collaborations, where I would like to thank, among others, Dr. Sieg for his collaboration in the SolNanoTOX project and beyond, I also had the opportunity to work with various external collaborators. Here I would like to mention in particular Dr. Fessard, who always had an open ear for my concerns and questions and supported me especially in the context of the SolNanoTOX cooperation project.

I would like to thank Dr. Huhse for many discussions, which were stimulating and instructive, as well as for many helpful comments on my dissertation.

Without help in the laboratory, many parts of this dissertation would not have been possible. I would especially like to thank Mrs. Nadine Dreiack, who was always open to my many different projects, for her extensive support in the lab. I would like to thank Mr. Philipp

Reichardt for his support especially in the area of ICP-MS and ToF-SIMS, he was always helpful to me. I would like to thank Mr. Nils Dommershausen and Mr. Julian Tharmann for help in the toxicological field and the everlasting willingness to be there for me with all other problems in the laboratory. I would also like to thank Mr. Roman Schmidt for his tireless work in keeping the ICP-MS operational.

I would like to thank the entire Department 7 for the friendly atmosphere, for many interesting discussions on a wide range of topics and for the good cooperation.

I also thank all my PhD student colleagues, especially Mrs. Morgane Even and Mrs. Nadja Mallock, for many nice conversations. In addition to being fun, these conversations have often led to other, new perspectives on my work, thus advancing it. In particular, I would like to thank Mr. Fabian Kriegel for the close cooperation during my doctoral studies and the great time we spent together in the office, as well as my other office colleagues Mr. Yves Hachenberger, Mr. Daniel Rosenkranz, Mr. Lars Leibrock and Mrs. Charlotte Kromer.

Finally, I would like to thank my family - my parents, my three brothers, my wife and my daughter - who have always supported me during the whole time, motivated me and thus only made it possible for me to successfully complete this work.

Table of contents

Abstract

Aluminum (Al) is the most common metal in the earth's crust and, with its natural occurrence and use in consumer products it is ubiquitous in human life. Al compounds are used in food packaging for food protection, but also as stabilizers, pH regulators and anti-caking agents. However, adverse health effects of Al have been discussed and neurodegenerative diseases have been linked to Al exposure. In the production and application of Al, nanoscaled particles are used intentionally but also unintentionally. Due to the unique characteristics of nanoparticles (NP), these can exhibit a different behavior than the respective bulk material. Their altered characteristics may also affect for example the oral uptake. A higher bioavailability due to increased solubility would also be conceivable. This may lead to a faster exceedance of the limit values for Al uptake. So far, the tolerable weekly intake value for Al from food do not differentiate between different forms of Al, such as ionic or nanoscale species. To gain a better understanding on whether Al NP could potentially cause adverse health effects, two nanoscale Al particles of similar size were characterized in this thesis by *in vitro* and *in vivo* experimentation. The obtained results were also compared to an ionic Al control.

For any meaningful *in vitro* or *in vivo* investigation, a proper and comprehensive characterization of the applied NPs is mandatory. This requires appropriate analytical techniques and the knowledge about their advantages and limits. The first part of this thesis compared different analytical methods for NP characterization. Particular attention was paid to techniques that can determine solubility and complexation behavior, since NPs can exhibit different properties in physiological media. To evaluate the possible differences between nanoparticulate metal and metal oxide Al forms, two similar sized particles, Al and Al_2O_3 NPs, were chosen. Fast screening techniques were evaluated for their suitability of characterizing hydrodynamic diameter and size distribution. More specialized techniques were applied to determine individual NP numbers and size. The use of complementary techniques confirmed the obtained results and highlighted the benefit of using more than one technique for a comprehensive NP characterization. With particle surface, another important property of NPs was investigated, revealing an important difference between the metal and metal oxide Al

NPs used. For all techniques applied, advantages and disadvantages were discussed, and possible complementary techniques suggested. The results obtained served as a basis for the following *in vitro* and *in vivo* studies.

During oral uptake, NPs from food or food contact material may reach the gastrointestinal tract. The second part of this thesis assessed the physicochemical fate of Al and Al_2O_3 NPs after passing through different compartments of the gastrointestinal tract. For this purpose, an artificial digestion approach was applied. A broad spectrum of techniques was used to characterize particle modifications during their passage. For comparison, ionic Al was used as a control. Three compartments, saliva, stomach and intestine, of the gastrointestinal tract were monitored. For saliva, no significant differences in particle size and shape were identified. In the gastric fluid, a strong agglomeration and an increased ion release were detected. In contrast, the subsequent exposure step to the intestinal fluid led to a reverse behavior, resulting in deagglomeration and decrease of free Al ions for all three Al species. A *de novo* formation of Al protein complexes in the nanoscale range was shown in intestinal fluid, even for the ionic Al control. The results suggest the possibility of nanoparticulate fractions reaching the intestinal epithelium. Different modifications and transitions may alter these NPs significantly. These findings stress the importance and necessity of a thorough characterisation of the NP under real-life conditions. It is suggested to consider a mutual conversion of particles and ions when evaluating toxicological experiments.

The oral uptake is a complex process and important factors like bioavailability and tissue distribution cannot be monitored in vitro. The third part of this thesis focused on a three-day oral gavage study with three different Al species (Al and Al_2O_3 NPs and ionic $AlCl_3$) in Sprague Dawley rats. For selected organs, the Al amount was determined to identify the systemic available Al burden and distribution. Three different concentrations of the two NP species were administered, while the ionic Al control was applied at one dose only for comparison. The development of a microwave assisted acid digestion approach followed by inductively coupled plasma mass spectrometry (ICP-MS) analysis enabled the quantification of Al burden of individual organs. Due to the complex matrices, sample matrix interferences on the calibration procedure were considered. After three days of exposure, the three Al species

tested showed a different distribution behavior within the investigated organs. High Al levels were found in liver and intestine for the ionic Al control, while upon treatment with Al NPs significant amounts of Al were detected in the latter only. High concentrations were detected in spleen following Al_2O_3 NP treatment, however in all other investigated organs Al was also determined. After the three-day oral exposure via gavage, for all three Al species a rapid absorption and systemic distribution was observed. The results suggest particle shape and surface composition as key factors for Al biodistribution and accumulation.

In summary, this thesis provides a strategy for a comprehensive characterization especially of aluminum-containing NPs, taking into account the advantages and limitations of known techniques for NP analysis. In addition, differences in both physicochemical properties and behavior of the two similar sized NPs used in physiological environments were determined. The results obtained here provide robust evidence that when evaluating Al after oral intake, when establishing recommended tolerable intake values, and when conducting future toxicological studies, a distinction must be made between different forms of Al, such as ionic or nanoparticulate species.

Zusammenfassung

Aluminium (Al) ist das häufigste Metall in der Erdkruste. Aufgrund seines natürlichen Vorkommens und der Verwendung in Lebensmitteln und Verpackungen ist es im menschlichen Leben allgegenwärtig. Neben den vielfältigen möglichen Anwendungen wird eine Rolle von Al bei der Entstehung verschiedener neurodegenerativer Krankheiten vermutet. Bei der Herstellung und Verwendung von Al werden absichtlich, aber auch unabsichtlich Al-Partikel im Nanobereich erzeugt. Aufgrund der einzigartigen charakteristischen Eigenschaften von Nanopartikeln (NP) können diese ein anderes Verhalten als das jeweilige Bulkmaterial aufweisen. Für die orale Aufnahme wäre eine veränderte Bioverfügbarkeit aufgrund einer erhöhten Löslichkeit denkbar. Dies kann zu einem schnelleren Überschreiten der Grenzwerte für die Al-Aufnahme führen. Bisher unterscheiden die empfohlenen Grenzwerte für die Freisetzung von Aluminium aus Lebensmitteln nicht zwischen verschiedenen Formen von Aluminium, wie z.B. ionischen oder nanoskaligen Spezies. Um ein besseres Verständnis darüber zu entwickeln, ob Al NP möglicherweise gesundheitsschädliche Auswirkungen haben könnte, wurden in dieser Arbeit zwei nanoskalige Al-Partikel ähnlicher Größe durch *in vitro*- und *in vivo*-Experimente charakterisiert. Die erhaltenen Ergebnisse wurden mit einer ionischen Al-Kontrolle verglichen.

Für jede aussagekräftige *in vitro*- oder *in vivo*-Untersuchung ist eine ordnungsgemäße und umfassende Charakterisierung der angewandten NPs obligatorisch. Dies erfordert geeignete analytische Techniken und das Wissen um deren Vorteile und Grenzen. Im ersten Teil dieser Arbeit wurden verschiedene analytische Methoden zur NP-Charakterisierung verglichen. Besonderes Augenmerk wurde auf Techniken gelegt, mit denen das Löslichkeits- und Komplexierungsverhalten bestimmt werden kann, da NPs in physiologischen Medien ein unterschiedliches Verhalten zeigen können. Um die möglichen Unterschiede zwischen Metall- und Metalloxid-Al-Formen zu untersuchen, wurden zwei NP ähnlicher Größe, zum einen aus Al und zum anderen aus Al_2O_3, ausgewählt. Schnelle Screening-Techniken wurden hinsichtlich ihrer Eignung zur Charakterisierung des hydrodynamischen Durchmessers und der Größenverteilung bewertet. Für die Untersuchung der Anzahl und Größe einzelner NPs wurden speziellere Techniken angewandt. Der Einsatz komplementärer Techniken bestätigte

die erzielten Ergebnisse und unterstrich den Vorteil der Verwendung von mehr als einer Technik für eine umfassende Charakterisierung. Mit der Partikeloberfläche wurde eine weitere wichtige Eigenschaft von NP untersucht, die einen wichtigen Unterschied zwischen den verwendeten Metall- und Metalloxid-NP aufzeigte. Für alle angewandten Techniken wurden die Vor- und Nachteile diskutiert und mögliche komplementäre Techniken vorgeschlagen. Die erzielten Ergebnisse dienten als Grundlage für die folgenden i*n vitro*- und *in vivo*-Studien.

Nach oraler Aufnahme können NP aus Lebensmitteln oder Material mit Lebensmittelkontakt den Magen-Darm-Trakt erreichen. Der zweite Teil dieser Arbeit untersuchte das physikalisch-chemische Verhalten von Al und Al_2O_3 NP nach der Passage verschiedener Kompartimente des Gastrointestinaltraktes. Zu diesem Zweck wurde ein künstlicher Verdauungsansatz angewandt. Ein breites Spektrum von Techniken wurde eingesetzt, um Partikelmodifikationen während ihrer Passage zu charakterisieren. Zum Vergleich wurde ionisches Al als Kontrolle verwendet. Modelle dreier Kompartimente des Gastrointestinaltraktes - Mund, Magen und Darm - wurden untersucht. In Speichel wurden keine signifikanten Unterschiede in Partikelgröße und -form beobachtet. In der Magenflüssigkeit wurde eine starke Agglomeration und eine erhöhte Ionenfreisetzung festgestellt. Im Gegensatz dazu führte die anschließende Exposition in Darmflüssigkeit zu einer Deagglomeration und einer Abnahme der freien Al-Ionen bei allen drei Al-Spezies. Es zeigte sich eine *de novo*-Bildung von Al-Proteinkomplexen im Nanobereich in der Darmflüssigkeit, die selbst für die ionische Al-Kontrolle beobachtet wurde. Die Ergebnisse deuten darauf hin, dass nanopartikuläre Fraktionen das Darmepithel erreichen können. Verschiedene Modifikationen und Übergänge können NP signifikant verändern. Dies unterstreicht die Notwendigkeit einer Charakterisierung in Bezug auf die jeweiligen Versuchsbedingungen und das Milieu, in dem die Partikel getestet werden. Diese Ergebnisse betonen die Bedeutung und Notwendigkeit einer gründlichen Charakterisierung der NP unter realen Bedingungen. Es wird vorgeschlagen, bei der Auswertung toxikologischer Experimente eine mögliche gegenseitige Umwandlung von Teilchen und Ionen in Betracht zu ziehen.

Die orale Aufnahme ist ein komplexer Prozess, und wichtige Faktoren wie die Bioverfügbarkeit und die Verteilung im Gewebe können nicht *in vitro* überwacht werden. Der dritte Teil dieser Arbeit konzentrierte sich auf eine dreitägige orale Aufnahmestudie mit drei verschiedenen Al-Spezies (Al und Al_2O_3 NP und ionisches $AlCl_3$) an Sprague-Dawley-Ratten. Für ausgewählte Organe wurde die Al-Belastung bestimmt, um die systemisch verfügbaren Al-Gehalte und die Verteilung zu ermitteln. Es wurden drei verschiedene Konzentrationen der beiden NP-Spezies verabreicht, während zum Vergleich die ionische Al-Kontrolle nur in einer Dosis appliziert wurde. Die Entwicklung eines mikrowellenunterstützten Aufschlussverfahrens, gefolgt von einer induktiv gekoppelten Plasma-Massenspektrometrie (ICP-MS)-Analyse, ermöglichte die Quantifizierung der Al-Belastung einzelner Organe. Aufgrund der komplexen Matrizen wurden die Interferenzen der Probenmatrix auf das Kalibrierverfahren berücksichtigt. Nach dreitägiger Exposition zeigten die drei getesteten Al-Spezies ein unterschiedliches Verteilungsverhalten innerhalb der untersuchten Organe. Für die ionische Al-Kontrolle wurden hohe Al-Gehalte in Leber und Darm gefunden, während bei der Behandlung mit Al NP signifikante Al-Mengen nur in letzterem nachgewiesen wurden. Nach der Behandlung mit Al_2O_3 NP wurden hohe Konzentrationen in der Milz festgestellt, aber auch in allen anderen untersuchten Organen wurde Al nachgewiesen. Nach der dreitägigen oralen Exposition wurde bei allen drei Al-Spezies eine schnelle Absorption und systemische Verteilung beobachtet. Die Ergebnisse deuten auf eine Schlüsselfunktion von Partikelform und Oberflächenzusammensetzung für Biodistribution und Akkumulation von Al hin.

Zusammenfassend bietet diese Arbeit eine Strategie für eine umfassende Charakterisierung insbesondere von aluminiumhaltigen NPs, unter Berücksichtigung der Vorteile und Grenzen bekannter Techniken zur NP-Analyse. Darüber hinaus wurden Unterschiede sowohl in den physikalisch-chemischen Eigenschaften als auch im Verhalten der beiden ähnlich großen NP in physiologischer Umgebung festgestellt. Die hier erzielten Ergebnisse liefern belastbare Anhaltspunkte dafür, dass bei der Bewertung von Al nach oraler Aufnahme, bei der Festlegung tolerierbarer Aufnahmewerte und bei der Durchführung zukünftiger toxikologischer Studien zwischen verschiedenen Formen von Al, wie ionischen oder nanopartikulären Spezies, unterschieden werden muss.

Abbreviations

AAS – Atomic absorption spectroscopy

ACH – Aluminum chlorohydrate

AES – Auger electron spectroscopy

AFM – Atomic force microscopy

AF4 – Asymmetric flow field flow fractionation

Al – Aluminum

Al_2O_3 – Aluminum oxide

ASTM – American Society of Testing and Materials

BAuA – Bundesanstalt für Arbeitsschutz und Arbeitsmedizin

BSI – British Standards Institution

CARS – Coherent anti-Stokes Raman spectroscopy

CI – Cascade impactor

DCS – Differential centrifugal sedimentation

DLS – Dynamic light scattering

DRF – Daily response factor

EDX – Energy-dispersive X-ray spectroscopy

EFSA – European Food Safety Authority

FFF – Field-flow fractionation

GFAAS – Graphite furnace atomic absorption spectrometry

IBM – Ion beam microscopy

ICP-AES – Inductively coupled plasma atomic emission spectroscopy

ICP-MS – Inductively coupled plasma mass spectrometry

ICP-OES – Inductively coupled plasma optical emission spectrometry

ISO – International Organization for Standardization

LA – Laser ablation

LDH – Lactate dehydrogenase

MA – Mobility analyzer

MCT – Monocarboxylate transporter

MTT – 3-(4,5-Dimethylthiazol-2-yl)-2,5-diphenyltetrazolium bromide

NAA – Neutron activation analysis

NIOSH – National Institute of Occupational Safety and Health

NOAEL – No observed adverse effect level

NP – Nanoparticle

NTA – Nanoparticle tracking analysis

OATP – Organo-anion transporting polypeptide

PTWI – Provisional tolerable weekly intake

ROS – Reactive oxygen species

SCCP – Scientific Committee on Consumer Products

SEC – Size exclusion chromatography

SEM – Scanning electron microscopy

SP-ICP-MS – Single particle inductively coupled plasma mass spectrometry

TEM – Transmission electron microscopy

ToF-MS – Time of flight mass spectrometer

ToF-SIMS – Time-of-flight secondary ion mass spectrometry

XPS – X-ray photon spectroscopy

1. Introduction

1.1 Aluminum – benefits and risks in daily use

About 8% of the earth's surface consists of aluminum (Al) and its compounds. It is the most abundant metal in the earth crust and naturally occurs in silicates, cryolite and bauxite. Al is redistributed in the environment mostly by natural processes and gets mobilized from natural sources by acidic precipitation [1].

The most important raw material to produce primary aluminum is bauxite. Bauxite is an ore containing mixture of aluminum oxide (Al_2O_3), silica, various iron oxides and titanium dioxide [2]. The Bayer process enables the purification of the Al_2O_3, which then can be refined to primary Al. Since the solubility of Al^{3+} in water is very low, sodium hydroxide is added to the bauxite ore. The mixture is then heated to 150-200 °C in a pressure vessel. This converts the insoluble aluminum oxide into the soluble sodium aluminate ($NaAl(OH)_4$). Filtering separates the aluminate from the waste and after cooling, $Al(OH)_3$ precipitates. To accelerate the precipitation, seed crystals in form of $Al(OH)_3$ are added to the solution [3]. About 90% of $Al(OH)_3$ are converted into Al_2O_3 by heating in rotary kilns at temperatures above 1000 °C. The remaining solution is recycled to extract accumulated gallium and vanadium. Most of the produced Al_2O_3 is used to generate primary aluminum using the Hall-Héroult process. The Hall-Héroult process uses Na_3AlF_6 (cryolite) to lower the high melting point (2072 °C) of Al_2O_3 and facilitate the electrolysis [4]. Cryolite is an advantageous electrolyte due to its enhanced alumina solubilization, electrical conductivity, resistance towards electrolytic dissociation at high voltages, as well as its low density at high temperatures when compared to aluminum [4]. The electrolysis is conducted by passing a low voltage (under 5 V) direct current at 100–300 kA through the cryolite. Liquid aluminum metal deposits on the cathode. The oxygen from the alumina forms carbon dioxide with carbon from the anode [4]. Additionally, Al is also recycled from scrap. This significantly reduces costs compared to the production of new Al, even after collecting, separating and recycling [5]. Recycling of Al does not alter its properties, which allows indefinite recycling circles of aluminum, while using only 5% of the energy required for Al production from bauxite ore [6]. In 2017, up to 63 million tons of primary Al

were produced [7]. More than 7 million tons of Al are recovered annually from recycled old scrap [1].

1.1.1 Applications of Al

Al is mostly used alloyed which improves its mechanical properties. Copper, zinc, magnesium, manganese and silicon are the most common alloys used in combination with Al [8]. Al and its alloys are utilized in the transportation industry, as building and construction materials, in packaging and as electrical equipment [9]. Because of its low density, Al is used in transportation and vehicles. For instance, automobiles, aircrafts or bicycles commonly use parts comprised of Al. In construction Al is chosen for its reflective properties and resistance to corrosion (i.e. windows, doors, roofing) [9]. Al use in packaging (cans, containers, foil) benefits from the non-adsorptive and splinter-proof properties. Application in the electricity sector is favored due to its relatively low costs, high electrical conductivity, low density and corrosion resistance [9]. In powder form, Al is applied in pigments and paints, fuel additives, explosives and propellants [1].

About 93% of Al_2O_3 is used for Al production [10]. With a Mohs hardness of 9, Al_2O_3 can be used excellently for various types of abrasives [10, 11]. It is exceptionally chemically inert, which allows applications in reactive environments. One example is the application of translucent alumina ceramics in the luminous tubes of sodium lamps, where it is resistant to the reaction with high-temperature sodium vapor [12]. In the purification of chemicals, Al_2O_3 is a common drying agent or absorbent [10, 13]. Industrial processes commonly utilize Al_2O_3 as catalyst, i.e. the Claus process, which is aimed to recover sulfur from hydrogen sulfite using an alumina catalyst [14]. Other processes benefit from the high surface area, thermal and mechanical stability when using Al_2O_3 as a support for noble metal catalyst applications [15]. An overview of various Al compounds, their application and the role of Al in these applications is shown in Table 1. In addition to Al_2O_3, aluminum sulfate ($Al_2(SO_4)_3$) and aluminum chlorides are important compounds with a wide range of applications.

For $Al_2(SO_4)_3$ both industrial and commercial applications are known, of which several million tons are produced annually [16]. A major proportion of the substance is used for waste water treatment, followed by paper manufacturing [16]. Other fields of application are mordants in

dyeing, seed pickling, mineral oil deodorization, leather tanning and in the production of other aluminum compounds [16].

Anhydrous aluminum chloride has a variety of applications as catalyst, i.e. in chemical and petrochemical industries, in dye production as well as in synthesis of various inorganic and organic compounds [16]. A well-known application of Al is its use in antiperspirants, where aluminum hydroxychlorides are utilized as astringent [16].

In medical applications, aluminum salts are used in vaccines as immune adjuvant to support the immune stimulant by increasing its potency. One possible mechanism as immune adjuvant is the adsorption of antigens to aluminum salts [17, 18].

In the food sector, preservatives, fillers, coloring agents, anti-caking agents, emulsifiers and baking powders can contain aluminum, mainly as stabilizer [1].

Table 1: Important Al compounds, their use and role of Al in these applications.

Al compound	**Application**	**Role of Al**	**Reference**
Primary Al	Transportation, building and construction, packaging and electrical equipment	Low density, corrosion resistant, lightness, non-adsorptive, splinter-proof properties, low costs	[9]
Al_2O_3	Al production, abrasives, chemical purification, Claus process, support for noble metal catalyst applications	Chemically inert, drying agent, absorbent, catalyst, high surface area, thermal/mechanical stability	[10-15]
$Al(OH)_3$	Medicine	Antacid	[19, 20]
$Al_2(SO_4)_3$	Water treatment, paper manufacturing, dyeing, seed pickling, food additive	Coagulant, retention agent, mordant, pickling agent, stabilizer	[16]
$AlCl_3$	Chemical industry, dye production, synthetization of organic and inorganic compounds	Catalyst	[16]
$Al_nCl_{(3n-m)}(OH)_m$	Antiperspirants, water purification, paper industry	Astringent, flocculating agent, fixing sizing agent	[16]

$NaAlO_2$	Water treatment, construction technology	Coagulant, remove dissolved silica, acceleration of concrete solidification	[16]
$Al(CH_3COO)_2(OH)$	Wound treatment	Antiseptic astringent	[21]
$AlPO_4$	Vaccines, ceramics, dental cement, cosmetics	Adjuvant, gelling agent, antacid	[1, 22, 23]
$LiAlH_4$	Organic chemistry	Reducing agent	[24, 25]
Organoaluminum	Organic chemistry	Lewis acid, cocatalyst	[26]

Aluminum is ubiquitous and widely used because of its excellent properties. Due to the use in industrial, commercial, and medical applications, the exposure of the consumer is conceivable by any uptake route. The next chapter will therefore deal with the different routes of human exposure to aluminum.

1.1.2 Biokinetics of Al

There are four main exposure routes for Al with ingestion being the most important one, followed by percutaneous and inhalative exposure. Due to the use of Al in adjuvants, also intramuscular injection is an investigated route of exposure. Absorbed Al is potentially distributed to all tissues in the body, while accumulation takes place mainly in bone, muscles, kidney and the brain [27-29]. Al which is not absorbed is excreted mainly via feces. Absorbed Al has a half-life time of about one day and is excreted via urine [29]. Upon a chronic exposure via the oral pathway the half-life time increases up to 50 years, which indicates aluminum accumulation in reservoirs in the body. Of great concern is especially the accumulation of Al in the brain tissue after becoming systemically available and the subsequent consequences for the nervous system. Al can cross the blood-brain barrier by two mechanisms, which are likely to occur simultaneously. One is the transport via citrate, the other mechanism includes the transferrin receptor, where Al is bound to transferrin [30, 31].

In the following parts the underlying processes will be described more in detail.

1.1.2.1 Ingestion

Different absorption mechanisms for ingestion, mainly from duodenum and small intestine, are described for Al, including passive diffusion, pinocytosis and transferrin/Vitamin D-

dependent active transport [32]. Some compounds can influence the uptake of Al in the body. An increased intestinal Al uptake was found after stimulation of renal synthesis of 1, 25-dihydroxycholecalciferol by parathyroid hormone [33, 34]. Reduced uptake of Al from the gut was shown in the presence of phosphates, which form insoluble aluminum phosphates and for iron, which occupies transferrin binding sites. Other food ingredients enhance Al uptake such as citric and other organic acids. Most of the absorbed Al in serum is present as Al^{3+} bound to transferrin (~90%), while the remaining 10% are bound to low molecular weight molecules like citrate, phosphate and citrate-phosphate complexes, predominantly Al citrate (7-8%) [35].

The interactions of Al^{3+} and Fe^{3+} with serum transferrin were studied using quantum mechanics, molecular mechanic and molecular dynamic simulations [36]. The experiments revealed that iron is released to the transferrin receptor 1 in peripheral cells (neurons, glial, blood-brain barrier) and is internalized via endocytosis. These results indicate interactions of both, Al^{3+} and Fe^{3+}, with serum transferrin. Depending on the pH value, near neutral in blood or 5.5 in endosomes, the binding of Al^{3+} and Fe^{3+} is different. Due to higher stability constants for the Fe^{3+} transferrin complex compared to Al^{3+}, no effective competition for serum Fe-binding sites exists. However, with about 70% unoccupied metal binding sites, transferrin is able to coordinate 2 Al^{3+} ions, transporting them to peripheral cells [36].

Besides increasing the bioavailability of Al in the gastrointestinal tract [1, 37, 38], citrate is also important as a substrate for the organo-anion transporting polypeptide (OATP) and can be taken up by the monocarboxylate transporter (MCT). This also explains the brain influx of citrate bound Al, as the MCT crosses the blood-brain barrier [31, 32].

When comparing the relative oral Al uptake and distribution of various Al compounds, no difference in whole blood concentrations after 7 days was detectable for Al citrate, $Al_2(SO_4)_3$, $AlCl_3$, $Al(OH)_3$, or $Al(NO_3)_3$ dissolved in deionized water. After 14 days whole blood Al levels decreased despite continued daily oral dosing, while the highest Al accumulation was found in liver, kidney and bone [39]. Those results were in contrast to a study described by the European Food Safety Authority (EFSA), where the uptake was highest for $Al_2(SO_4)_3$ followed

by Al citrate > $AlCl_3$ > $Al(NO_3)_3$ > $Al(OH)_3$ [40]. However, only a single dose of 50 mg administered by intubation was used in this study [39], compared to the repeated oral dose in the other [40]. Extensive investigations were carried out to elucidate the bioavailability and tissue accumulation of Al citrate. Citrate can bind Al^{3+} at three different coordination sites forming an octahedron with three water molecules. Depending on the pH value, citrate binds Al^{3+} at two carboxylic and an alkoxy group, followed by second and third ionization with increasing pH. Binding of Al^{3+} shifts pKa values of citrate resulting in a high uptake from the gut [41]. Furthermore, those mechanisms also enhance the interaction of Al with MCT and OATP transporters, Al sequestration in different intracellular compartments and facilitate Al efflux from the central nervous system [31, 42].

In summary, bioavailability of ingested Al depends on aqueous solubility of the physical and chemical form. After oral uptake from food, Al compounds are poorly absorbed (max. 1%)[27]. The average absorption from food is 0.1%, while about 0.3% are absorbed from drinking water [27, 43]. Absorption depends on the aluminum compound, but also on pH value, iron and calcium levels. Furthermore, the absorbed Al amount as well as the presence of other compounds have an influence. Lactate, citrate and fluoride enhance the uptake, while silicates and especially phosphates significantly lower the absorption.

1.1.2.2 Percutaneous absorption

Besides ingestion, humans are also exposed to Al via the dermal route, for example from cosmetics. Widely used is aluminum chlorohydrate (ACH) as antiperspirant and for treatment of hyperhidrosis [44]. In an *in vivo* study on two persons (a woman and a man), the very rare isotope ^{26}Al in the form of ACH was applied to one armpit at a time. In order to determine the absorbed amount, urine was collected. Based on 53 days of urinary excretion and the comparison to the excretion rate of absorbed Al an average absorption rate of 0.014% was calculated [45]. A more comprehensive clinical study showed a comparable absorption rate through intact skin [46]. This led to the conclusion, that intact skin is an effective barrier for Al [1].

An aqueous solution of 5% $AlCl_3$ was used for one or seven days of repeated application to investigate the deposition of Al in the stratum corneum. After application on the forearm followed by air drying, volunteers were examined after rest and after a moderate physical activity [47]. With the help of two ultraviolet light-emitting cameras changes of the treated skin due to $AlCl_3$ were recorded. Single $AlCl_3$ application led to deposition in microrelief lines of the skin, while the repeated dose showed an accumulation on the plateaus delimited by the microrelief lines. Information on local irritation caused by $AlCl_3$ was not given. The authors of the study concluded a low irritant potential for $AlCl_3$. However, some important information were missing, for example purity of the used test compound, pH values before and after treatment of the skin or the application technique used [47, 48].

Alongside antiperspirants, aluminum salts are also used for the treatment of hyperhidrosis. A study with topical use of a 20% $AlCl_3$ solution on palm skin of 127 patients for one month showed a significant reduction of sweat production rate [49]. Like in other studies, important information, for example on the pH value of the solution given or irritations due to the treatment, were not provided. The staining of the stratum corneum with hematoxylin-eosin revealed intact eccrine sweat ducts before the treatment but indicated filled ducts after the $AlCl_3$ treatment. Histology of the treated skin showed an Al complex on the surface of the stratum corneum and in casts filling the sweat ducts. However, no Al accumulation was found in either the eccrine sweat duct or in the sweat gland.

To investigate skin penetration for dermal exposure assessment, the Franz® diffusion cell system can be applied as a realistic *in vitro/ex vivo* method [50]. This model was used to determine the transdermal penetration of Al after topical application of ACH (6-24h at 37 °C) [51]. This *in vitro* study investigated penetration of Al for different cosmetic formulations (deodorant, roll-on, stick). Interestingly, significant amounts of Al were found in the stratum corneum, the uppermost barrier of the skin. After damaging the stratum corneum with tape-stripping, the penetration increased to 10.7% [51]. However, only a very low amount of 0.1 µg/cm² Al was found in the Franz® receptor fluid, which corresponded to 0.012% of the applied dose. Due to the limitations of an *in vitro* model, personal habits and different rates and types of Al application could not be considered in this study.

Systemic hyperaluminemia (plasma Al = 104.7 µg/L) was diagnosed after four year daily use of ACH antiperspirant, while also complaints of bone pain occurred [52]. These findings led to the calculation of the highest systemic Al uptake of 0.1 mg/kg per day following topical application of commercial antiperspirants [53].

In summary, it can be concluded that intact skin is an effective barrier to Al absorption [54]. However, if the skin is damaged, the absorption of Al may increase significantly.

1.1.2.3 Inhalation

As described earlier, inhalative exposure represents only a minor exposure route compared to ingestion. However, aluminum workers can be exposed to Al fumes and particulates of different size (<10 - <100 µm) at their workplace. After deposition in the respiratory tract, a fraction can be absorbed from the lung, but most is eliminated in urine (>95%) [1, 55]. The exposure and related urinary Al concentrations depend on the respective activity (i.e. bauxite mining, Al refining, reduction, casting, fettling, slagging, welding, and AlF_3 production) and the Al forms present. Inhalative uptake of Al dust and fume by workers was estimated to be about 6 µg/kg per day [1].

Besides areas with aluminum mining no significant exposition from ambient air is expectable [43]. However occupationally exposed people can inhale larger amounts, for example insoluble dusts of Al. Up to 25% of the total Al body burden may be deposited in the lung of people with high occupational exposure [56]. Lung absorption of Al is not well investigated. Absorption rate seems to be between 1.5-2%, but it is not certain if also oral absorption via mucociliary cleaning or nasal absorption may occur [1, 27, 35].

1.1.2.4 Intramuscular injection

Several aluminum compounds are used as adjuvants in vaccines, including Al hydroxide, Al phosphate and Al potassium sulphate [57]. Nearly one century since the first use of Al in vaccines [58], extensive studies have been done on Al and its use as adjuvant [17, 22, 59-61]. Like for Al ingestion, the bioavailability and systemic uptake from vaccine depots depend on the chemical form the Al adjuvant [61, 62]. In most cases, $Al(OH)_3$ is present as poorly crystallized AlO(OH), while $AlPO_4$ can be detected in the form of $HAlO_5P$ [63, 64]. Based on a

study with a single intramuscular injection of AlO(OH) and $AlPO_4$, where the former was found in a 4-fold higher concentration in macaque muscles after 3-6 months [61], an eventual absorption of 100% was concluded [1]. After 12 months, Al concentrations in muscles decreased to less than the analytical limit of detection (≤ 25 µg/g muscle).

In a study, comparing the uptake of the both adjuvants AlO(OH) and $AlPO_4$ in rabbits, a more rapid uptake into the blood was observed for AlO(OH). With a single intramuscular injection of 0.85 mg Al, given as $^{26}Al(OH)_3$, the plasma ^{26}Al level reached 2 ng/ml after one h [62]. This concentration is about 7% of the normal Al plasma level in rabbits. In total, 13-22% of the given dose was taken up and distributed to the investigated organs (kidney > spleen > liver > heart > lymph nodes > brain). After equivalent injection of both adjuvants, initial plasma ^{26}Al concentrations were three-fold higher for AlO(OH) compared to $AlPO_4$. Interestingly, after 28 days mean peripheral tissue concentrations in rabbits dosed with $AlPO_4$ were three times higher compared to those exposed to AlO(OH). For more than 28 days, Al was taken up from the vaccine depot, while only 6% and 22% of the injected ^{26}Al had been excreted via the urine for AlO(OH) and $AlPO_4$, respectively. With an extrapolation of the rabbit plasma concentration related to the time profile, it could be concluded, that the Al dose of a single intramuscular adjuvant injection leads to an increase of 0.8% or less versus normal concentrations (2.7–6.2 µg Al/L) [1, 62].
The data demonstrate that Al burden increases only minimally, which can be neglected compared to the added value of immunization.

1.1.3 Toxicity of Al

Mainly responsible for Al toxicity is the systemic available amount of Al. Therefore, the absorbed amount of Al via the different uptake routes (dermal, oral, inhalative) is crucial for the overall toxicity of Al.

According to the current state of the art, Al is neither genotoxic nor carcinogenic [27, 28]. However, there has been a controversial discussion about the correlation between Al uptake and the development of breast cancer for many years. Although some studies postulate this relationship, there is no proof for Al causing the development of cancer so far [65-68]. In an

in vivo study on mice with high doses of 850 mg/kg body weight per day no cancerogenic effects were observed [69]. In two epidemiologic case studies, no correlation between the use of antiperspirants and the occurrence of breast cancer could be demonstrated [70, 71]. In fact, some studies indicate an accumulation of Al in breast cancer tissue as a result of cancer development [71, 72]. This assumption gets strengthened since also other elements, for example iron, nickel, chromium and lead, accumulate significantly in tumor tissues [73].

After oral Al treatment of rabbits and dogs, reduced testis weight and sperm quality was observed. The no observed adverse effect level (NOAEL) was between 27 and 88 mg/kg body weight per day for dogs [27]. Only doses clearly above 100 mg/kg body weight per day showed harmful effects on embryos [27]. Doses above 200 mg/kg bodyweight per day led to behavioral disorders. In an *in vivo* study on rats, disorders of the vestibulo-ocular reflex were investigated and a NOAEL of 30 mg/kg body weight per day was determined [27]. Increased Al blood levels in humans, for example in dialysis patients resulted in the development of dialysis encephalopathy [74]. In addition to brain damage, this disease also causes anaemia and a vitamin D-resistant disorder of bone mineralization [75]. Al often gets associated with Alzheimer's disease. Pathological amyloid deposits in the brain are assumed to be the cause of this disease. Studies showing increased Al concentrations in damaged brain regions of Alzheimer patients could not clarify whether the Al deposits were causative or symptomatic of the disease [76]. In addition, the neuropathological changes in Alzheimer's disease differ significantly from those in dialysis encephalopathy, so that triggering of Alzheimer's disease is considered unlikely [27, 29, 77, 78]. EFSA determined developmental neurotoxicity as the most critical endpoint for calculation of tolerable intake quantity [27]. Several *in vivo* studies on mice showed decreased motor activity, decreased grip strength and startle responsiveness as well as reduced brain weights [79-81]. The lowest NOAEL was found to be 10 mg/kg body weight per day and was used for the calculation of tolerable intake quantity. Another critical endpoint for determination of the NOAEL was the development of hydronephrosis in rats. The calculated NOAEL was 30 mg/kg body weight per day [29].

The current research points to the importance of several physicochemical parameters for assessing health risks caused by exposure to inorganic Al. Furthermore, the route of

administration is crucial as well as duration, frequency and concentration of the exposure. The exclusive consideration of the Al dose, that is measured and interpreted as “total Al” [82], without differentiation of specific forms [83] may possibly give rise to inadequate conclusions regarding Al health risks.

1.2 Role of oral uptake in total Al burden

Given the significance of the oral intake, the focus of this work is the Al intake after exposure with food and food contact materials. Oral uptake represents the most important exposure route for Al burden in man except for aluminum workers. Most healthy adults show no adverse effects when exposed orally to repeated high doses Al [1, 82]. In contrast children or adults with compromised kidney function can experience symptoms Al intoxication at much lower doses [1, 82].

1.2.1 Dietary intake

As an ubiquitous element, the presence of aluminum in daily food is remarkable. However, compared to gastric antacids, dietary intake of Al only adds a small part (0.07–0.2%) to the total oral Al uptake. However, there are numerous sources of aluminum intake from food, including beverages, fish and seafood, coffee, vegetables, cereals, chocolate, cocoa, non-dairy creamers and salts. In the following, some major aluminum sources in different countries are summarized, indicating that aluminum exposure is quite diverse, reflecting different dietary habits.

Beverages, especially tea infusions, can contribute to a doubling of daily Al intake [84, 85]. Other aluminum sources are formulas [86], in particular formulas for milk and processed cheese [87]. Highest Al food levels in France were found in fish and its products [88, 89]. An increased Al level was detected after baking or grilling with aluminum foil or in other Al-kitchenware [90]. Wines from different regions also add to the aluminum intake. The main source here is bentonite, which is added as clarifying agent to reduce proteins and particles. Sedimentation occurs by binding of the positively charged particles to the negatively charged surface of the bentonite[91].

EFSA calculated Al doses for toddlers (11.3–156.2 mg/kg-week), children (26.9–286.8 mg/kg-week) and adults (2.3–100.4 mg/kg-week) after an assumed consumption of five Al-containing food additives at their highest permitted levels [92]. All the calculated values were greater than the provisional tolerable weekly intake (PTWI).

The mentioned studies show the broad variety of Al sources for daily uptake from food with peak exposures from different products. They also point out that Al exposure varies from

country to country due to different lifestyles, but the PTWI values for children are often significantly exceeded. This is a cause for concern, which has already been mentioned above in relation to the toxicity of Al.

Gastrointestinal uptake of Al varies strongly depending on the present form. Hydrated Al silicates show almost no detectable uptake [93, 94], while sodium Al phosphates in foods can be taken up to levels between 0.1 to 0.3%. $AlCl_3$ can be detected up to 0.2% compared to organic Al which showed much higher values (> 2.0%) after ingestion [1, 40]. Therefore, it can be problematic for human health risk assessments to summarize different Al exposures as "total Al". As already discussed for the toxicity assessment of Al, summarizing Al exposure as total Al can also lead to inadequate results when assessing Al in food, since Al compounds with higher solubility can have a better bioavailability and should therefore be distinguished from low soluble Al compounds.

In summary, it can be stated that Al occurs in numerous foods and raw materials. Therefore, a certain Al background cannot be avoided. In the following, further areas and processed products are described which may cause additional exposure to aluminum.

1.2.2 Consumer products

An important parameter affecting the Al burden of the consumer products is the migration from certain metallic and ceramic products [95, 96], from glass bottles [97] and leaching from aluminum foil [98]. Tobacco and marijuana also show an Al content of about 0.4% [99]. Via olfactory pathways, Al may enter the brain [31, 100-102]. Furthermore, intentional drug abuse via intravenous injection can lead to Al intoxication [103]. Different calcium dietary supplements and gastric antacids in form of capsules or chewable tablets contain Al at concentration levels, that may cause a daily intake of around 200 µg Al/kg body weight of a 60 kg adult [104]. The use of Al-based phosphate binders decreased in most of North America and the United Kingdom but is continuously applied in Australia, Germany, Spain, Italy and New Zealand [105]. By controlling Al serum levels and replacing Al phosphate binders with calcium-containing alternatives, the risk for dialysis encephalopathy has been almost eliminated. Nevertheless, the data situation remains ambiguous as very high Al plasma and

serum levels were observed after daily intake of the customary about 4 g of Al-based phosphate chelators [106, 107].

1.2.3 Drinking water

Although food is the major source for Al exposure, drinking water should not be ignored. Health Canada reported mean Al concentrations of 20–174 µg/L in finished municipal tap water [108]. In potable water Al was measured using three analytical techniques (graphite furnace atomic absorption spectrometry (GFAAS), inductively coupled plasma mass spectrometry (ICP-MS) and inductively coupled plasma atomic emission spectroscopy (ICP-AES)). The element was found in different forms depended upon water source pH, temperature, the concentration of organic carbon, and the nature of the suspended particles [109]. At lower Al concentrations and at pH 5.5–6.5, the fluorides (AlF^{2+}, AlF_2^{+}, AlF_3^{0}, and AlF_4^{-}) and sulfates ($AlSO_4^{+}$, and $Al(SO_4)_2^{-}$) predominated, while at higher Al concentrations and at neutral pH, the hydroxides ($AlOH^{2+}$, $Al(OH)_2^{+}$, and $Al(OH)_4^{-}$) and organic Al (e.g., fulvic and humic acids) were the major species [109].

Drinking water is considered to contribute approximately 1.2% of a typical Egyptian's daily Al intake [87]. This conclusion is consistent with another study which found that adults living in six Japanese cities who consumed 2 liters of water each day received 80 ± 7 µg Al/day or 2.2% of their total mean daily Al dietary intake (3600 ± 1370 µg/day) [110]. In the United States, comparable concentrations were found in finished municipal drinking water with a median Al concentration of 0.112 mg/l, resulting in a daily ingested dose of 160 µg Al/kg (consumption of 1.4 l/day) or about 1% of the Al contribution by food for a 70 kg adult [1, 55].

1.3 Nanotechnology and its implication for dietary Al intake

Nanotechnology describes the manipulation of matter at atomic and molecular scale [111]. Nanoparticles (NP) are most often defined or described using their size, which ranges between 1 to 100 nm. Metallic NPs have unique chemical and physical properties compared to their bulk material. Properties like lower melting points, higher specific surface areas, specific optical properties, mechanical strengths, and specific magnetizations are interesting for industrial and medicinal applications. Of particular interest are the optical properties, which lead to different colors for differently sized particles of the same metal. NPs of same chemical composition but of different shapes and sizes may result in various light absorption [111]. There are several definitions for NPs by different organizations (see table 2).

Table 2: Definition of nanoparticles by different organizations: International Organization for Standardization (ISO), American Society of Testing and Materials (ASTM), National Institute of Occupational Safety and Health (NIOSH), Scientific Committee on Consumer Products (SCCP), British Standards Institution (BSI), Bundesanstalt für Arbeitsschutz und Arbeitsmedizin (BAuA) modified from [111]

Organization	**Definition of nanoparticle**
ISO	A particle spanning 1–100 nm (diameter)
ASTM	An ultrafine particle whose length in 2 or 3 places is 1–100 nm
NIOSH	A particle with diameter between 1 and 100 nm, or a fiber spanning the range 1–100 nm.
SCCP	At least one side is in the nanoscale range.
BSI	All the fields or diameters are in the nanoscale range.
BAuA	All the fields or diameters are in the nanoscale range.

NP synthesis can be performed by two different approaches. One way is the breakdown of the bulk material, also called top-down approach. The other possibility is the buildup by assembling basic units into larger structures, also known as bottom-up approach. For both approaches, a vast amount of different synthetic methods can be used to achieve the specific requirements imposed on the NPs (Fig. 1).

The above-mentioned properties of NPs allow their application in different fields. An overview of selected properties with the area of application is given in Table 3.

Table 3: NP properties and their application in different areas [111].

Nanoparticle property	**Area of application**
Optical properties	Use in paints or for materials with little light absorption, dispersion or reflection
High specific surface area	High selective catalysts
Electrical properties	Superconductive materials
Mechanical	Improvement of mechanical strengths of materials mixed with NPs
Surface plasmon resonance	Use in medical treatments for diagnosis
Antimicrobial properties	Food packaging

In the last two decades, nanotechnology was increasingly used to either improve certain abilities of food packaging materials or to introduce new functionalities. This includes enhanced mechanical and barrier functions, extension of food shelf-life based on antimicrobial properties of added NPs as well as oxygen scavenging [112]. By applying nanotechnology, even elements that do not occur in conventionally produced food contact materials, such as nanoscale Al, can be introduced into the food. Widely used are clays which contain Al. A common example is montmorillonite clay which is applied as a nanocomponent in different polymers, i.e. polyethylene, polyvinyl chloride, nylon and starch [113]. The addition of clay reduces the permeability of gases and water vapor, while improving the mechanical strength of biopolymers [114-116].

Besides food packaging, Al dietary intake might derive from food additives and kitchenware [35]. With the use of food packaging, food additives and kitchenware, combined with an increase in the use of acidic food, the exposure and oral intake of aluminum is significant [117]. Studies determined various metals in food. Significant amounts of these were found to be present as nano-sized particles [118, 119]. Some studies provide hints that NPs can migrate from food packaging into food [120, 121], although the application of standardized migration tests did not reveal a significant release from Low Density Polyethylene Polymer as a worst-case matrix [122, 123]. All these facts underline the necessity to further analyze, characterize and study the oral intake of aluminum, because it is the most prominent way to absorb Al in human.

1.3.1 Particle characterization

Since NPs can migrate from food packaging into the food and subsequently can cause human exposure, it is important to investigate their fate after oral uptake. Therefore, the characterization of NPs is essential to obtain information on the behavior of NPs. The characterization is also very important, since the different physicochemical properties may have an impact on their toxicity. Contrary to the respective bulk material, it is insufficient to know the chemical composition and concentration. As the high surface-to-volume ratio increases the reactivity electronic, optical and chemical parameters of the NP might be affected [124]. Parameters such as size, shape, chemical composition, surface area, charge and solubility are considered to significantly influence behavior of NPs in biological systems and consequently their toxicity [125]. For the characterization and investigation of these parameters a broad spectrum of analytical techniques are available. However, since no technique can give information on all the necessary properties, a combination of different methods is needed to provide all relevant parameters. The use of complementary techniques further strengthens the obtained results [126, 127]. The characterization of NP depends strongly on the question of interest. For a given application certain NP characteristics are used. These mostly include surface area, bulk chemical composition, surface chemistry, size, size distribution, morphology/shape, surface charge, agglomeration/aggregation state, crystal structure, and solubility [128]. An overview of the properties focused on in this thesis including the respective analytical techniques is given below (Figure 1). Beside different parameters, that are needed for proper and reliable characterization, additional challenges arise in environmental contexts. Several methods have detection limits above concentrations, at which NPs still can have adverse effects. Such low concentrations often occur in environmental samples, preventing the use of such methods. High background levels of the investigated analyte may also cause problems, as it becomes difficult to distinguish between the background and the analyte [129, 130]. Mixtures of NPs pose another common problem, since especially counting methods cannot differentiate between differently composed particles [130].

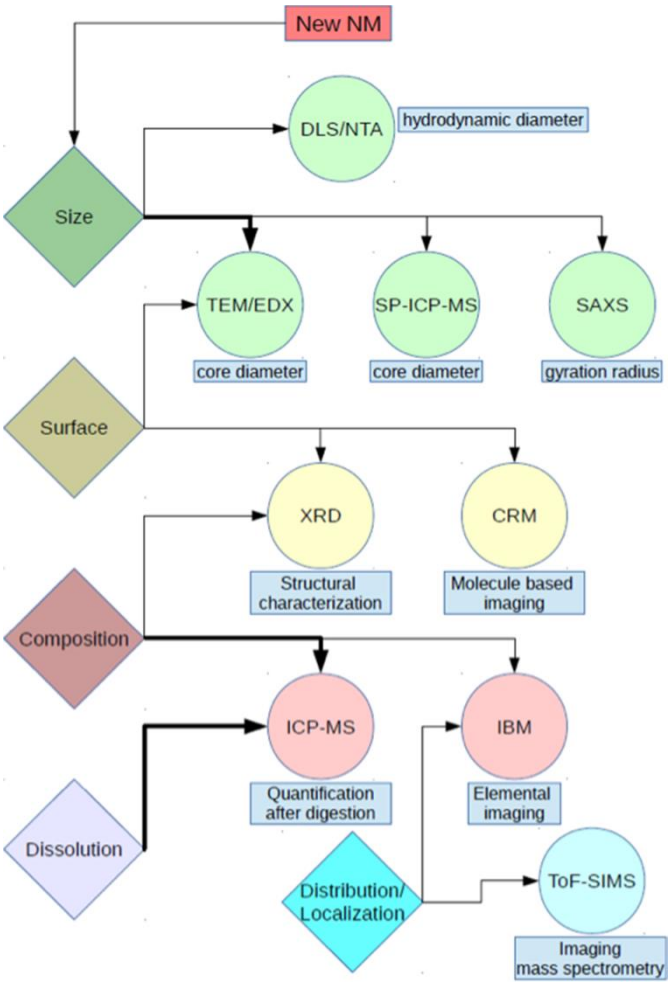

Figure 1: Overview of key NM characteristics (colored rhombi) and methods (colored circles) used in this study for characterization. Arrows in bold imply the main method for the linked characteristic. Abbreviations: DLS – dynamic light scattering; NTA – nanoparticle tracking analysis; TEM – transmission electron microscopy; EDX – energy dispersive X-ray spectroscopy; SP-ICP-MS – single particle inductively coupled plasma mass spectrometry; SAXS – small angle Xray scattering; XRD – X-ray diffraction; CRM – confocal Raman microscopy; ICP-MS – inductively coupled plasma mass spectrometry; IBM – ion beam microscopy; ToF-SIMS – time of flight mass spectrometry [127].

1.3.1.1 ICP-MS – the all-in-one device for NP characterization

Since ICP-MS represents a key technique in this thesis, it will be discussed in more detail in the next section. The basic principles, advantages and disadvantages as well as possible applications are considered.

A quadrupole ICP-MS consists of:

- Sample introduction system
- Inductively coupled plasma

- Interface
- Ion optics
- Mass analyzer
- Detector.

In the sample introduction system, the nebulization of liquid samples take place. An aerosol is created, which then will be transported into the argon plasma. Due to the high temperature of the plasma, atomization and ionization of the sample occur. In the interface region, the generated ions will be extracted into the ion optics, which are a set of electrostatic lenses. Here, the ion beam is focused and transferred into the quadrupole mass analyzer. Based on their different mass to charge ratio (m/z) the ions are separated in the analyzer and finally measured at the detector.

As with every analytical technique, there are advantages and disadvantages when using them. Some of the most prominent are shown in Table 4.

Table 4: Advantages and disadvantages of ICP-MS for analysis of trace elements [131].

Advantages	**Disadvantages**
Multi-element technique	Equipment cost
Large analytical range	Operating cost (argon)
Low detection limit	Multiple high purity gases required
High sample throughput	High level of staff expertise
Low sample volume	Interferences need to be controlled
Simple sample preparation	Laboratory set up costs (air-conditioning, HEPA filters, pipe work, dust reduction measures)
High-resolution and tandem mass spectrometry (triple-quadrupole) instruments offer a very high level of interference control	

One of the most relevant advantages is the capability of measuring multi-element samples in a single analysis, which is not possible with other elemental analysis techniques like GFAAS. In addition, short analysis time and easy sample preparation result in high sample throughput. On the other hand, both, the device and the needed high purity gases are quite costly, while

also the required expertise is quite high.

ICP-MS for the trace elemental analysis in different fields, like in food, feed, consumer products but also in biological fluids in clinical or medical areas, is well-established. Another interesting possibility is to operate the ICP-MS in the single particle mode (SP-ICP-MS) [132]. The basic assumption behind this technique is that, given a sufficiently short dwell time and low particle number concentration, one pulse represents a single particle event. There is a direct relationship between the number of pulses and the number concentration of particles (particle number per volume). With the intensity of the pulse (i.e., the height) and assumptions about the particle geometry, the particle size can be determined by the particle mass [127]. It provides information about the core diameter of a NP, since coatings with a composition different to the investigated element are ignored. Aside from the above-mentioned determination of the particle size via single pulses, there is always a background originating from the ionic fraction of the analyzed sample. In addition to the primary particle size, information about the dissolution rate of a NP sample can also be obtained. While quantification is more difficult, a qualitative estimate of the ions released can be derived [127]. With low number concentration and size detection limits (10 to >200 nm, depending on the investigated element) [133], this technique is particularly appropriate for the determination of biological samples, where low concentrations of particles can be present. An advantage of this technique is the possibility to differentiate between ionic and particulate form of the analyte in contrast to the classical ICP-MS method. In biological media, this is very advantageous, because NPs can undergo several processes and change their form, for example after oral uptake and transport in the gut [134]. For complex samples with higher agglomeration SP-ICP-MS struggles to differentiate between single particles and agglomerates. In addition, ICP-MS is less sensitive to certain elements, which can result in poor ionization and detection [135]. Another challenge can be the quantification of NPs in the presence of calcium, phosphorous and sodium, which naturally occur in biological samples and can cause isobaric interferences [136]. In addition, metal speciation is not possible and carbon-based NPs cannot be characterized.

In summary, the ICP-MS technique is a very versatile method for the analysis and characterization of NP properties in different media and conditions and was employed for

different key aspects in this thesis. In the following, the most important NP properties and their possible characterization techniques will be described.

1.3.1.2 Size

Particle size describes the external dimensions of a particle. It is one of the most studied parameters when characterizing nanoparticles [126]. A multitude of analytical techniques are available to determine the size of a NP at different conditions. However, the obtained results may differ significantly, as aspects of particle dimensions or distribution averages are chosen differently. In addition, sample preparation for the used technique can change the effective particle size [137]. Depending on the state NPs are present, there are various techniques for size determination. Airborne particles can be measured by cascade impactors (CI), mobility analyzers (MA) or time-of-flight mass spectrometers (ToF-MS) [138, 139]. For suspended NPs, techniques like dynamic light scattering (DLS), laser diffraction, field-flow fractionation (FFF) coupled to DLS or (SP-)ICP-MS, nanoparticle tracking analysis (NTA), size exclusion chromatography (SEC), differential centrifugal sedimentation (DCS) and atomic force microscopy (AFM) can be used [127, 140-143].

Also for dry samples, promising techniques are available, including electron microscopy, atomic force microscopy and X-ray diffraction methods [127, 143].

1.3.1.3 Shape

Shape or morphology not only describe the outer form of a NP, but also the surface topography, including pores, cracks or ridges [137]. Morphology is an important parameter, as it influences the dispersion, functionality and therefore also toxicity of a NP. Unlike size characterization, the investigation of particle morphology requires a visualization of particles, which can be achieved by electron microscopy or atomic force microscopy [137]. A difficulty arising from the use of microscopic techniques is the measurement of single particles, which requires a large sample size to be representative. Moreover, sample preparation and orientation of particles need to be taken into account [144].

1.3.1.4 Chemical composition and crystal structure

Chemical composition defines the atomic elements a NP is made of. Several techniques, depending if a bulk analysis or a single particle analysis is needed, are available for the

determination of the chemical composition. Techniques able to determine the composition of complete samples include atomic absorption spectroscopy (AAS), inductively coupled plasma optical emission spectroscopy (ICP-OES), or ICP-MS, nuclear magnetic resonance spectroscopy (applicable for suspensions or solid samples), neutron activation analysis (NAA), and X-ray techniques (diffraction, absorption and fluorescence) [137]. Single particle techniques are, as described above, electron microscopy techniques with elemental detectors such as energy-dispersive X-ray analysis or electron energy loss spectroscopy [137].

Another property is the crystal structure of a NP, which can be crystalline or amorphous. The crystal structure is the repetition of a three-dimensional unit of atoms. Crystallinity describes the ratio between crystalline and amorphous phases. Crystal structure is an important parameter when investigating the material stability and the dissolution behavior of a NP. Since dissolution is relevant for multiple areas, e.g. toxicology, getting information on the crystal structure can be crucial. The most common technique is X-ray diffraction for determination of crystal structure and crystal size [137].

1.3.1.5 Surface area

Surface area is a key parameter responsible for the reactivity of a NP and is important for surface ligand interactions. The surface area of a powder normalized to mass or volume is defined as specific surface area. Same as for other parameters, surface area can be measured by different methods, indirectly and directly [137]. Airborne NPs can be investigated indirectly by real-time diffusion chargers that determine the active surface area. Active surface area is defined as the area interacting with surrounding gas or ions which can only be accessed from outside [145]. Alternatively, electrical mobility analyzers can be used to calculate spherical equivalent diameters. These are converted via geometric relationships to mobility-based surface areas [146]. Since these methods do not distinguish between the NP to be analyzed and incidental background particles, caution is required especially in complex environments. In addition, porosity and other surface irregularities are not accounted and may therefore lead to inaccurate results [145, 147]. Direct surface area measurements can be achieved using inert gas adsorption. Therefore, the sample must be present in a clean and dry state and is then exposed to the adsorbate gas under varying pressure conditions. A gas coverage monolayer is aimed for, from which the needed number of adsorbate gas molecules together with the

cross-sectional area of adsorbed gas molecules are related to total surface area (including external area and internal pores and cavities) with the help of Brunauer-Emmett-Teller equation [148]. It is important to keep in mind, that for gas adsorption, samples must be outgassed under vacuum and/or heated to remove surface water and contaminants. The investigated material needs to be inert to such preparation steps in order not to alter its surface properties.

1.3.1.6 Surface chemistry and charge

Compared to the bulk material, a significantly higher proportion of atoms is present on the surface of NPs. Since those surface atoms are in direct contact with solvents, they influence dissolution and sorption of other molecules, for example proteins. In addition reactivity is dependent on surface atoms, since they are able to produce reactive oxygen species [144]. Moreover, NPs may have a core-shell structure, with a surface different from their core composition. Different techniques are available for surface analysis, including X-ray photon spectroscopy (XPS), Auger electron spectroscopy (AES) and Time-of-flight secondary ion mass spectrometry (ToF-SIMS). While XPS and AES describing thicker surfaces of 1-5 nm, ToF-SIMS is also able to determine just the top layer of a sample (few angstroms) [130, 144].

Surface charge describes the charge that occurs due to adsorption or desorption of protons on hydroxylated sites or chemical modification such as amination and sulfonation on a NP surface and is determined by titration. Often used as a parameter is the zeta potential, which defines the shear-plane charge near the NP surface in suspension. It can be an indicator for colloidal stability in dispersions, while it also predicts the NP uptake by cells. The Zeta potential is a calculated value, that depends on the NP and its surrounding medium. Therefore, a description of measurement temperature, composition, pH, viscosity and dielectric constant of medium is needed to calculate the zeta potential from the Henry equation [137, 149].

1.3.1.7 Solubility

Solubility of a solute is the analytical composition of a saturated solution, given as the proportion of a designated solute in a designated solvent. The solubility can be represented as a concentration, molality, mole fraction, mole ratio, etc. [150]. Often water is the investigated solvent and compared to more complex liquids, for example biological fluids, it is

easy to analyze. In literature, the terms solubility, dissolution, biodurability and biopersistence are often used interchangeably however they are not the same. In contrast to solubility, dissolution is a kinetic process, which is quantified by its rate (typical unit is mol/s). It describes the interactions of a solute with the solvent, that results in the stabilization of a solute in the solvent [150]. In biological fluids or matrices, the dissolution rate is defined as biodurability. The clearance of a material from the lung, by physical (mucocilliary or cell-mediated action) and chemical (dissolution) processes is called (bio)persistence [137]. Techniques commonly applied to determine the ion concentration in solvents are AAS, ICP-OES and ICP-MS with ICP-MS generally being the most sensitive. As these techniques provide a total elemental concentration and do not distinguish between dissolved and particular forms, it is important to avoid particles present in the sample as it would increase the mass of a dissolved analyte.

In order to ensure particle-free samples, different separation methods are available. Based on the underlying principle they can be classified into physical, mechanical and chemical separation methods. Size exclusion, hydrodynamic chromatography and field-flow fractionation rank among the physical techniques. Mechanical separation can be achieved using membranes (like in dialysis) and/or centrifugation processes. Liquid-liquid and solid-liquid extraction are possible chemical separation approaches. Cost, complexity and efficiency are different for those techniques, which makes them strongly dependent on the respective problem, as there is no universal separation method for every question [137]. One example is centrifugal ultrafiltration, which uses membranes with a very low cut-off. However, these membranes often contain chloride, which will bind to analytes like silver, resulting in the loss of analyte [151].

Separation is an additional step of sample preparation, which lead to the development of separation-free analytical techniques. One appropriate technique, where a separation of particulate and ionic part of the sample is not necessary, is SP-ICP-MS.

1.3.2 Methods for the investigation of aluminum NPs in environmental matrices

The broad application profile of engineered NPs in consumer products leads to their release into the environment and potentially to human exposure. Information on the fate of nanomaterials after their release into the environment is important to predict effects after

uptake into organisms [152]. Little is known about biodistribution, localization and accumulation of NPs in biological systems. Studies exist about NPs in biological media focusing on medical questions. However, functionalized NPs at high concentrations are being used in these experiments [153, 154]. On the other hand, engineered NPs released to the environment often are non-functionalized and occur in much lower concentrations, leading to completely different behavior compared to functionalized NPs [155]. Characterization and quantification of NPs in biological samples with common analytical techniques is possible [156], yet challenging in certain complex biological media [157, 158]. Many of the analytical methods provide mass-based concentrations, while not taking into account, that particle number or volume-specific surface areas may exhibit a specific toxicity of the NPs [159]. Methods for quantification and characterization of NPs in complex matrices, such as food, cosmetic products and soil were developed [160-162]. Due to the complexity of these methods, they are rarely used in toxicological assessments [158].

Analytical techniques for NP investigation in biological media can be divided into *in situ* and *ex situ* methods. An advantage of *in situ* methods is that only minimal sample preparation is needed, which sometimes leads to artifacts [158]. Most *in situ* techniques are either imaging or spectrometry techniques. Electron microscopy (transmission, TEM, or scanning, SEM) is commonly used for NP investigation in complex matrices. Coupled to an energy-dispersive X-ray spectrometer (EDX) or in combination with synchrotron-based techniques, it allows localization and speciation of NPs down to the cellular level [163, 164]. ICP-MS can quantify NPs *in situ*. With detection limits in the µg/l range and as multi-element method, it can be used for different analytical problems [165]. Coupling of ICP-MS with laser ablation (LA) enables quantification of metallic NPs in solid samples [155].

Electron microscopy (EM) as an imaging technique can be used for visualization of NPs in cells, although artifacts (e.g. cell structure distortion, relocation or extraction of NPs) can occur due to sample preparation steps (like chemical fixation, drying of the samples, dehydration at room temperature or slow freezing attempts) [166]. High pressure freezing could be an alternative for sample preparation [167], yet it is rarely used [168].

The application of EDX enables the identification of the elemental composition with high resolution in micro- and nanometer range [163]. This combination can detect metallic NPs in

biological media [169] and was applied for intracellular localization of metal NPs [170, 171]. Drawback of this hyphenation is the small sample section, which is normally analyzed, resulting in a time-consuming analysis, especially for low amounts of analyte. Furthermore, no information about size or aggregation state can be obtained.

Besides labeling techniques, which may cause interferences with the sample, there are label-free techniques, for example coherent anti-Stokes Raman scattering (CARS) and the two-photon laser technique. These techniques were successfully used to detect metallic NPs in fish gills and for three-dimensional particle tracking in living cells [172, 173].

Dark-field microscopy can be used for detection and characterization of NPs [174]. Here an incident beam illuminates the sample and the scattered radiation is collected by a microscope objective and can be coupled to a spectrometer for analysis. This technique enables fast analysis of NPs and their properties (size, shape, composition) [175].

Laser ablation coupled to ICP-MS enables elemental analysis of solid samples. This technique has already been applied for quantification of different NPs at single cell level [176, 177]. Disadvantages are low resolution and the destruction of the sample. With improved resolution, the technique was applied for different NPs in various biological samples in the recent years [178-180].

After extraction of NPs from biological media, application of ex-situ techniques is possible for particle characterization. For complex samples with high polydispersity, asymmetric flow field flow fractionation (AF4) can be used to facilitate the characterization with other techniques, such as light scattering or (SP-)ICP-MS. AF4 has been applied for NP separation from complex matrices [181]. However, it cannot distinguish between particles and complex matrices, since the fractionation is based on the hydrodynamic diameter. After coupling to ICP-MS, elemental information on the fractions can be obtained. AF4-ICP-MS was used for separation and characterization of NPs in complex matrices [160, 182]. Limiting factors such as particle-membrane interactions or protein corona formation may modify the particles' elution time [183, 184]. In addition, the mass-based data needs to be converted to a particle number size distribution, which has limitations based on the analytical method [185].

Ex-situ techniques can be a valuable alternative, if no in-situ techniques are suitable. *Ex-situ* techniques may reveal parameters like size, size distribution and particle number

concentration. However, it must be kept in mind, that sample preparation can severely alter particles and therefore change their behavior leading to inaccurate results.

1.3.3 Modes of nanomaterial-induced toxicity

Nanoparticles can lead to different toxicological effects, based on their physicochemical properties. For soluble NPs toxic effects seem to be caused mainly by their dissolved fraction [186, 187]. However, there are also investigations on more inert NPs, where size and specific surface area have a significant impact on the reactive oxygen species (ROS) production [188]. The production of ROS has been described to be responsible for most of the toxic effects attributed to NPs *in vitro* and *in vivo* [189]. Modest amounts of ROS are important for the modulation of several cellular actions, such as signal transduction, protein redox regulation, gene expression and proliferative response [190, 191]. However, higher ROS levels indicate oxidative stress and may result in cell damage due to lipid peroxidation, altered proteins, DNA disruption, interference with signaling functions and gene transcription modulation [159]. Cancer, renal diseases, neurodegeneration, cardiovascular or pulmonary diseases may be the consequence [189]. To test *in vitro* toxicity, several assays like lactate dehydrogenase (LDH) for cell membrane integrity, MTT for mitochondrial function or immunochemistry markers for apoptosis and necrosis exist. These assays give little information about reasons or mechanisms of the toxicity [189]. On the other hand, *in vivo* studies are used to assess aspects, which cannot be investigated *in vitro*, for example the toxico-kinetics of tested materials. However, *in vivo* tests are expensive, time-consuming and ethically questionable. Nevertheless, *in vivo* studies are capable of addressing various exposure routes while providing information on neurological, cardiovascular, reproductive, immunological and developmental toxicity of the tested NPs.

Physicochemical properties of a respective NP strongly influence the toxicity mechanisms outlined above. Knowledge of size, shape, chemical composition, surface area, charge and solubility is not only important to evaluate their biokinetic behavior but also to investigate their toxic potential. An overview about potential effects of these properties on toxicity and physiological response to NPs is given below (Figure 2).

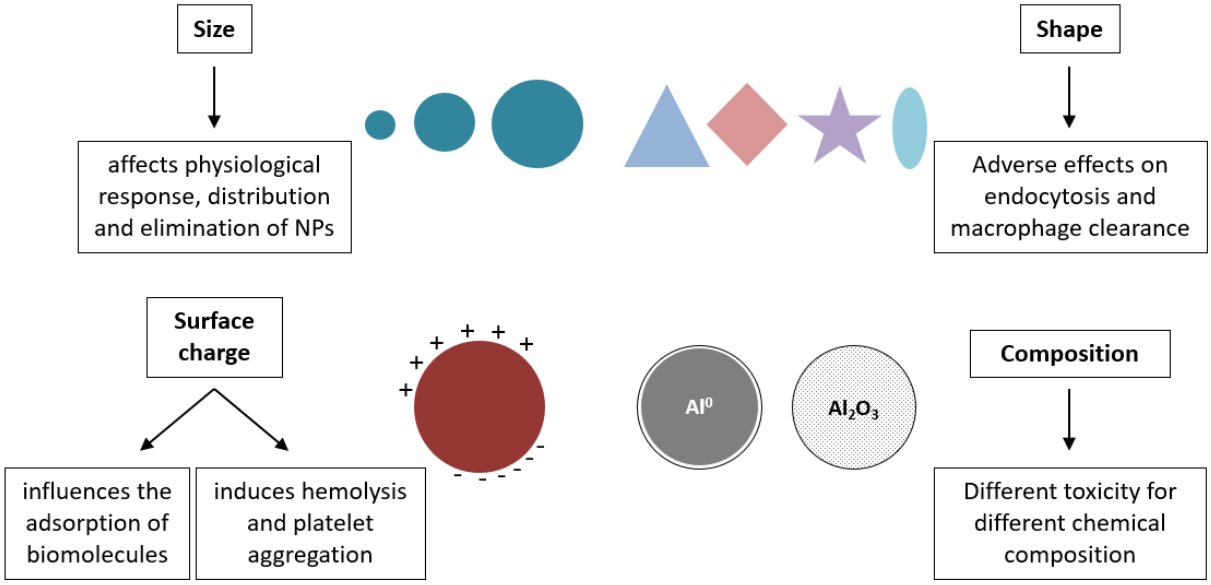

Figure 2: Overview on selected physicochemical properties of NPs and how these properties may affect the NP toxicity and the physiological response.

In the following sections, some of those parameters are discussed in more detail.

1.3.3.1 The importance of size for NP toxicity

Particle size and surface area are important parameters when assessing the toxicity of a NP. Interactions with NPs occur at their surface. The specific surface area increases exponentially with decreasing particle size, resulting in more surface atoms present in comparison to the corresponding bulk material. This means an increase in the surface reactivity of the NP. It was demonstrated that treatment of NPs (e.g uptake, distribution, elimination) by the endocytic pathway is dependent on particle size [144, 192, 193]. Nanoparticles are often regarded as harmful because they can enter biological systems in a size-dependent manner. Furthermore, they may modify proteins by the formation of nanoparticle-protein complexes or accelerating their degradation [194, 195].

1.3.3.2 The importance of shape for NP toxicity

The shape and the aspect ratio of NPs are two other parameters that determine the NP toxicity. Shape dependent toxicity was mostly investigated *in vitro*. Adverse effects on endocytosis and macrophage clearance are suspected to be the main reasons for shape

dependent toxicity *in vivo* [189]. *In vitro* investigations showed that shape can have impact on the membrane wrapping process which occurs in endocytosis and phagocytosis [196]. One example are spherical NPs, which are better and faster endocytized compared to rod-shaped or fiber-like NPs [197].

1.3.3.3 The importance of surface charge for NP toxicity

The surface charge of NPs is another important parameter for toxicity assessment. Surface charge influences the adsorption of biomolecules and can therefore change the cellular or organism's response towards the NP. Adhesion alters the biological identity of the particle, changing not only the hydrodynamic size but also the absorption and toxicity mechanisms. Since surface charge also largely determines the colloidal behavior of a NP, there is an additional impact on the organism's response due to aggregate or agglomerate formation [198]. There is evidence that cationic surface charges are more toxic than anionic ones because they are more likely to induce hemolysis and platelet aggregation, while neutral surface charges are most biocompatible [199].

1.3.3.4 The importance of composition for NP toxicity

While size and surface area are generally considered to be more important for toxicity, composition of NPs is a relevant parameter for investigation of cell molecular chemistry and oxidative stress [189]. Studies on zebrafish with NPs of the same size but different chemical composition showed different toxicities [200, 201]. It appears that the solubility of the tested NPs had an impact on the toxicity, as nanosilver and nanocopper and the corresponding soluble forms showed toxicity in different organisms, while TiO_2 induced no toxic effects [201].

Based on the discussed influences of different physicochemical properties, toxicity seems to be affected by different particular parameters, including chemical composition, surface charge, size, and shape.

2. Aim and objectives

The aim of this dissertation was to identify differences in the bioavailability of different Al species after oral uptake. Therefore, the three following aspects were investigated in detail.

1. For NP characterization, suitable techniques for the analysis of NPs in complex matrices needed to be identified and implemented first. A broad spectrum of analytical methods was used for particle characterization purposes to identify those techniques that would allow for the determination of NP key parameters. Special attention was put on the characterization of size, surface and the solubility of different Al-containing NPs. An ionic Al control was used in comparison.

2. An artificial digestion was used for the *in vitro* simulation of the gastrointestinal tract to simulate the behavior of NPs after oral uptake. The previously identified analytical techniques were applied to characterize the mixtures resulting from the artificial digestion and to relate them to an ionic aluminum control. A great advantage of the artificial digestion approach is that it is an *in vitro* method. As a more mechanistic approach, it is suitable to specifically investigate individual digestion steps, which is not easily possible in an *in vivo* study.

3. Finally, an *in vivo* study in rats was performed to determine whether possible differences, which were expected to occur during the artificial digestion approach could be confirmed *in vivo*. For this purpose, the organ burden after oral uptake of Al-containing NPs was determined and compared to an ionic Al control. Special emphasis was put on the analysis of the intestinal tract and important excretion organs, e.g. intestine, liver, kidney. In addition, the distribution via blood was another parameter that was investigated.

All these objectives should serve to provide a differentiated statement on whether the behavior of different aluminum-containing species varies after oral intake and in biological media. The results will contribute to the risk assessment of Al and help to understand the different toxicokinetic behavior of its speciations.

3. Results

For a better understanding, publications used in this thesis are shown in a non-chronological order. Abbreviations and units have been defined within the respective publication. The publication in chapter 3.3 contains an “author contributions” section to display the individual involvement of the authors.

3.1 Characterization of aluminum, aluminum oxide and titanium dioxide nanomaterials using a combination of methods for particle surface and size analysis

B. Krause,* T. Meyer, H. Sieg, C. Kästner, P. Reichardt, J. Tentschert, H. Jungnickel, I. Estrela-Lopis, A. Burel, S. Chevance, F. Gauffre, P. Jalili, J. Meijer, L. Böhmert, A. Braeuning, A. F. Thünemann, F. Emmerling, V. Fessard, P. Laux, A. Lampen and A. Luch

*Corresponding author

This chapter was published online on 17 Apr 2018 in:

RSC Advances, Vol. 8, H. 26S. 14377-14388

DOI: 10.1039/c8ra00205c

Link: https://doi.org/10.1039/C8RA00205C

Involvement of the author within this publication: Project planning (55%), project execution (80%), data analysis (70%), writing of the manuscript (70%).

The supplementary material of the publication can be found in Annex I.

RSC Advances

PAPER

View Article Online
View Journal | View Issue

Cite this: *RSC Adv.*, 2018, **8**, 14377

Characterization of aluminum, aluminum oxide and titanium dioxide nanomaterials using a combination of methods for particle surface and size analysis†

B. Krause, *[a] T. Meyer,[b] H. Sieg,[c] C. Kästner, [d] P. Reichardt,[a] J. Tentschert,[a] H. Jungnickel,[a] I. Estrela-Lopis,[b] A. Burel,[e] S. Chevance, [f] F. Gauffre, [f] P. Jalili,[g] J. Meijer,[h] L. Böhmert,[c] A. Braeuning,[c] A. F. Thünemann, [d] F. Emmerling, [i] V. Fessard,[g] P. Laux, [a] A. Lampen[c] and A. Luch [a]

The application of appropriate analytical techniques is essential for nanomaterial (NM) characterization. In this study, we compared different analytical techniques for NM analysis. Regarding possible adverse health effects, ionic and particulate NM effects have to be taken into account. As NMs behave quite differently in physiological media, special attention was paid to techniques which are able to determine the biosolubility and complexation behavior of NMs. Representative NMs of similar size were selected: aluminum (Al^0) and aluminum oxide (Al_2O_3), to compare the behavior of metal and metal oxides. In addition, titanium dioxide (TiO_2) was investigated. Characterization techniques such as dynamic light scattering (DLS) and nanoparticle tracking analysis (NTA) were evaluated with respect to their suitability for fast characterization of nanoparticle dispersions regarding a particle's hydrodynamic diameter and size distribution. By application of inductively coupled plasma mass spectrometry in the single particle mode (SP-ICP-MS), individual nanoparticles were quantified and characterized regarding their size. SP-ICP-MS measurements were correlated with the information gained using other characterization techniques, *i.e.* transmission electron microscopy (TEM) and small angle X-ray scattering (SAXS). The particle surface as an important descriptor of NMs was analyzed by X-ray diffraction (XRD). NM impurities and their co-localization with biomolecules were determined by ion beam microscopy (IBM) and confocal Raman microscopy (CRM). We conclude advantages and disadvantages of the different techniques applied and suggest options for their complementation. Thus, this paper may serve as a practical guide to particle characterization techniques.

Received 8th January 2018
Accepted 22nd March 2018

DOI: 10.1039/c8ra00205c

rsc.li/rsc-advances

Introduction

The specific properties of NMs depend on their physicochemical characteristics. Optical properties build upon the size, the shape and the surface structure,[1,2] while higher reactivity, for example, may result from a high surface area,[3,4] specific surface coatings[5] or a surface charge.[6–8] An important factor for increasing their activity is the self-assembly of NMs. Here, NMs associate *via* non-covalent interactions resulting in organized structures of higher-order. Different applications based on advanced functions were

[a]*German Federal Institute for Risk Assessment (BfR), Department of Chemical and Product Safety, Max-Dohrn-Straße 8-10, 10589 Berlin, Germany. E-mail: benjamin-christoph.krause@bfr.bund.de*

[b]*Institute of Medical Physics and Biophysics, University of Leipzig, Härtelstrasse 16-18, 04275 Leipzig, Germany*

[c]*German Federal Institute for Risk Assessment (BfR), Department of Food Safety, Max-Dohrn-Straße 8-10, 10589 Berlin, Germany*

[d]*Federal Institute for Materials Research and Testing (BAM), Unter den Eichen 87, 12205 Berlin, Germany*

[e]*MRIC TEM BIOSIT, Université de Rennes 1, 2 av pro Leon Bernard, France*

[f]*Univ Rennes, CNRS, ISCR UMR6226, F-35000 Rennes, France*

[g]*ANSES, French Agency for Food, Environmental and Occupational Health and Safety, Fougères Laboratory, 10B rue Claude Bourgelat, 35306, Fougères Cedex, France*

[h]*Felix Bloch Institute for Solid State Physics, Faculty of Physics and Geosciences, Division of Nuclear Solid State Physics, University of Leipzig, Linnéstraße 5, 04103 Leipzig, Germany*

[i]*Federal Institute for Materials Research and Testing (BAM), Richard-Willstätter-Straße 11, 12489 Berlin, Germany*

† Electronic supplementary information (ESI) available: NTA size distributions for Al^0, Al_2O_3, NM103, NM104, DLS number-based distribution for Al^0, Al_2O_3, NM103, NM104, TEM measurement of TiO_2 NMs in DMEM, SAXS data for Al^0, Al_2O_3 and $AlCl_3$ in BSA and DMEM after 24 and 48 h, impurities of used NMs determined by IBM, aluminium aqua complexes at different pH values, CRM surface investigations, colocalization pattern by IBM for Al_2O_3, CRM spectra displaying protein modifications, ToF-SIMS measurements of Al and Al_2O_3 NMs in DMEM, ToF-SIMS measurements of TiO_2 NMs in DMEM. See DOI: 10.1039/c8ra00205c

reported, for example formation of mesoporous TiO_2 mediated by ionic liquids for solar cell conversion, catalysis or electronic devices.[9–11] Another application is the self-assembly of biomolecules, like lipids and proteins, mediating inner-particle mesoporosity in a macroporous TiO_2 structure.[12]

TiO_2 NMs are classified as granular biodurable particles (GBPs) of low toxicity.[13] They occur in the form of anatase or rutile as well as in mixtures thereof. While significant accumulation was shown in the liver of rats in the case of orally administered TiO_2 NMs,[14] this was different in studies with Al^0 NMs in mice, in which predominant accumulation in the brain, thymus and lung was revealed.[15] Characterization is important for both *in vitro* and *in vivo* studies. Currently, the human health risk assessment of NMs is mainly based on *in vivo* experiments in rodents.[16,17] However, due to the high number of new NMs,[18] it is not ethical or feasible to conduct such studies for each individual NM. On the other hand, *in vitro* systems proved useful, *e.g.* to generate high throughput data.[19] Extrapolation to the *in vivo* situation remains limited, in particular due to the insufficient comparability of applied dose and particle biotransformation.[20,21] An accurate characterization of NMs in *in vitro* systems by the application of up-to-date analytical methods may therefore help to establish reliable methods for determination of nanomaterial uptake and translocation as key parameters that affect NM-related toxicity. Such an approach would therefore help to reduce the number of materials that need to be subjected to animal testing. We investigated rather soluble Al^0 and rather insoluble Al_2O_3 and TiO_2 NMs (Fig. 1).

This classification is important for NMs because even the same chemical composition can exhibit differences in physicochemical properties. Compared to bulk material, variations are much higher for NMs.[22,23]

For the characterization of test materials, we applied a combination of techniques based on different measuring principles. With DLS as intensity-weighted method, we assessed the hydrodynamic diameter and the polydispersity of the materials in aqueous suspensions and cell culture media (CCM). To validate the results, the more reliable, number-based approach of NTA was applied. The two methods, DLS and NTA, were performed in two different laboratories, allowing for a direct comparison of the results achieved. For particle surface investigation, XRD was used to test whether the aluminum was already oxidized. The core diameter of Al^0, Al_2O_3 and both TiO_2 NMs was measured by SP-ICP-MS. These results were compared to TEM measurements. As a further technique for estimation of the core diameter, SAXS was applied. Additionally, IBM and CRM were performed to analyze the interaction of NMs with biomolecules as well as to quantify impurities in the NM composition. ToF-SIMS is capable of visualizing the formation of complexes out of Al^0 and Al_2O_3 NMs with components of the environmental media. This allows investigation of the behavior of NMs within physiological fluids such as CCM.

With respect to uptake, the dissolution of NMs in different media is of high importance. For example, during an artificial digestion procedure, different pH values, as well as proteins, enzymes and other compounds, mimic the oral uptake route for NMs. For Al^0 and Al_2O_3 NMs, an increased dissolution within the gastric environment was noticed.[24] However, to properly interpret and compare the results, precise knowledge of the properties of the starting materials and of their state in CCM is required. Although there are a lot of studies dealing with silver and copper-containing NMs and their dissolution behavior in biological media,[25–27] to our knowledge, no study accounts for Al^0 NMs. Furthermore, the dissolution behavior of aluminum-containing nanomaterials may be very different since aluminum ions already have a different complexation behavior compared to silver or copper ions. By means of the methods described earlier (Fig. 2), we were able to obtain valuable information to hypothesize the behavior of NMs in biological media and to extrapolate to the *in vivo* situation. With these assumptions, it is much easier to understand and explain future data resulting from more complex scenarios.

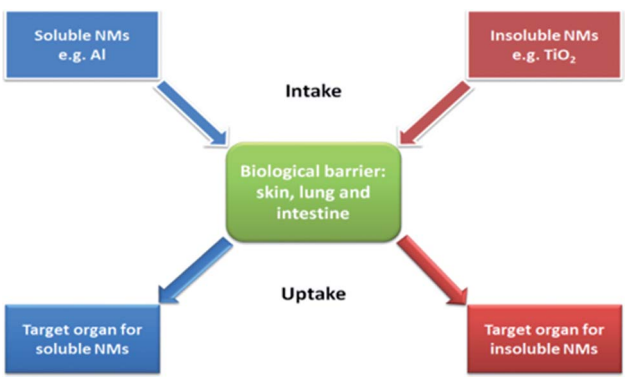

Fig. 1 Hypothesis of different behavior of soluble and insoluble NMs after uptake.

Experimental

Materials and methods

Al^0 NMs (mean diameter 18 nm (TEM), 99.9%) and Al_2O_3 NMs (mean diameter 20 nm (TEM), 99+%) were purchased from IoLiTec Ionic Liquids Technologies GmbH, Heilbronn, Germany. TiO_2 NMs (NM103 and NM104, mean diameter 25 nm (TEM)) were purchased from JRC Joint Research Centre, Ispra, Italy. Bovine serum albumin (BSA) was bought from Sigma Aldrich. CCM (DMEM, high glucose (4.5 g l^{-1}), with sodium pyruvate; with L-glutamine; with 1% penicillin/streptomycin (P/S)) and fetal bovine serum were purchased from PAA Laboratories GmbH, Paching, Austria. All other chemicals used in this study were reagent grade.

Sample preparation

NM dispersions were prepared following the NanoGenoTOX dispersion protocol "Final protocol for producing suitable manufactured NMs exposure media" (October 2011).[28]

For cell culture experiments, stock dispersions of NMs were diluted in DMEM with 10% fetal calf serum (FCS) to either 10 or 100 μg ml^{-1}.

For ion release testing, stock dispersions were diluted in 0.05% BSA to 100 and 10 μg ml^{-1} to reflect a high and a low

concentration used in cell culture experiments. 1 ml was taken and centrifuged at 16000 × *g* for 1 h (Hettich Zentrifuge Mikro 220R). 500 µl of the supernatant were taken, 750 µl of HNO_3 (69%) were added and Millipore water was used to fill up to 15 ml.

For IBM and CRM, NMs were centrifuged at 8000 × *g* for 10 min, supernatant was taken away, mpH_2O was added and the sample was vortexed. The procedure was repeated 3 times. Finally, a small drop of the sample was given on polypropylene foil for IBM and on quartz glass for CRM. The dry samples were measured.

Dynamic light scattering measurements

The distributions of the hydrodynamic diameters of the NMs were determined using a Malvern Nano ZS (Malvern Inc., UK) or a Brookhaven ZetaPALS (Brookhaven Instruments Corporation, USA). A stock dispersion (2.56 mg ml^{-1} in 0.05% BSA) was diluted to the concentration of 100 µg ml^{-1}. The NM dispersions in 0.05% BSA as well as in DMEM were analyzed 5–10 min after preparation. Thermal equilibration time was set to 60 s at 25 °C. Each intensity-weighted size distribution represents the average of six individual DLS analyses, three replicates and at least three independent experiments using automatic optimization of analytical conditions and data treatment by general purpose size analysis.

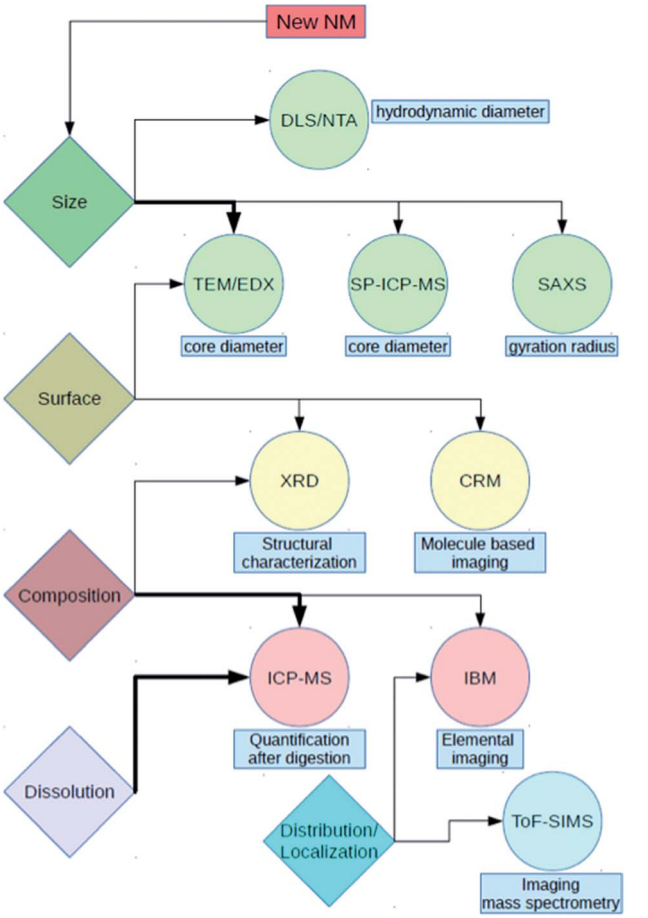

Fig. 2 Overview of key NM characteristics (colored rhombi) and methods (colored circles) used in this study for characterization. Arrows in bold imply the main method for the linked characteristic. Abbreviations: DLS – dynamic light scattering; NTA – nanoparticle tracking analysis; TEM – transmission electron microscopy; EDX – energy dispersive X-ray spectroscopy; SP-ICP-MS – single particle inductively coupled plasma mass spectrometry; SAXS – small angle X-ray scattering; XRD – X-ray diffraction; CRM – confocal Raman microscopy; ICP-MS – inductively coupled plasma mass spectrometry; IBM – ion beam microscopy; ToF-SIMS – time of flight mass spectrometry.

Nanoparticle tracking analysis measurements

NTA measurements were performed with a NanoSight LM20 and LM10 (NanoSight, Amesbury, UK), equipped with a 632 nm laser or 532 nm laser. The samples were injected into the sample chamber with sterile syringes. All measurements were performed at room temperature. The samples were diluted to a final concentration of approx. 10^8 particles per ml with mpH_2O, depending on the NMs and media. The software used for recording and analyzing the data was NTA 2.3 and NTA 3.0. All samples were measured for 60 s at five positions. All measurements were performed with at least three independent experiments.

X-ray diffraction measurements

The XRD measurements were achieved on powder samples using a D5000 diffractometer (Siemens AG, Munich, Germany) in Bragg Brentano geometry. A linear detector, a curved Ge(111) monochromator and Cu K_α radiation (λ = 0.1542 nm) were used. The analysis was performed over the 2θ range of 10 to 90° and at a step size of 0.02° and scanning speed of 2° per step. The experiments were carried out independently three times.

Single particle ICP-MS measurements

For single particle analysis of the NM solutions, a quadrupole ICP-MS (Thermo Scientific XSERIES II, Thermo Fisher Scientific, Waltham, MA, USA) with a PFA ST Nebulizer, a quartz cyclonic spray chamber and a 2.5 mm quartz O-ring-free injector (all from ESI Elemental Service & Instruments GmbH, Mainz, Germany) were used. Using the time-resolved analysis (TRA) mode for data acquisition, intensities as a function of time (counts per dwell-time interval) were collected. The acquisition time for each run was set to 60 s with a dwell time (or data acquisition rate) of 3 ms. The gas flow for the plasma, the nebulizer and the auxiliary (all Ar) was set to 13 l min^{-1}, 0.89 l min^{-1} and 0.7 l min^{-1} respectively. The flow rate of the sample was 0.34 ml min^{-1}. Data were exported to a spreadsheet for further processing. For data processing, an established procedure according to Pace *et al.*[29] was followed. Determination of nebulizer efficiency was performed using a described method with reference nanoparticles of known particle size.[29] 60 nm gold reference nanoparticles from the U.S. National Institute of Standards and Technology (NIST, RM 8013) were used as reference nanoparticles.

Small angle X-ray scattering measurements

The measurements were conducted in a flow-through capillary with a Kratky-type instrument (SAXSess, Anton Paar, Austria) at 21 ± 1 °C. The SAXSess has a low sample-detector distance of 0.309 m. Deconvolution of the SAXS curves was carried out with the SAXS-Quant software. Curve fitting was performed with the McSAS software (Monte Carlo method, version 1.0.1). The experiments were performed with 120 measurement cycles (each averaged over 10 s). NMs and controls were dispersed according to NanoGenoTOX protocol and diluted into DMEM in a sample concentration of 100 μg ml^{-1}. Samples were incubated for a time of 24 and 48 h at 37 °C and 5% CO_2 in a cell incubator until sample injection. Stock dispersions were injected directly after ultrasonication.

Ion beam microscopy

Label-free IBM measurements were performed with the LIPSION Nanoprobe. A 2.25 MeV proton beam was applied by a Singletron™ particle accelerator. A vacuum with a pressure of 5×10^{-5} to 10^{-7} torr was applied and the beam was focused to a spot size of around 1 μm. For spatial resolved element analysis, micro proton induced X-ray emission (μPIXE) and micro Rutherford backscattering spectroscopy (μRBS) were recorded simultaneously. The μPIXE detector (Canberra, Meriden, CT, USA) consists of a high-purity Ge crystal covered with a 60 μm polyethylene layer, which covers the detector for backscattered protons. μRBS spectra were detected by a Canberra PIPS detector.

Confocal Raman microscopy

Spectroscopic analysis of NMs was performed by CRM. A Witec alpha300 confocal Raman spectrometer (Witec GmbH, Germany) with a 532 nm laser with 30 mW power was used. Control4.1 (Witec GmbH, Germany) software was used to record and analyze the spectra. The spectra were recorded at an integration time of 0.15 s per point and with a step size of 250 nm.

Transmission electron microscopy

The samples were deposited on a 400-mesh copper grid. The grids were prepared by sample adsorption and left free-standing on top of a 0.8 mg ml^{-1} solution of NMs for 20 s. Excess solution was removed by placing the grid on a filter paper and the sample was dried for 24 h. For samples in DMEM, the grid was washed by dipping the grid in a droplet of water before. Examination was performed with a JEOL 1400 transmission electron microscope, equipped with a tungsten filament and supplied with GATAN Orius 1000 camera. TEM operated at 80 kV (DMEM) or at 120 kV with magnification of 200 000×.

Time-of-flight mass spectrometry

Ion images and spectra were acquired using a ToF-SIMS V instrument (ION-TOF GmbH, Münster, Germany) with a 30 keV nano-bismuth primary ion beam source ($[Bi]x^{(y+)}$-cluster ion source with a BiMn emitter). The ion currents were 0.5 pA at 5 kHz using a Faraday cup. A pulse of 0.7 ns from the bunching system resulted in a mass resolution that usually exceeded 6000 (full width at half-maximum) at $m/z < 500$ in positive ion mode. The primary ion dose was controlled below 1012 ions cm^{-2} to ensure static SIMS conditions. Charge compensation on the sample was obtained by a pulsed electron flood gun with 20 eV electrons.

The primary ion gun scanned a field of view of 500 μm × 500 μm applying a 512 × 512 pixel measurement raster. Once the primary ion gun was aligned, a ToF-SIMS mass spectrum was generated by summing the detected secondary ion intensities and plotting them against the mass channels. The data were evaluated using the Surface Lab software (ION-TOF GmbH, Münster, Germany).

Results and discussion

We point to the advantages and disadvantages of the methods used and explain whether or not methods can provide complementary results to other techniques. We also analyzed possible dissolution characteristics of different matrix media (BSA and DMEM) for pristine Al^0 and oxide (Al_2O_3 and TiO_2) NMs. Characterization data already published on TiO_2 were retrieved according to JRC report.[30] In conclusion, we will present data where the dissolution of NMs in complex media has an impact on particle media interactions. These results were obtained by ToF-SIMS and show the efficiency of that method for obtaining insights into elemental compositions with TEM, IBM, CRM and ToF-SIMS. An overview about the main characterization techniques and their limits is given in Table 3.

A very common and frequently used method for determining the size distribution and polydispersity of NMs in solution is DLS. Fast and easy sample preparation as well as quick measurement give rapid initial indications of the sample. NTA is more appropriate for evaluating polydisperse samples with

Table 1 *Z*-averages with standard deviation (SD) and polydispersity index (PDI) of Al^0, Al_2O_3, NM103 and NM104 NMs in different media determined by dynamic light scattering (DLS). All results represent the average of six repeats. BSA: bovine serum albumin; DMEM: Dulbecco's modified eagle medium; FCS: fetal calf serum

DLS measurements and comparison				
	Lab 1 (Malvern)		Lab 2 (Brookhaven)	
	Z-average [nm]	PDI	*Z*-average [nm]	PDI
Stock solution (0.05% BSA in H_2O)				
Al^0 NM	250 ± 10	0.17 ± 0.01	270 ± 40	0.18 ± 0.02
Al_2O_3 NM	170 ± 10	0.24 ± 0.02	210 ± 40	0.21 ± 0.06
NM103	270 ± 10	0.28 ± 0.05	610 ± 190	0.21 ± 0.30
NM104	220 ± 10	0.26 ± 0.03	370 ± 90	0.15 ± 0.03
DMEM (with 10% FCS)				
Al^0 NM	200 ± 10	0.18 ± 0.01	220 ± 10	0.21 ± 0.02
Al_2O_3 NM	70 ± 10	0.52 ± 0.03	230 ± 60	0.18 ± 0.07
NM103	240 ± 20	0.24 ± 0.01	270 ± 10	0.25 ± 0.01
NM104	190 ± 10	0.28 ± 0.02	230 ± 10	0.18 ± 0.02

various aggregate populations, since it is based on single particle tracking as both techniques determine the hydrodynamic diameter. Due to the fixed working ranges of DLS and NTA, the used concentration of media various. Since NTA is a counting method, also proteins would be counted and would significantly lower the hydrodynamic diameter of the NM dispersion. Therefore, the particles, as well as the medium were diluted directly before measurement with mpH_2O to avoid agglomeration effects.

For all particles with a primary size of approximately 20 nm, a hydrodynamic diameter between 200 and 270 nm was measured by DLS in DMEM (Table 1). In contrast, different aggregate fractions of NMs in DMEM with a mean value of about 150 nm were found by means of NTA (Fig. S1†). This difference can be explained by the fact that NTA is a particle counting system, sensitive to large as well as small fractions in the sample, and DLS is an intensity-weighted system, highly responsive to the large fractions. In all cases, the NTA size distribution is asymmetrical with a steep slope on the left side (small particles) and a gentle slope on the right side, representing the fraction of agglomerates. Additionally, a calculation of number-based size distribution out of intensity-weighted DLS data was done (Table S1†).

In the case of NM103 and NM104 dispersed in 0.05% BSA water solution, a very high mean value and a large error was measured by the Brookhaven device, while NTA exhibits broad distributions with some fractions and a mean value of around 180 nm. This can be explained by unstable particle agglomerates, which are observed by the DLS.

Comparing the two DLS devices, one can observe that the Malvern DLS detects 15% smaller particles than the Brookhaven machine in 0.05% BSA water solution as well as in DMEM. This systematic deviation could be related to different detection angles of scattered intensity, 90° for Brookhaven and 173° for Malvern, since larger particles mostly scatter light at forward angles. Backscattering at 173° will not overestimate larger particles as much as measurements at 90°.

In the case of NM103 and 104 in BSA and Al_2O_3 in DMEM, the results were not consistent for the two devices. *Z*-averaged diffusion coefficients were calculated by applying the cumulant method, which is applicable to polydisperse and non-multimodal systems. In contrast, NTA results show the presence of different particle populations. The applied cumulant algorithms are not suitable in certain cases for getting reliable DLS results. Furthermore, it should be kept in mind that the inversion of the DLS autocorrelation function is part of a poorly formulated mathematical problem. It works quite well in the case of monodisperse or low polydisperse particles. Applications of multiangle DLS and sophisticated algorithms are thus necessary to obtain trustworthy results of NM size distributions by means of DLS.[31,32]

Investigations on primary particle size

With the European commission's definition of a nanomaterial, that is, a nanomaterial should contain 50% or more particles in number size distribution with one or more size dimensions between 1–100 nm, it is obviously necessary to obtain information about the primary particle size of the investigated particles. TEM as well as SAXS can be used to solve this problem.

Looking at advantages and disadvantages of TEM, the following issues should be considered. Since TEM measurements are performed under high vacuum, only dried samples are observed. For this reason, TEM is not representative of the sample in its solution state. In particular, agglomeration and coffee stain effect[33] may occur during the drying process, resulting in a non-homogenously covered surface. Size distributions can be determined from TEM pictures by measuring the size of each particle using image analysis software.[34] The size of individual nanoparticles may be difficult to extract from agglomerated samples but, recently, some implementations have been proposed.[35] In addition, for irregular particles with ill-defined shapes, which dimension should be taken? In practice, size analysis can be time-consuming and TEM generally yields a poor statistical representation of the sample.[34] Electron microscopy also enables chemical and crystallographic analysis of the particles. The contrast in TEM is directly linked to the atomic number of electrons, heavier atoms giving higher contrast. This is an advantage when observing metal nanoparticles in a biological environment. However, care should be taken for mineral salts from buffers that may precipitate on the grid when drying. Aqueous washing of the grid after sample deposition might be appropriate in this case.

Fig. 3 shows the dispersion in water with 10% BSA. The shape of Al^0 NMs is globally spherical with rod-like excrescences and the primary particle size varies between 2–50 nm, which matches the manufacturer specification. The Al_2O_3 NMs are not spherical but have rather a needle-like shape. The width is about 10 nm, while the longest dimension varies a bit more between 20–50 nm. The shape of TiO_2 NM104 is rod-like, with a width of approx. 10 nm and length of 20–50 nm (Fig. S2†). Working with a more complex medium, such as CCM, was challenging for TEM analysis. However, we were able to image the particle in DMEM, with very little differences compared to BSA dispersion. Using relatively low voltage, the protein coating can be observed (see Fig. S2†).

SAXS was used for characterization of the primary particle size of NMs. SAXS allows to analyze a broader variety of different sample types than most other techniques. Compared to TEM, the samples can easily be investigated *in situ*. Additionally, SAXS provides statistically more reliable data for particle size distribution quantification since more than 10^6 particles are typically measured, in contrast to TEM, where rarely more than a few

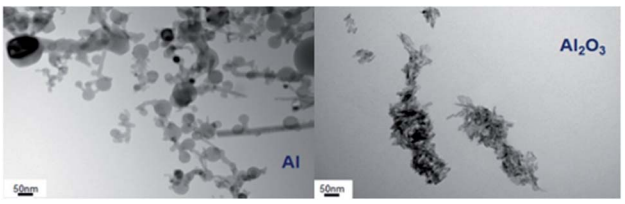

Fig. 3 Comparison of TEM pictures of Al^0 and Al_2O_3 NMs in BSA solution after applying the dispersion protocol.

hundred particles are counted. Size distribution of NMs can be quantified in the range of 1 to 100 nm if the shape is known from a complementary technique like TEM. The classical radius of gyration (Guinier radius) is accessible in any case.

In this study, we observed the size parameters of the particles in BSA as a stock solution and after addition in DMEM at different times of $t = 0$ h, 24 h and 48 h (Fig. 4). Since the particle cores scatter much stronger than the surrounding particle shell, the shell becomes practically invisible. Therefore, SAXS determines the size distribution of the core radii. The resulting distributions of the particles' stock solutions are shown in Fig. 4. Their corresponding SAXS curves are displayed in the ESI (Fig. S3–S5†). The accessible size range of the radii is given by the range of the scattering vector q: $R_{min} = \pi/q_{max}$ and $R_{max} = \pi/q_{min}$. In the present case of the q-range of 0.1 $nm^{-1} < q < 6$ nm^{-1} corresponds to radii of 30 nm > R > 0.5 nm.

The Al^0 NMs showed a broad size distribution including primary particles with radii > 10 nm. Since the detection limit is 30 nm (radius) in this case, bigger aggregates cannot be detected directly. However, from the steep slope of the SAXS curve (Fig. S3†) at low q values, it can be assumed that bigger aggregates are present. The defined characterization of these particle aggregates has to be performed using a complementary method like TEM. The inset in Fig. 4a shows that the radii distribution of the Al^0 NMs did not change significantly either after addition in DMEM or 24 h and 48 h thereafter. In contrast to the Al^0 NMs, the Al_2O_3 NM in BSA displays a distribution which consists of small primary particles and aggregates. The sample shows an amount of 75% primary particles with a mean radius of 7.1 ± 0.5 nm. The detected aggregates display radii of > 10 nm. Upon the addition in DMEM, the radii distribution shifts slightly to higher radii of 8.4 ± 0.2 nm. These characteristics did not change significantly over the time of 48 h in DMEM.

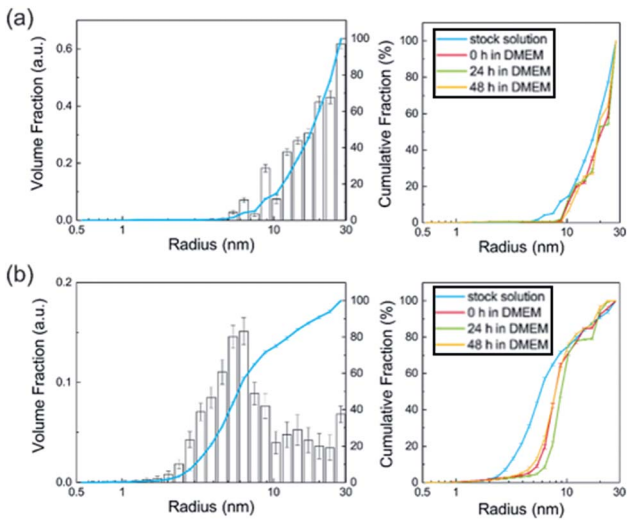

Fig. 4 Volume-weighted radii distributions of Al^0 NMs (a) and Al_2O_3 NMs (b) derived from SAXS measurements. The displayed radii distribution (right panel, black bars) and cumulative fraction presentation (blue line) correspond to the NMs in stock solution (BSA). Left panel shows particle distribution in cumulative fraction presentation at different stages: in stock solution (blue line) and in DMEM after 0 h (red line), 24 h (green line) and 48 h (orange line).

No particles were detected in the ionic control substance $AlCl_3$. In contrast, immediately after addition in DMEM, nano-scaled particles with sizes of 1–30 nm were observed. Since all curves are background-corrected with the respective solvent control, solvent effects can be excluded and the particles derive directly from the aluminum species. In conclusion, SAXS yields the size distribution of nanoparticles and its changes in DMEM.

SP-ICP-MS is another technique to determine primary particle sizes. The fundamental assumption behind this technique is that, at a sufficiently short dwell time and low particle number concentration, a pulse will represent a single particle event.

There is a direct correlation between the number of pulses and the number concentration of particles (particle number per volume). With the intensity of the pulse (*i.e.* height) and assumptions about the particle geometry, the particle size through particle mass can be determined.

Aside from single pulses, there is always a background, which originates from the ionic part of the analyzed sample. In addition to primary particle size, information about the dissolution rate of a NM sample can be achieved. While quantification is more difficult, a qualitative assessment of ions released can be inferred. For Al^0, a broad distribution (Fig. 5, left) up to 200 nm is observed compared to Al_2O_3 (Fig. 5, right). This fits very well with the data obtained from TEM analysis. Compared to the Au NIST reference material, which shows almost no dissolution, a higher background for Al^0 NMs was detected, indicating potential ion release.

Particle surface – impact on dissolution in complex media

Al^0 NMs usually become quickly passivated at the surface by the formation of an oxide layer. This event is likely to change the dissolution behavior and the overall physicochemical

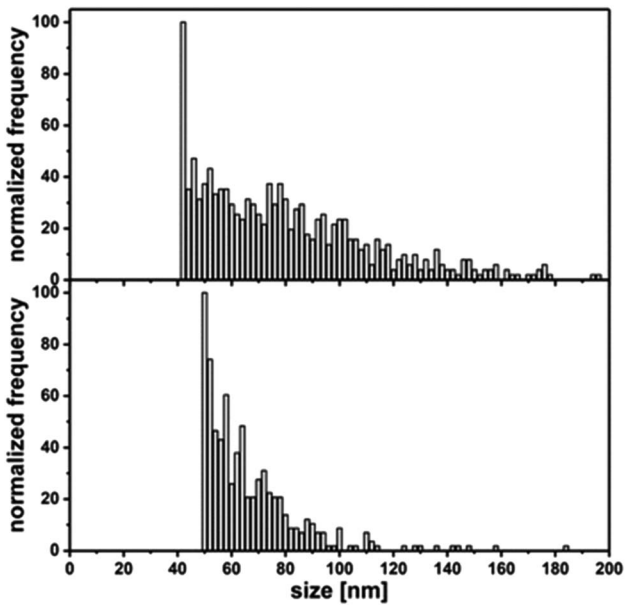

Fig. 5 Top: primary particle size distribution of Al^0 in 0.05% BSA determined by SP-ICP-MS; bottom: Primary particle size distribution of Al_2O_3 in 0.05% BSA determined by SP-ICP-MS.

characteristics of Al^0 NMs. For comparison, we also investigated Al_2O_3 particles of similar size. To prevent the surface oxidation of Al^0 NMs, its processing and handling in an inert gas atmosphere was evaluated.

Investigation by XRD revealed a thin aluminum oxide layer at the surface of the Al^0 NMs (Fig. 6, left). This was confirmed by TEM measurements and has also already been shown in the literature for another Al^0 NM by TEM measurements (2.5 nm oxide layer).[36] The occurrence of an oxide layer can be explained by partial passivation of the material due to manufacturer's processing.

In comparison with Al^0 NMs, the diffractogram of Al_2O_3 particles showed clear differences (Fig. 6, right). The diffractogram of Al^0 NMs showed a higher intensity for the aluminum peaks, *e.g.* at 38°, 45°, 66° and 78° (Fig. 6, left) as compared to Al_2O_3 peaks, *e.g.* at 37°, 46° and 67° (Fig. 6, right). This demonstrates that even though there is an Al oxide layer at the surface of the Al NMs they are not completely oxidized.

To confirm these results, we used electron energy loss spectroscopy (EELS). Here the sample becomes exposed to an electron beam with defined kinetic energy. Some electrons undergoing inelastic scattering are collected in a detector. The loss of energy reflects the chemical composition of the sample.

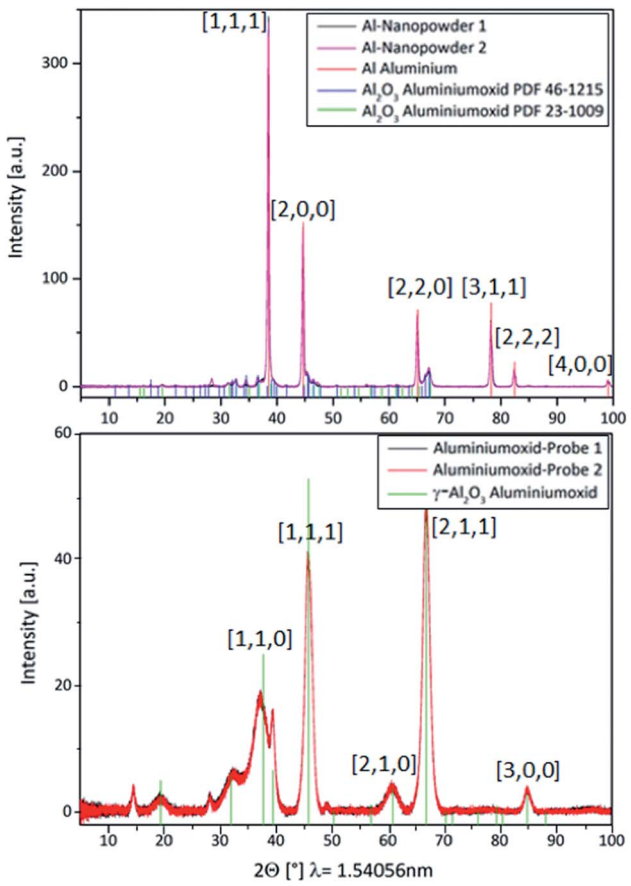

Fig. 6 Top: XR-diffractogram of Al^0 NMs red: database entry for Al; blue; (green: database entry for Al_2O_3), space group: *Fm3m*, lattice constants: $a = 4.0494$ Å; bottom: diffractogram of Al_2O_3 NMs (red: database entry for Al_2O_3), space group: *Fd3m*, lattice constants: $a = 7.906$ Å.

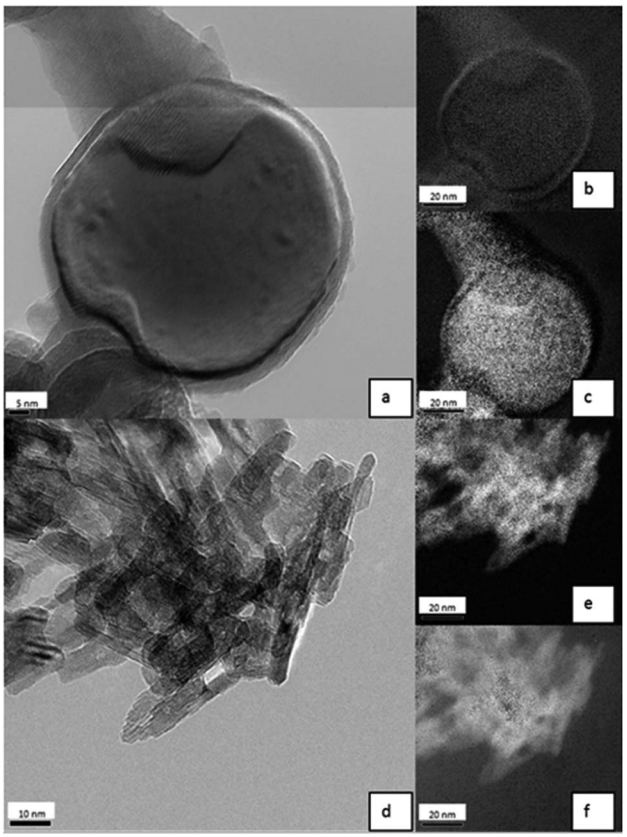

Fig. 7 (a): TEM picture of Al^0 NMs, 200 k magnification; (b) oxygen mapping of left TEM picture; (c) Aluminum mapping of left TEM picture. (d) TEM picture of Al_2O_3 NMs, 200 k magnification; (e) aluminum mapping of left TEM picture; (f) oxygen mapping of left TEM picture.

Analysis of Al^0 NMs in 0.05% BSA (Fig. 7a) revealed a core–shell structure. By means of EELS, it was proven that the shell is rich in oxygen (Fig. 7b), while the core consists of elemental aluminum (Fig. 7c). The TEM results indicate an oxide layer of about 2 to 5 nm.

Elemental mapping of Al_2O_3 NMs showed a quite different picture compared to pure Al^0 NMs (Fig. 7d). The distribution of aluminum and oxygen was homogenous over all NMs (Fig. 7e and f). These results show that Al_2O_3 NMs are fully oxidized while elemental Al^0 NMs were passivated by an oxide layer. It is

Table 2 Ion release of Al^0 and Al_2O_3 NMs compared to recovery of $AlCl_3$ in 0.05% BSA and DMEM

		Ion release in BSA [%]	Ion release in DMEM [%]
Al^0 NMs	10 μg ml^{-1}	0.4 ± 0.1	0.5 ± 0.1
	100 μg ml^{-1}	0.3 ± 0.1	0.4 ± 0.1
Al_2O_3 NMs	10 μg ml^{-1}	0.4 ± 0.1	1.4 ± 0.1
	100 μg ml^{-1}	0.2 ± 0.1	0.4 ± 0.1
$AlCl_3$	10 μg ml^{-1}	140 ± 9	112 ± 4
	100 μg ml^{-1}	94 ± 4	66 ± 3

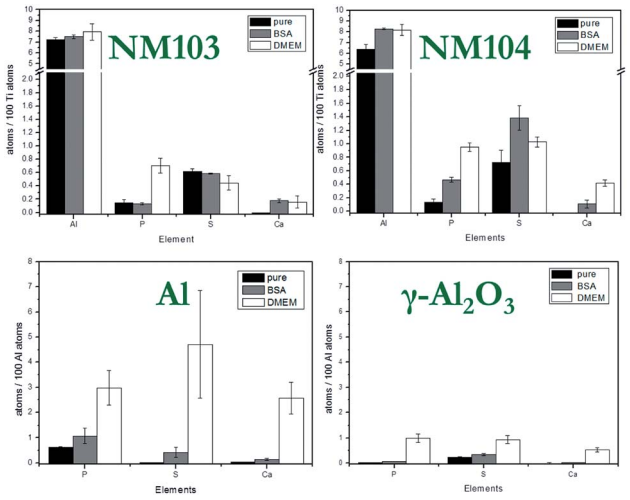

Fig. 8 IBM element analysis of NM103, NM104, Al and Al_2O_3 NMs. NMs as purchased and diluted in water (pure), NMs with albumin corona in H_2O (BSA) and NMs under cell exposure conditions (DMEM). The graph demonstrates the ratio of atoms of several elements compared to 100 atoms of titanium or aluminum.

also visible because Al^0 NMs are dark grey to black, while Al_2O_3 NMs are white.

The results from surface investigations *via* XRD and EELS suggest a different solubility of Al^0 compared to Al_2O_3. Indeed, the thin oxide layer on Al^0 allows the release of ions while the fully oxidized Al_2O_3 particle should be much more inert. Nevertheless, due to the highly specific surface, a higher solubility compared to Al_2O_3 bulk material could be expected as more potentially ion releasing Al atoms are present on the surface.

Influence of particle composition and impurity patterns

Compared to particle size and surface, the particle composition has a much higher impact on the solubility and dissolution behavior of NMs. One of the most widely used methods due to its high sensitivity, broad range for nearly all elements and detection limits down to the sub-ppb level is the ICP-MS. Unknown samples can be not only detected but also quantified. For more complex samples, microwave-assisted digestion prior to ICP-MS analysis could be performed. In this study, we confirmed the already known composition of the NMs by XRD and EELS measurements as well as ICP-MS analysis. For the assessment of particle toxicity, it is also important to take impurities into account which might alter ion release behavior. Due to element-specific μRBS and μPIXE, IBM became the method of choice for these investigations. The main impurities of aluminum-containing NMs were phosphorus, sulfur and chlorine, which could lead to a different ion release compared to pure materials (see Fig. S6†).

Solubility investigations on Al^0 and Al_2O_3 NMs

To verify our hypothesis that Al^0 NMs are more soluble than Al_2O_3, we performed ion release experiments in stock dispersions and DMEM. Adjusting the pH value was not necessary due to almost neutral pH values of 7.3 in stock dispersion compared to 7.2 in DMEM. Keeping in mind that aluminum is an amphoteric material due to the aluminum aqua complexes, one can assume that dissolution of Al^0 NMs in complex media is highly pH-dependent. Compared to an acid, the aluminum aqua complex reacts as a base and *vice versa*. At a neutral pH value, reactivity is very low, thus only low ion release should occur. The possible aluminum aqua complexes at the different pH values are shown in Fig. S7.†

The ion release for both Al^0 and Al_2O_3 NMs after one hour was very low, about 0.2–0.4% in BSA and 0.3–0.5% in DMEM (with 10% FCS) (Table 2). As already described above, this was expected at a neutral pH value. For *in vitro* experiments, this will

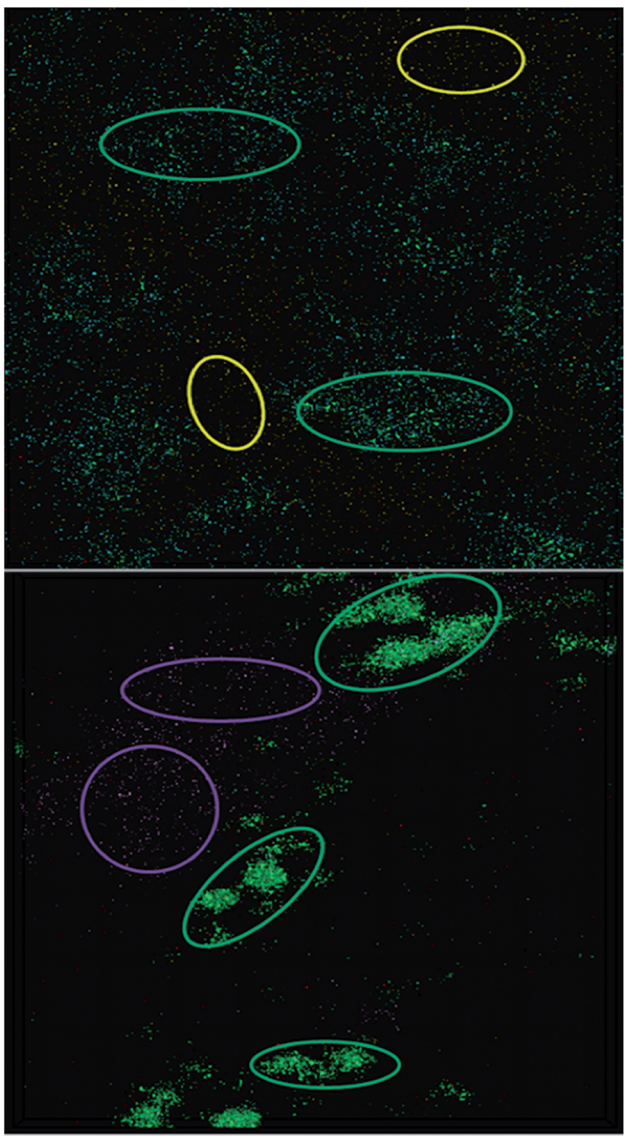

Fig. 9 ToF-SIMS reconstructed ion overlay image (500 μm × 500 μm) of Al NM (top) and Al_2O_3 (bottom) agglomerates of different chemical entities from a DMEM solution; yellow: Al NM, purple: Al_2O_3 NM, green: aluminum(III)–serine; orange: phenylalanine aluminate; red: leucine aluminate; blue: polyoxo-aluminum complex.

Table 3 Main characterization techniques and their limits[a]

Methods		TEM	EELS-TEM	XRD	SAXS	SP-ICP-MS	ICP-MS	ToF-SIMS	IBM, atom number %	CRM
Aluminum	Results	Primary particle size and shape: 2–50 nm, nearly spherical	Core–shell structure, thin (2–5 nm) oxide layer	Aluminum surface; partially oxidized	Particle radius: > 10 nm	Primary particle size: 54–80 nm	Ion release: 0.2–0.5%	Particle-amino acid agglomerates	Impurities: P (1%); biocorona: S (5%), protein; adsorption from DMEM; $Ca_3(PO_4)_2$ coating: P (3%)	No data available
	Limits	No element-specific limits	Light core of Al hinders detailed measurements	No element-specific limits	No element-specific limits	No limits known; results show limit of 54 nm	Detection limit of 10 μg g^{-1} in DMEM	No element-specific limits	From Al to higher atomic mass	Raman active molecules
Al_2O_3	Results	Primary particle size and shape: 10 × 20–50 nm, grain-like shape	Fully oxidized particle	Fully oxidized surface	Primary particle radius: 7.1 nm aggregates' radius: > 10 nm	Primary particle size: 50–80 nm	Ion release: 0.2–0.4%	Particle-amino acid agglomerates; polyoxo-aluminates	Impurities: S (0.2%); biocorona: S (1%), protein adsorption from DMEM; $Ca_3(PO_4)_2$ coating: P (1%)	No data available
	Limits	No element-specific limits	Light core of Al hinders detailed measurements	No element-specific limits	No element-specific limits	No limits known; results show limit of 50 nm	Detection limit of 10 ng g^{-1} in DMEM	No element-specific limits	From Al to higher atomic mass	Raman active molecules
TiO_2 NM103	Results	Primary particle size and shape: 20–100 nm, nearly spherical[b]	No data available	Rutile; crystallite size: 20 nm[b]	Gyration diameter: 26 nm[b]	Primary particle size: 60–100 nm	No solubility in BSA, low soluble in DMEM[b]	Particle-amino acid agglomerates	Impurities: Al (7%), S (0.6%); biocorona: S (0.5%), protein; exchange in DMEM; $Ca_3(PO_4)_2$ coating: P (0.5%)	Decrease of aliphatic/aromatic compounds on NM surface; higher protein exchange in DMEM
	Limits	No element-specific limits	No element-specific limits	No element-specific limits	No element-specific limits	Limit of ∼90 nm[39]	Detection limit of 7.5 ng g^{-1} in DMEM	No element-specific limits	From Al to higher atomic mass	Raman active molecules
TiO_2 NM104	Results	Primary particle size and shape: 10–50 nm, nearly spherical	No data available	Rutile; crystallite size: 21 nm[b]	Gyration diameter: 26 nm[b]	Primary particle size: 60–100 nm	No solubility in BSA, low soluble in DMEM[b]	Particle-amino acid agglomerates	Impurities: Al (6%), S (0.7%); biocorona: S (1%); protein; exchange in DMEM; $Ca_3(PO_4)_2$ coating: P (0.8%)	Decrease of aliphatic/aromatic compounds on NM surface; higher protein exchange in DMEM

Table 3 (*Contd.*)

Methods	TEM	EELS-TEM	XRD	SAXS	SP-ICP-MS	ICP-MS	ToF-SIMS	IBM, atom number %	CRM
Limits	No element-specific limits	No element-specific limits	No element-specific limits	No element-specific limits	Limit of ~90 nm[39]	Detection limit of 7.5 ng g^{-1} in DMEM	No element-specific limits	From Al to higher atomic mass	Raman active molecules
General limits	1 nm to 2 μm; only dried samples	Organic matrix contaminates sample	Only powder and crystallite samples	r = 0.5–30 nm (depending on the available q-range)	Only highly diluted samples, limits: Au 10 nm, Ag 20 nm	Sub ng g^{-1} level for most elements	No single particles visible, only agglomerates	Only dry samples under vacuum condition, detection limit: few ppm	Only raman active molecules observable

[a] Abbreviations: TEM – transmission electron microscopy; EELS – electron energy loss spectroscopy; XRD – X-ray diffraction; SAXS – small angle X-ray scattering; SP-ICP-MS – single particle inductively coupled plasma mass spectrometry; ICP-MS – inductively coupled plasma mass spectrometry; ToF-SIMS – time of flight mass spectrometry; IBM – Ion beam microscopy; CRM – confocal Raman microscopy; BSA – bovine serum albumin; DMEM – Dulbecco's modified eagle medium; ppm – parts per million. [b] Data taken from (ref. 30).

mean that the effects will originate mainly from particles and not from Al ions. The application of an artificial digestion procedure for mimicking *in vivo* situation showed, that the particle dissolution and complexation behavior was quite different in all three studied gastrointestinal compartments.[24] After no significant changes in the saliva, the gastric environment leads to a significant increase of the dissolution rate as well as very strong agglomeration of NMs. The addition of intestinal fluid results in a nearly neutral pH value which leads to a decrease in the dissolution rate, a deagglomeration of particles and even *de novo* particle formation in ionic aluminum control.

Particle-CCM interactions

It is of major interest to evaluate the elemental and molecular changes on the particle surface during sample preparation for cell experiments (Fig. S8 and S9†). Additionally, two steps were chosen to investigate the surface modification of particles during the sample preparation process. Firstly, the NMs were dispersed. In this step, NMs were covered with albumin corona and are referred to as "BSA" in the text below. The second step was to investigate the NMs under cell culture conditions, diluted in DMEM. After each step, the particles were washed three times in Millipore water. The results of the element analysis, performed by IBM, are shown in Fig. 8.

The variation of the element content represents changes on the surface of NMs, *e.g.* attachment of amino acids, fatty acids, proteins and/or ions to the surface of the NMs. An increase in the Ca and P amount was observed for all studied NMs exposed to DMEM. The highest content of these elements was found in the case of Al NMs. It is suggested that calcium and phosphate ions interact strongly with the albumin corona of NMs and build a calcium phosphate layer on the particle surface. It is known that calcium phosphate has a high affinity to proteins and can increase the efficiency of uptake.[37,38]

The amount of sulfur on the NMs was analyzed under different conditions. Sulfur was found in association with proteins forming a corona around the NMs. Al and Al_2O_3 NMs acquire more proteins on their surface when exposed to DMEM as compared to dispersion in 0.05% BSA (Fig. S11†). In the case of Al and Al_2O_3, the proteins from the culture medium contribute to additional adsorption compared to the existing albumin corona of the particles alone. DMEM shows more physiologic relevant conditions. The salts might induce shielding effects on the protein, so the amount of proteins is likely to be increased. Due to the larger variety of available proteins, a more complex corona will self-assemble on the surface of the particles. In contrast, a decreased amount of proteins was found in the case of NM103 and 104 NMs exposed to DMEM. Substitution of the relatively dense BSA on the particle surface with less dense proteins from the culture media is suggested. This exchange of proteins has a stabilizing effect on TiO_2 NMs in DMEM and results in a strong decrease of aggregate size in DMEM media (Table 1). This finding is also supported by CRM investigations (Fig. S10†).

ToF-SIMS was used to image Al NMs and Al_2O_3 NMs as well as nanoparticle agglomerates in cell culture medium and to assess the chemical composition of the nanoparticle agglomerates. The analyses revealed nanoparticle-specific agglomerates, consisting of polyoxo-aluminum complexes, aluminum(III)–serine and amino acid aluminate complexes (leucine and phenylalanine aluminate). These complexes were not observed when ionic $AlCl_3$ was added to the cell culture medium. ToF-SIMS images revealed a rather homogenous agglomerate distribution with only a slight accumulation of Al NMs in certain areas (see yellow circles in Fig. 9, top) and aluminum(III)–serine and polyoxo-aluminum complexes in others (see green circles in Fig. 9, top). While the aluminates co-locate with both areas, aluminates can be found in regions with predominantly Al NMs and in areas with predominantly aluminum(III)–serine and polyoxo-aluminum. Fig. 9 shows the ToF-SIMS image for Al_2O_3 NMs (bottom). Larger agglomerate areas (green circles in Fig. 9, bottom), where aluminum(III)–serine and polyoxo-aluminum complexes were present in higher amounts, can be distinguished from areas with predominantly smaller nanoparticle agglomerates made of Al_2O_3 NMs (see purple circles in Fig. 9, bottom).

In DMEM with Al NMs, areas where predominantly Al NMs localize, depicted as yellow circles in Fig. 9, top, are distinct from areas where polyoxo-aluminum complexes and aluminum(III)–serine particles localize (green circles). Generally, smaller agglomerates of different chemical entities, Al NMs, aluminum(III)–serine, leucine aluminate, phenylalanine aluminate and polyoxo-aluminum complexes, which do not co-localize in the same area, were observed. In addition to areas where predominantly Al_2O_3 NMs (purple) localize, Al_2O_3 NMs in DMEM show a similar pattern with areas where all chemical entities co-localize but are clearly separated from each other. This indicates a starting mineralization of the larger agglomerates, where different chemical entities co-localize and form mixed agglomerates of Al_2O_3 NMs, amino acids and aluminum salts. Further agglomerate compositions and chemical entities were detected (Fig. S11–14†). For ToF-SIMS measurements for TiO_2 NM103 and 104 in DMEM see Fig. S15–18.†

Conclusions

An extensive characterization of NMs in their different states, from dispersion to *in vitro* conditions, should precede any toxicological testing. In this study, we have characterized two different types of NMs, one metal and one metal oxide. For this purpose, we used a wide range of complementary analytical techniques to characterize particle size, surface and composition in more detail. An in-depth insight into the dissolution, one of the most important determinants of NM toxicity, was achieved by investigation by the examples of Al^0 and Al_2O_3 NMs. A very low dissolution rate and a small percentage of ion release was observed at a neutral pH value, while higher rates for acidic environment we already reported earlier.[24] A significant difference between the surface and the extent of oxidation of Al^0 and Al_2O_3 NM forms was detected. In contrast to the fully oxidized Al_2O_3 with a rather homogenous distribution of Al and O atoms, Al^0 NM showed a core–shell structure with an oxide layer only a few nm thick. This was proven with XRD and the EELS technique, which emphasizes the benefit of using different techniques to get reliable results. It was demonstrated with the help of ToF-SIMS that both aluminum forms are subject to a surprisingly different complexation in biological media: while Al^0 NMs were shown to form complexes with amino acids, Al_2O_3 NMs mostly formed polyoxo-complexes out of two or more Al_2O_3 molecules. Based on the collected results, all of the investigation methods applied have their own benefits. Thus, with the methods described in this study focusing on size, surface and complex formation, dissolution investigations can perhaps become a bit more predictable. Right now, the recommended limit for aluminum release from food is 5 mg kg^{-1} food. The various aluminum forms, *e.g.* ions, micro- and nanomaterials, pure Al^0 or Al_2O_3, are not differentiated here. With this study, it becomes obvious that there should be differentiation for the different forms, as they may be taken up and react differently. For future analytical investigations on aluminum-containing NMs, we propose considering not only Al_2O_3 but also Al^0 NMs and their interaction with the corresponding ions.

Conflicts of interest

There are no conflicts to declare.

Acknowledgements

This French-German bilateral project SolNanoTOX was funded by the German Research Foundation (DFG, Project ID: DFG (FKZ LA 3411/1-1 and LA 1177/9-1)) and the French National Research Agency (ANR, Project ID: ANR-13-IS10-0005). The authors would like to thank Simone Rolf from the Federal Institute for Materials Research and Testing (BAM) for the XRD measurements, Claudia Kästner from BAM for the SAXS measurements and Dr Uwe Mühle from the Fraunhofer Institute for Ceramic Technologies and Systems (IKTS) for the TEM measurements with elemental information.

Notes and references

1 A. Moores and F. Goettmann, *New J. Chem.*, 2006, **30**, 1121–1132.
2 K. L. Kelly, E. Coronado, L. L. Zhao and G. C. Schatz, *J. Phys. Chem. B*, 2003, **107**, 668–677.
3 D. M. Brown, M. R. Wilson, W. MacNee, V. Stone and K. Donaldson, *Toxicol. Appl. Pharmacol.*, 2001, **175**, 191–199.
4 S. Hussain, S. Boland, A. Baeza-Squiban, R. Hamel, L. C. J. Thomassen, J. A. Martens, M. A. Billon-Galland, J. Fleury-Feith, F. Moisan, J. C. Pairon and F. Marano, *Toxicology*, 2009, **260**, 142–149.
5 Y. Zhang, N. Kohler and M. Q. Zhang, *Biomaterials*, 2002, **23**, 1553–1561.
6 A. Cockburn, R. Bradford, N. Buck, A. Constable, G. Edwards, B. Haber, P. Hepburn, J. Howlett, F. Kampers, C. Klein, M. Radomski, H. Stamm, S. Wijnhoven and T. Wildemann, *Food Chem. Toxicol.*, 2012, **50**, 2224–2242.
7 I. A. Rahman, P. Vejayakumaran, C. S. Sipaut, J. Ismail and C. K. Chee, *Mater. Chem. Phys.*, 2009, **114**, 328–332.

8 S. E. A. Gratton, P. A. Ropp, P. D. Pohlhaus, J. C. Luft, V. J. Madden, M. E. Napier and J. M. DeSimone, *Proc. Natl. Acad. Sci. U. S. A.*, 2008, **105**, 11613–11618.
9 Y. Zhou and M. Antonietti, *J. Am. Chem. Soc.*, 2003, **125**, 14960–14961.
10 S. K. Das, M. K. Bhunia and A. Bhaumik, *Dalton Trans.*, 2010, **39**, 4382–4390.
11 Z. Q. Sun, T. Liao, L. Y. Sheng, L. Z. Kou, J. H. Kim and S. X. Dou, *Chem.–Eur. J.*, 2016, **22**, 11357–11364.
12 X. N. Ren, L. Wu, J. Jin, J. Liu, Z. Y. Hu, Y. Li, T. Hasan, X. Y. Yang, G. Van Tendeloo and B. L. Su, *RSC Adv.*, 2016, **6**, 26856–26862.
13 M. Moreno-Horn and T. Gebel, *Crit. Rev. Toxicol.*, 2014, **44**, 849–875.
14 J. X. Wang, G. Q. Zhou, C. Y. Chen, H. W. Yu, T. C. Wang, Y. M. Ma, G. Jia, Y. X. Gao, B. Li, J. Sun, Y. F. Li, F. Jiao, Y. L. Zhao and Z. F. Chai, *Toxicol. Lett.*, 2007, **168**, 176–185.
15 E. J. Park, H. Kim, Y. Kim and K. Choi, *Toxicol. Environ. Chem.*, 2011, **93**, 120–133.
16 Y. R. Kim, S. Y. Lee, E. J. Lee, S. H. Park, N. W. Seong, H. S. Seo, S. S. Shin, S. J. Kim, E. H. Meang, M. K. Park, M. S. Kim, C. S. Kim, S. K. Kim, S. W. Son, Y. R. Seo, B. H. Kang, B. S. Han, S. S. Aan, B. J. Lee and M. K. Kim, *Int. J. Nanomed.*, 2014, **9**, 67–78.
17 K. Loeschner, N. Hadrup, K. Qvortrup, A. Larsen, X. Y. Gao, U. Vogel, A. Mortensen, H. R. Lam and E. H. Larsen, *Part. Fibre Toxicol.*, 2011, **8**, 18.
18 J. H. E. Arts, M. Hadi, A. M. Keene, R. Kreiling, D. Lyon, M. Maier, K. Michel, T. Petry, U. G. Sauer, D. Warheit, K. Wiench and R. Landsiedel, *Regul. Toxicol. Pharmacol.*, 2014, **70**, 492–506.
19 A. R. Collins, B. Annangi, L. Rubio, R. Marcos, M. Dorn, C. Merker, I. Estrela-Lopis, M. R. Cimpan, M. Ibrahim, E. Cimpan, M. Ostermann, A. Sauter, N. E. Yamani, S. Shaposhnikov, S. Chevillard, V. Paget, R. Grall, J. Delic, F. G. de-Cerio, B. Suarez-Merino, V. Fessard, K. N. Hogeveen, L. M. Fjellsbo, E. R. Pran, T. Brzicova, J. Topinka, M. J. Silva, P. E. Leite, A. R. Ribeiro, J. M. Granjeiro, R. Grafstrom, A. Prina-Mello and M. Dusinska, *Wiley Interdiscip. Rev.: Nanomed. Nanobiotechnol.*, 2017, **9**, e1413.
20 P. Laux, C. Riebeling, A. M. Booth, J. D. Brain, J. Brunner, C. Cerrillo, O. Creutzenberg, I. Estrela-Lopis, T. Gebel, G. Johanson, H. Jungnickel, H. Kock, J. Tentschert, A. Tlili, A. Schäffer, A. J. A. M. Sips, R. A. Yokel and A. Luch, *NanoImpact*, 2017, **6**, 69–80.
21 J. M. Cohen, J. G. Teeguarden and P. Demokritou, *Part. Fibre Toxicol.*, 2014, **11**, 20.
22 S. Dekkers, A. G. Oomen, E. A. J. Bleeker, R. J. Vandebriel, C. Micheletti, J. Cabellos, G. Janer, N. Fuentes, S. Vazquez-Campos, T. Borges, M. J. Silva, A. Prina-Mello, D. Movia, F. Nesslany, A. R. Ribeiro, P. E. Leite, M. Groenewold, F. R. Cassee, A. J. A. M. Sips, A. Dijkzeul, T. van Teunenbroek and S. W. P. Wijnhoven, *Regul. Toxicol. Pharmacol.*, 2016, **80**, 46–59.
23 A. D. Maynard, R. J. Aitken, T. Butz, V. Colvin, K. Donaldson, G. Oberdorster, M. A. Philbert, J. Ryan, A. Seaton, V. Stone, S. S. Tinkle, L. Tran, N. J. Walker and D. B. Warheit, *Nature*, 2006, **444**, 267–269.
24 H. Sieg, C. Kastner, B. Krause, T. Meyer, A. Burel, L. Bohmert, D. Lichtenstein, H. Jungnickel, J. Tentschert, P. Laux, A. Braeuning, I. Estrela-Lopis, F. Gauffre, V. Fessard, J. Meijer, A. Luch, A. F. Thunemann and A. Lampen, *Langmuir*, 2017, **33**, 10726–10735.
25 J. M. Zook, S. E. Long, D. Cleveland, C. L. A. Geronimo and R. I. MacCuspie, *Anal. Bioanal. Chem.*, 2011, **401**, 1993–2002.
26 K. Loza, J. Diendorf, C. Sengstock, L. Ruiz-Gonzalez, J. M. Gonzalez-Calbet, M. Vallet-Regi, M. Koller and M. Epple, *J. Mater. Chem. B*, 2014, **2**, 1634–1643.
27 Z. Y. Wang, A. von dem Bussche, P. K. Kabadi, A. B. Kane and R. H. Hurt, *ACS Nano*, 2013, **7**, 8715–8727.
28 A. M. Tavares, H. Louro, S. Antunes, S. Quarre, S. Simar, P. J. De Temmerman, E. Verleysen, J. Mast, K. A. Jensen, H. Norppa, F. Nesslany and M. J. Silva, *Toxicol. in Vitro*, 2014, **28**, 60–69.
29 H. E. Pace, N. J. Rogers, C. Jarolimek, V. A. Coleman, C. P. Higgins and J. F. Ranville, *Anal. Chem.*, 2011, **83**, 9361–9369.
30 K. Rasmussen, J. Mast, P. J. de Temmerman, E. Verleysen, N. Wegeneers, F. van Steen, J. C. Pizzolon, L. de Temmerman, E. van Doren, K. A. Jensen, R. Birkedal, M. Levin, S. H. Nielsen, I. K. Koponen, P. A. Clausen, V. Kofored-Sørensen, Y. Kembouche, N. Thieriet, O. Spalla, C. Giuot, D. Rousset, O. Witschger, S. Bau, B. Bianchi, C. Motzkus, B. Shivachev, L. Dimowa, R. Nikolova, D. Nihtianova, M. Tarassov, O. Petrov, S. Bakardjieva, D. Gilliland, F. Pianella, G. Ceccone, V. Spampinato, G. Cotogno, P. Gibson, C. Gaillard and A. Mech, JRC Science and Policy Reports, 2014, http://publications.jrc.ec.europa.eu/repository/handle/JRC86291.
31 M. Naiim, A. Boualem, C. Ferre, M. Jabloun, A. Jalocha and P. Ravier, *Soft Matter*, 2015, **11**, 28–32.
32 P. A. Hassan and S. K. Kulshreshtha, *J. Colloid Interface Sci.*, 2006, **300**, 744–748.
33 R. D. Deegan, O. Bakajin, T. F. Dupont, G. Huber, S. R. Nagel and T. A. Witten, *Nature*, 1997, **389**, 827–829.
34 P. J. De Temmerman, E. Van Doren, E. Verleysen, Y. Van der Stede, M. A. D. Francisco and J. Mast, *J. Nanobiotechnol.*, 2012, **10**, 24.
35 P. Muneesawang and C. Sirisathitkul, *J. Nanomater.*, 2015, **2015**, 8.
36 R. J. Griffitt, A. Feswick, R. Weil, K. Hyndman, P. Carpinone, K. Powers, N. D. Denslow and D. S. Barber, *Environ. Toxicol.*, 2011, **26**, 541–551.
37 T. T. Morgan, H. S. Muddana, E. I. Altinoglu, S. M. Rouse, A. Tabakovic, T. Tabouillot, T. J. Russin, S. S. Shanmugavelandy, P. J. Butler, P. C. Eklund, J. K. Yun, M. Kester and J. H. Adair, *Nano Lett.*, 2008, **8**, 4108–4115.
38 G. Dordelmann, D. Kozlova, S. Karczewski, R. Lizio, S. Knauer and M. Epple, *J. Mater. Chem. B*, 2014, **2**, 7250–7259.
39 S. Lee, X. Y. Bi, R. B. Reed, J. F. Ranville, P. Herckes and P. Westerhoff, *Environ. Sci. Technol.*, 2014, **48**, 10291–10300.

3.2 Impact of an Artificial Digestion Procedure on Aluminum-Containing Nanomaterials

Holger Sieg, Claudia Kästner, Benjamin Krause, Thomas Meyer, Agnès Burel, Linda Böhmert*, Dajana Lichtenstein, Harald Jungnickel, Jutta Tentschert, Peter Laux, Albert Braeuning, Irina Estrela-Lopis, Fabienne Gauffre, Valérie Fessard, Jan Meijer, Andreas Luch, Andreas F. Thünemann and Alfonso Lampen

*Corresponding author

This chapter was published online on 13 September 2017 in:

Langmuir 2017, 33, 40, 10726–10735

DOI: doi: 10.1021/acs.langmuir.7b02729

Link: https://doi.org/10.1021/acs.langmuir.7b02729

Involvement of the author within this publication: Project planning (25%), project execution (40%), data analysis (30%), writing of the manuscript (20%).

The supplementary material of the publication can be found in Annex II.

LANGMUIR

Article

pubs.acs.org/Langmuir

Impact of an Artificial Digestion Procedure on Aluminum-Containing Nanomaterials

Holger Sieg,[†] Claudia Kästner,[§] Benjamin Krause,[‡] Thomas Meyer,[∥] Agnès Burel,[⊥] Linda Böhmert,*[,†] Dajana Lichtenstein,[†] Harald Jungnickel,[‡] Jutta Tentschert,[‡] Peter Laux,[‡] Albert Braeuning,[†] Irina Estrela-Lopis,[∥] Fabienne Gauffre,[⊥] Valérie Fessard,[#] Jan Meijer,[▽] Andreas Luch,[‡] Andreas F. Thünemann,[§] and Alfonso Lampen[†]

[†]German Federal Institute for Risk Assessment, Department of Food Safety, Max-Dohrn-Straße 8-10, 10589 Berlin, Germany

[‡]German Federal Institute for Risk Assessment, Department of Chemical and Product Safety, Max-Dohrn-Straße 8-10, 10589 Berlin, Germany

[§]Bundesanstalt für Materialforschung und -prüfung (BAM), Unter den Eichen 87, 12205 Berlin, Germany

[∥]Institute of Medical Physics and Biophysics, Leipzig University, Härtelstrasse 16-18, 04275 Leipzig, Germany

[⊥]Institut des Sciences Chimiques de Rennes, UMR-CNRS 6226, Université de Rennes, 35700 Rennes, France

[#]Fougères Laboratory, Toxicology of contaminants unit, ANSES, French Agency for Food, Environmental and Occupational Health and Safety, 10B rue Claude Bourgelat, 35306 Cedex, Fougères, France

[▽]Felix Bloch Institute for Solid State Physics, Leipzig University, Linnéstraße 5, 04103 Leipzig, Germany

Supporting Information

ABSTRACT: Aluminum has gathered toxicological attention based on relevant human exposure and its suspected hazardous potential. Nanoparticles from food supplements or food contact materials may reach the human gastrointestinal tract. Here, we monitored the physicochemical fate of aluminum-containing nanoparticles and aluminum ions when passaging an in vitro model of the human gastrointestinal tract. Small-angle X-ray scattering (SAXS), transmission electron microscopy (TEM), ion beam microscopy (IBM), secondary ion beam mass spectrometry (TOF-SIMS), and inductively coupled plasma mass spectrometry (ICP-MS) in the single-particle mode were employed to characterize two aluminum-containing nanomaterials with different particle core materials (Al^0, γAl_2O_3) and soluble $AlCl_3$. Particle size and shape remained unchanged in saliva, whereas strong agglomeration of both aluminum nanoparticle species was observed at low pH in gastric fluid together with an increased ion release. The levels of free aluminum ions decreased in intestinal fluid and the particles deagglomerated, thus liberating primary particles again. Dissolution of nanoparticles was limited and substantial changes of their shape and size were not detected. The amounts of particle-associated phosphorus, chlorine, potassium, and calcium increased in intestinal fluid, as compared to nanoparticles in standard dispersion. Interestingly, nanoparticles were found in the intestinal fluid after addition of ionic aluminum. We provide a comprehensive characterization of the fate of aluminum nanoparticles in simulated gastrointestinal fluids, demonstrating that orally ingested nanoparticles probably reach the intestinal epithelium. The balance between dissolution and de novo complex formation should be considered when evaluating nanotoxicological experiments.

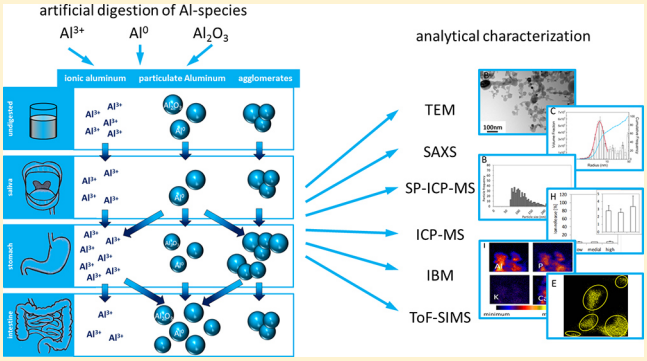

INTRODUCTION

Aluminum is the most common metal in the biosphere and therefore ubiquitously present in food and consumer products.[1] However, no essential physiological role of aluminum is known, possibly due to its inflexible trivalent oxidation state and its relatively low reactivity.[2,3] Most aluminum on earth is bound in minerals that are in a chemically inactive state.[4] In the last two centuries, more and more aluminum has been transferred into the metallic and the more reactive ionic form, in the course of industrial activities and environmental acidification.[5,6] Activation of aluminum seems to be triggered by an acidic pH.[4] Chronic exposure to aluminum can be harmful for certain groups of people, for example, for those with renal dysfunction.[7] The suspected hazardous potential of aluminum on human health recently increased public attention on this topic, as a correlation between the use of aluminum-containing

Received: August 4, 2017
Revised: September 13, 2017
Published: September 13, 2017

DOI: 10.1021/acs.langmuir.7b02729
Langmuir 2017, 33, 10726−10735

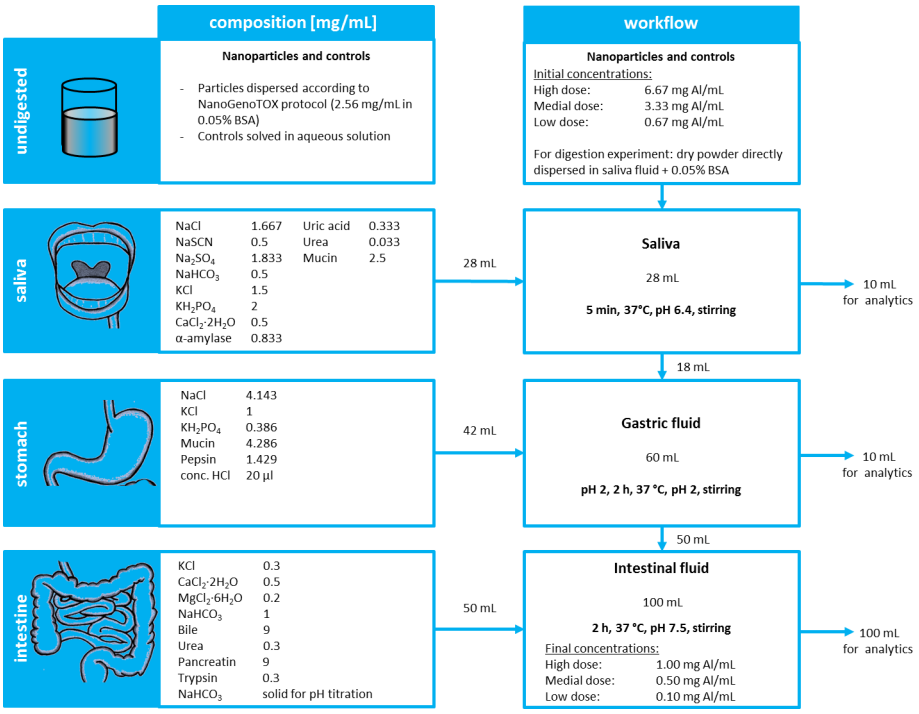

Figure 1. Scheme of particle dispersion and in vitro digestion including the composition of digestion fluids, experimental workflow, and nanoparticle concentrations.

products and Alzheimer's disease or breast cancer has been proposed.[8,9]

Oral ingestion is an important uptake route for aluminum. Exposure might result from natural sources, such as drinking water, but also from food additives, packaging, and kitchenware.[3] The use of aluminum-containing packaging, consumer products, and kitchenware has increased,[10] as well as the use of chemical solvents, leaches, and acids. Several metal species are present in a significant amount in food as nanoscaled particles[11,12] and migrate into food from packaging material.[13−15] Like other orally ingested metals, aluminum passes the different compartments of the human digestion tract. During this process, the chemical environment changes remarkably, from mouth to stomach and intestine, with regard to shifts in pH as well as to the presence of a complex mixture of salts, proteins, and intestinal bile acids with surface-active properties. The changing environment may modify aluminum nanoparticles, resulting in dissolution, agglomeration, or deagglomeration, and thereby affect intestinal uptake of the metal. Gastrointestinal metal uptake differs significantly between dissolved ions and nanoparticles, depending on their size, shape, and physicochemical properties.[16] These properties include surface coating, protein corona composition, and the biological environment.[17] Therefore, it is crucial to characterize nanoparticles under realistic conditions.

To mimic these conditions, different modifications of physiologically buffered fluids have been applied in research, with some of them using buffered solutions with only pH changes,[18] while others use more complex systems which include salts, digestion enzymes, proteins, or even other food components.[19,20] Such high-complexity models are appropriate to monitor changes in the physicochemical characteristics of metallic nanoparticles and also enable detailed studies on the toxicological potential of particles following intestinal digestion.[21]

The chemical state of aluminum is an important factor for its toxicological potential. This study focuses on the fate and behavior of different aluminum species during the digestion process after oral uptake. Therefore, three different aluminum species were used which represent soluble ionic aluminum ($AlCl_3$), elementary metallic aluminum (Al^0), and mineral oxidized aluminum (Al_2O_3). These three representative aluminum entities were analyzed separately in a complex artificial digestion system consisting of three steps, namely saliva, gastric juice, and intestinal juice. Differences in ionic content, particle size, shape, element attachment, agglomeration state, and stability were investigated using elemental analysis, small-angle X-ray scattering (SAXS), transmission electron microscopy (TEM), single particle inductively coupled plasma mass spectrometry (SP-ICP-MS), ion beam microscopy (IBM), and time-of-flight secondary ion mass spectrometry (ToF-SIMS).

EXPERIMENTAL SECTION

Chemicals and Nanoparticles. Chemicals were purchased from Sigma-Aldrich (Taufkirchen, Germany), Merck (Darmstadt, Germany), or Carl Roth (Karlsruhe, Germany) in the highest available purity.

Nanomaterials (Al^0-core surface-passivated nanoparticles and γ-Al_2O_3 nanoparticles) were supplied by IoLiTec (Heilbron, Germany). Al^0 nanoparticles were stored and weighted under an argon atmosphere. Both particles were freshly dispersed at a concentration of 2.56 mg/mL according to the modified NanoGenoTOX protocol (ultrasonication applying an energy of 1176 kJ/mL dispersion using an acoustic power of 7.35 W), stabilized by 0.05% BSA/water before use. BSA was supplied by Carl Roth (Albumin Fraction V, ≥98%) and $AlCl_3$ was supplied by Sigma-Aldrich (Hexahydrate, ≥97%).

Artificial in Vitro Digestion. Artificial in vitro digestion was originally based on DIN ISO 19738 and distinctly modified for scientific investigations on metals, metallic nanoparticles,[19−24] and other nanoparticles and biopolymers.[25,26] As depicted in Figure 1, the artificial in vitro digestion consists of three steps with the indicated

DOI: 10.1021/acs.langmuir.7b02729
Langmuir 2017, 33, 10726−10735

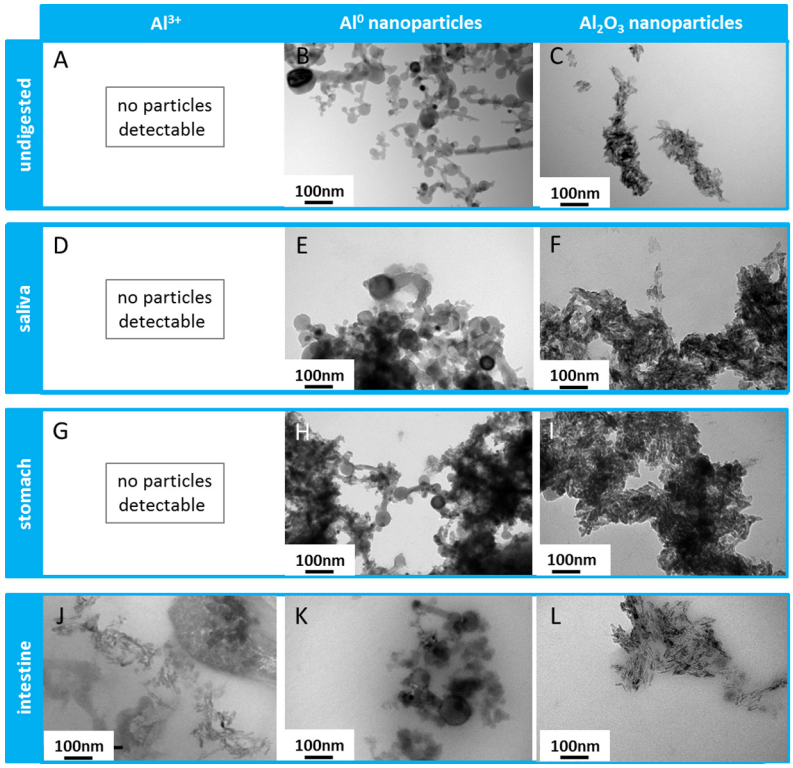

Figure 2. Representative TEM pictures of aluminum-containing samples after standard dispersion (A–C), in artificial saliva (D–F), gastric fluid (G–I), and intestinal fluid (J–L). The sample concentration applied to the grid was 0.8 g/L. $AlCl_3$-containing samples showed no measurable particles in stock, saliva, and gastric fluid. Representative images are depicted.

compositions. Before starting the digestion process, nanomaterials were freshly dispersed via ultrasonication in saliva and 0.05% BSA, prior to addition of digestion enzymes. As a control, ionic aluminum ($AlCl_3$) was used in the same concentration ranges and treated accordingly. Then, 28 mL of synthetic saliva with the corresponding samples was heated to 37 °C in a water bath and stirred for 5 min. Subsequently, a 10 mL sample was taken for further analysis, 42 mL of artificial gastric juice was added to the solution, and the pH value was adjusted to 2 using hydrochloric acid. The solution was stirred for 2 h at 37 °C, and the pH value was checked every 30 min. Prior to the following digestion step, a 10 mL sample was taken for further analysis. Then, 50 mL of artificial intestinal juice were added, the pH value was set to 7.5 by adding sodium bicarbonate powder to the reaction solution, and the solution was stirred for 2 h. Subsequently, intestinal samples were taken for further analysis.

The activity of the digestion enzymes was verified prior to every set of experiments for each step of the digestion process using model substrates of the respective enzymes: amylase activity was confirmed using amylopectin azure, pepsin activity by using an albumin/bromophenol blue complex, tryptic activity by using azocasein, and lipase activity by using 4-methylumbelliferyl oleate. All resulting cleavage products were monitored photometrically.

Transmission Electron Microscopy (TEM). A drop of each, digested or undigested, sample was placed on a Formvar carbon-coated 300 mesh grid for 20 s for adsorption. Excess fluid was wiped off using a filter paper before grids were air-dried. All grids were examined with a JEOL 1400 transmission electron microscope (JEOL, Peabody, MA) operated at 120 kV and supplied with a GATAN Orius 1000 camera (GATAN Inc., Pleasanton, CA).

Small-Angle X-ray Scattering (SAXS). SAXS measurements were conducted in a flow-through capillary with a Kratky-type instrument (SAXSess from Anton Paar AG, Graz, Austria) at 21 ± 1 °C. The SAXSess has a low sample–detector-distance of 0.309 m which is appropriate for the investigation of dispersions with low scattering intensities. The experiments were performed with 120 measurement cycles (each averaged over 10 s). The measurements were background-corrected with the respective mixture of aqueous BSA solution or digestive juices without addition of aluminum species. Deconvolution (slit length desmearing) of the SAXS curves was performed with the SAXS-Quant software (Anton Paar AG). Samples analyzed with SAXS were used as prepared. Curve fitting was performed with the software McSAS (Monte Carlo method, version 1.0.1). This procedure has been described before.[27]

Single-Particle Inductively Coupled Plasma Mass Spectrometry (SP-ICP-MS). For single particle analysis of the nanoparticle solutions a quadrupole ICP-MS (Thermo Scientific iCAP Q, Thermo Fisher Scientific GmbH, Dreieich, Germany) with a PFA ST Nebulizer, a quartz cyclonic spray chamber and a 2.5 mm quartz O-ring-free injector (all from ESI Elemental Service & Instruments GmbH, Mainz, Germany) was used. Using the time-resolved analysis mode for data acquisition, intensities as a function of time (counts per dwell-time interval) were collected. The acquisition time for each run was set to 60 s with a dwell time (or data acquisition rate) of 3 ms. The gas flow for the plasma, the nebulizer, and the auxiliary (all Ar) was set to 13, 0.89, and 0.7 L/min. The flow rate of the sample was 0.34 mL/min. Data were exported to a spreadsheet developed by RIKILT (Imperial Quality Control of Agricultural and Horticultural Products for further processing, University of Wageningen, The Netherlands). For data processing, an established procedure according to Pace et al.[28] was followed. Determination of nebulizer efficiency was performed according to the described method with reference nanoparticles of known particle size. Here 60 nm gold reference nanoparticles from the U.S. National Institute of Standards and Technology (NIST, RM 8013) were used as reference nanoparticles.

Ion Beam Microscopy (IBM). IBM experiments were performed at LIPSION© nanoprobe. The singletron particle accelerator was used to apply a 2.25 MeV proton beam according to a previously described protocol.[29] To avoid interactions between the ion beam and air molecules a vacuum with a pressure of 5×10^{-5} and 10^{-7} Torr was applied. By focusing the beam, a spatial resolution of around 1 μm was reached. For element analysis we used the X-ray fluorescence technique μ proton-induced X-ray emission (μPIXE) and

DOI: 10.1021/acs.langmuir.7b02729
Langmuir 2017, 33, 10726–10735

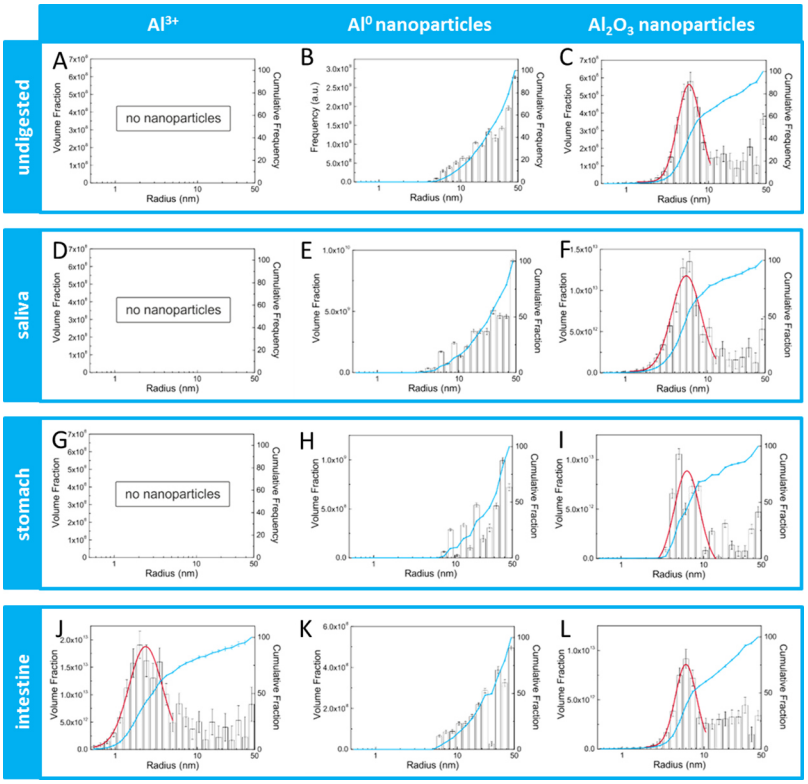

Figure 3. Volume-weighted size distributions, as derived by SAXS measurements. Samples containing Al^0 nanoparticles, Al_2O_3 nanoparticles, or $AlCl_3$ were analyzed after standard dispersion (A–C), in artificial saliva (D–F), gastric fluid (G–I), and intestinal fluid (J–L). The distributions of undigested stock solutions and digested Al^0 nanoparticles, Al_2O_3 nanoparticles, and $AlCl_3$ in their highest concentration are given (6.67 mg Al/mL at the beginning of the digestion process in saliva, and a final conecentration of 1 mg Al/mL in intestinal fluid). $AlCl_3$-containing samples showed no measurable particles in stock solution, saliva, and gastric fluid. The right-hand *y*-axes mark the cumulative particle fraction given in blue solid lines. The size distributions are fitted by a log-normal distribution function (red solid lines).

μ Rutherford Backscattering spectroscopy (μRBS). Detection of μPIXE signals was done by using a High Purity Germanium crystal detector (Canberra, Meriden, CT). A 60 μm polyethylene layer was used to cover the detector for backscattered protons. A Canberra PIPS-detector was used to detect the μRBS signal. For element analysis, the standard dispersion as well as gastric fluid was investigated. The concentration of the nanoparticles in the digestion fluid was set to 1000 μg aluminum/mL. Samples were prepared for measurements by centrifugation at 8000*g* for 10 min. Afterward, the supernatant was removed and replaced by mpH_2O followed by vortexing of the sample. This procedure was repeated three times. Finally, a small drop of the dispersion was placed on polypropylene foil and the liquid was vaporized.

Time of Flight Secondary Ion Mass Spectrometry (ToF-SIMS). Volumes of 10 μL of digested samples were dropped on gold wafers and air-dried. Ion images and spectra were acquired as described before[30] using a ToF-SIMS V instrument (ION-TOF GmbH, Münster, Germany) with a 30 keV nano-bismuth primary ion beam source $(Bi)x^{(y+)}$-cluster ion source with a BiMn emitter). The ion currents were 0.5 pA at 5 kHz using a Faraday cup. A pulse of 0.7 ns from the bunching system resulted in a mass resolution that usually exceeded 9000 (full width at half-maximum) at $m/z < 500$ in positive ion mode. The primary ion dose was controlled below 10^{12} ions cm^{-2} to ensure static SIMS conditions. Charge compensation on the sample was obtained by a pulsed electron flood gun with 20 eV electrons.

The primary ion gun scanned a field of view of 80 μm × 80 μm applying a 512 × 512 pixel measurement raster. Once the primary ion gun was aligned, a ToF-SIMS mass spectrum was generated by summing the detected secondary ion intensities and plotting them against the mass channels. The data were evaluated using the Surface Lab software (ION-TOF GmbH, Münster, Germany).

Ion Release Measurements. Ion release of nanoparticles in stock dispersions and digestion fluids was determined by ultracentrifugation (100 000*g* for 1 h at 4 °C) followed by acidic hydrolysis of the supernatant (69% HNO_3, 180 °C for 20 min in an MLS-ETHOS Microwave system), and element analysis was conducted using a quadrupole ICP-MS (Thermo Scientific iCAP Q, Thermo Fisher Scientific GmbH) comparable to previous studies.[31] LOD and LOQ for Al were determined as 0.6 and 1.8 ppb, respectively. Results are given as percentile of the initially used amount of aluminum.

RESULTS AND DISCUSSION

Aluminum is one of the most abundant metals on earth, occurs in our food and is therefore also taken up orally. The chemical state of aluminum is an important factor for its bioavailability and toxicological potential.[3,32] Therefore, this study focused on the behavior of different aluminum species during the digestion process after oral uptake. Three different aluminum species were used, which represent elementary metallic aluminum, mineral oxidized aluminum, and completely dissolved ionic aluminum. These three representative substances vary strongly in their physicochemical properties including reactivity, solubility and bioavailability[2,33] and therefore were analyzed stepwise throughout the digestion procedure (before digestion, in saliva, stomach fluid, and intestinal fluid). Each step is characterized by a typical composition of buffer, salts, protein components and pH value. Differences in ionic aluminum content, aluminum particle size, shape, element attachment, agglomeration, and stability were analyzed using complementary techniques, namely, element analysis, SAXS, TEM, SP-ICP-MS, ToF-SIMS, and IBM.

DOI: 10.1021/acs.langmuir.7b02729
Langmuir 2017, 33, 10726–10735

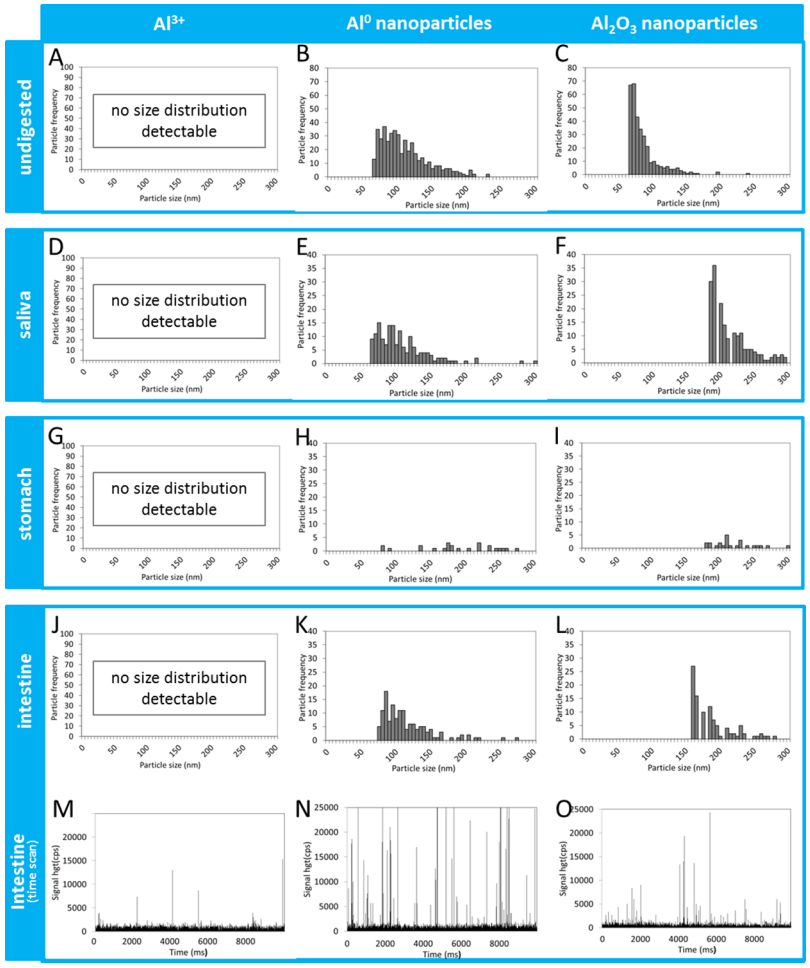

Figure 4. Number-weighted size-distributions of aluminum samples after standard dispersion (A–C), in artificial saliva (D–F), gastric fluid (G–I), and intestinal fluid (J–L). Representative images and size distributions are calculated from 60 s measuring time each run. For intestinal samples, the time scan is shown, too (M–O). The number of measurable particles in $AlCl_3$-containing samples was too low to calculate a size distribution.

Shape of the Nanoparticles. TEM analysis of undigested nanoparticles in Figure 2 shows polydisperse spherical particles with diameters between 10 and 100 nm with prominent fingerlike outgrowths for Al^0, and needlelike nanoparticles of about 5 × 30 nm^2 size in loosely packed agglomerates for Al_2O_3. No particles were detectable in $AlCl_3$ solution. During the digestion process both nanoparticle species appeared to agglomerate and to be surrounded by organic material, while their size ranges had not substantially changed. However, it has to be kept in mind that preparation for TEM analysis may cause agglomeration due to the necessary drying step. Deagglomeration was observed in intestinal fluid. For aluminum ions, nanoparticle-like structures with different densities were observed in intestinal fluid. These were not detectable in undigested samples, saliva, or gastric fluid.

Size Distribution and Agglomeration of the Nanoparticles. SAXS results are shown in Figure 3 and Supporting Information Figure 1. The two nanoparticle species displayed different agglomeration characteristics in undigested dispersion. Elementary Al^0 nanoparticles displayed a broad size distribution with primary particle radii ≥ 8 nm. In contrast, Al_2O_3 nanoparticles showed a narrower size distribution of primary particles with core radii between 5 and 10 nm (Figure 3B,C). Populations with higher radii resulted from agglomerates and aggregates of these primary particles, as proven by TEM (Figure 2). These species represented either aluminum nanoparticles or Al_2O_3-nanoparticles depending on the nanoparticle species used, as proven by ToF-SIMS (see Figure 6). Aluminum ions formed no detectable particles in undigested stocks. In comparison to the undigested dispersions, the SAXS core radii for both aluminum species did not change notably by the transfer into saliva (Figure 3E,F). Also, no nanoparticles were detected for ionic aluminum samples (Figure 3D). In contrast to the saliva, the next steps of the digestion procedure strongly influenced the agglomeration behavior of the nanoparticles. Especially in gastric juice at low pH, SAXS measurements showed an increased mean radius (Supporting Information Figure 1). This effect was most prominent at the lowest concentration of Al_2O_3 nanoparticles. The next digestion step, the intestine, implies a pH shift to 7.5. Deagglomeration occurred in the intestinal fluid, which resulted in primary particles in the nanoscaled range. The determined core radii were in the range of the original state of the particles, as found in the saliva. Surprisingly, the ionic aluminum samples also showed detectable nanoscaled particles in the last step of the digestion process (Figure 3J) which could be attributed to aluminum particles using ToF-SIMS analysis (see Figure 6G).

As a second method to determine particle size distributions, SP-ICP-MS measurements were performed (Figure 4). Both particles species tended to stay unaffected in the saliva while in

DOI: 10.1021/acs.langmuir.7b02729
Langmuir 2017, 33, 10726–10735

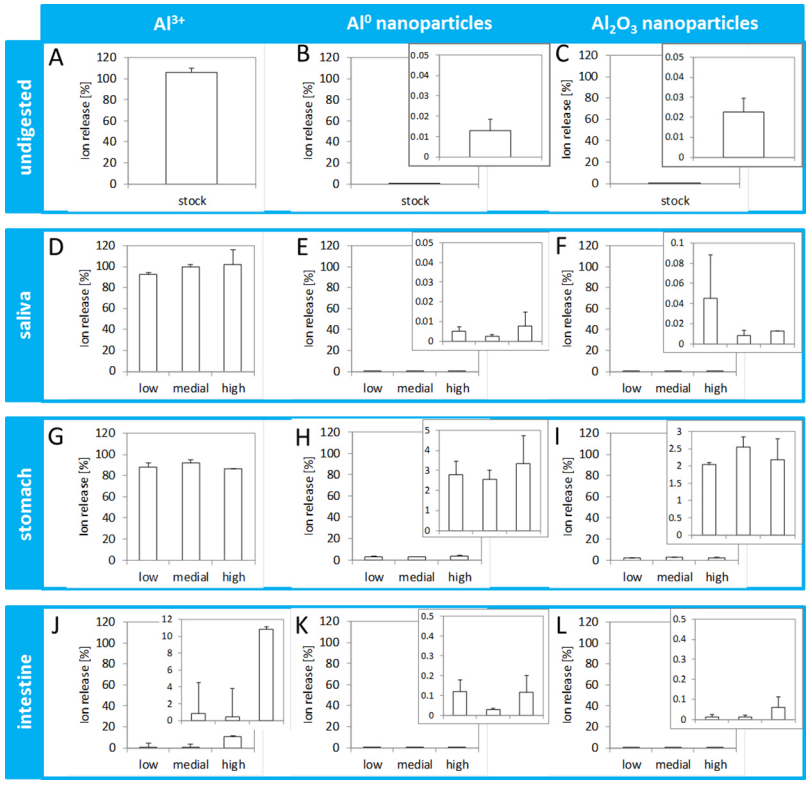

Figure 5. Determination of free aluminum ions in aluminum-containing samples after standard dispersion (A–C), in artificial saliva (D–F), gastric fluid (G–I), and intestinal fluid (J–L). Quantification of the ionic fraction is given, as determined by UC followed by nitric acid digestion and ICP-MS. Each sample was processed in duplicate and measured twice. Error bars show the standard deviation of the mean values.

the stomach only a small fraction of nanoparticles still remained in the nanoscaled range. Especially for Al_2O_3 nanoparticles, the data indicate very high diameters that derive from agglomeration in every artificial fluid. The lower limit of the SP-ICP-MS, based on the particle mass, is directly dependent on the particle density, which leads to a particle-specific cutoff diameter. In digested Al_2O_3 samples, there were no primary particles visible up to 200 nm. This may be due to nonspherical particles and the resulting agglomerates, which was confirmed by TEM measurements (Figure 2). As a second reason, this can result from the complex medium that impedes mathematical calculation. Up to now, based on the used mathematical algorithm for SP-ICP-MS, reliable size determination is limited to spherical entities. Given the analytical background of aluminum as a consequence of the ubiquitous presence of this element, the limit of detection is higher as compared to rare elements, e.g. gold. On the other hand, de novo emerged nanoscaled particles formed from $AlCl_3$ could not be proven by this method. Some signals were present in the time scan which, however, did not lead to calculable size distributions.

Ion Release of the Nanoparticles. The free ionic fraction of aluminum was separated by centrifugation from the particulate and matrix-bound aluminum fraction and analyzed via ICP-MS after acidic hydrolysis (Figure 5). As shown in Figure 5B,C, both particle species displayed a very low intrinsic ion release below 0.03% in undigested dispersion. Similar values were obtained for the ionic content in saliva (Figure 5E,F). In gastric media (Figure 5H,I), metallic Al^0 nanoparticles released slightly more ions, whereas Al_2O_3 nanoparticles appeared to be more inert in terms of solubility. In intestinal fluid, free ions disappeared almost completely. Ion controls showed almost 100% free ions in stocks, saliva, and gastric fluid (Figure 5A,D,G), while there was a pronounced decrease of free ions in the intestinal fluid (Figure 5J). This matches well with the TEM data and SAXS spectra showing particle formation from dissolved aluminum (Figures 2 and 3).

Element Distribution of Aluminum: Time of Flight Secondary Ion Mass Spectrometry (TOF-SIMS). ToF-SIMS results are shown in Figure 6. No pronounced agglomeration was found in saliva samples (Figure 6B,C),

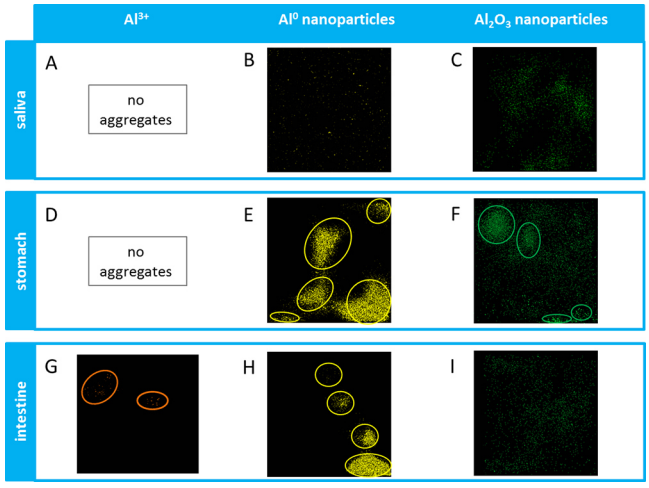

Figure 6. Representative ToF-SIMS images of aluminum-containing samples in artificial saliva (A–C), gastric fluid (D–F), and intestinal fluid (G–I). $AlCl_3$-containing samples showed no measurable particles in saliva and gastric fluid. Densitograms show local agglomerations of measured aluminum species, indicated by colored circles.

DOI: 10.1021/acs.langmuir.7b02729
Langmuir 2017, 33, 10726–10735

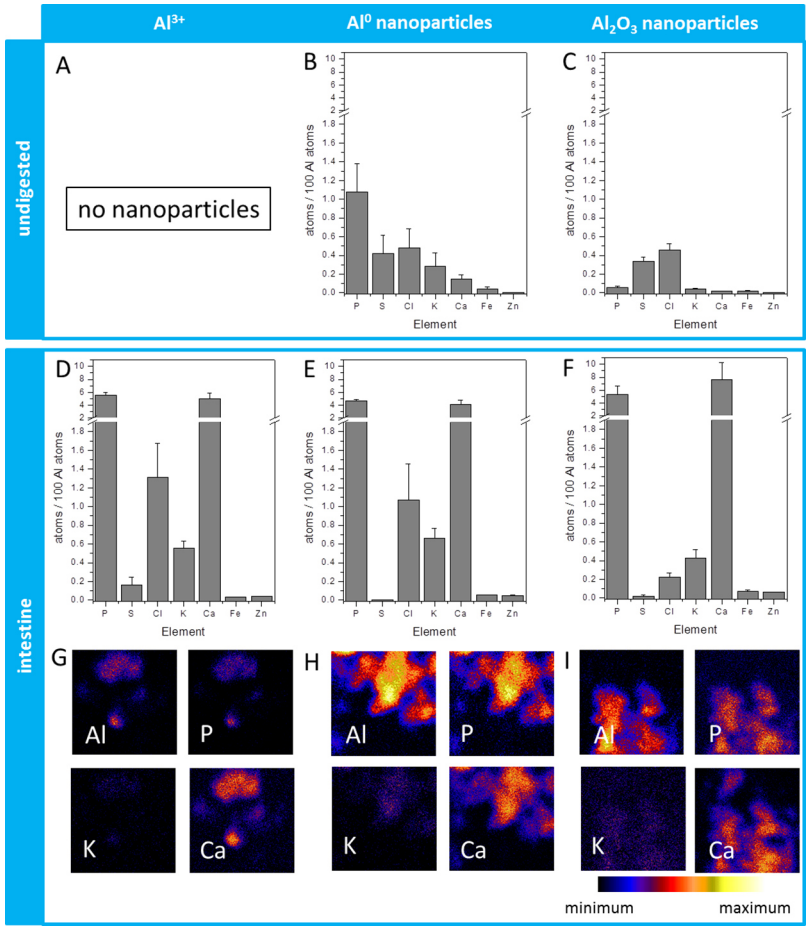

Figure 7. Impact of digestion on surface modification of aluminum nanoparticles. (A–F) Element analysis of Al, of Al_2O_3, and de novo-emerged particles resulting from $AlCl_3$. Samples were prepared from standard dispersion (A–C) as well as from intestinal fluid after the full artificial digestion protocol (D–F). Each sample was measured at least three times on different positions. Error bars represent the standard deviation of the mean values. (G–I) μPIXE images of element distributions in aluminum species after the artificial digestion process. All images display an area of 25 × 25 μm^2. The color code is as follows: minimal concentration is displayed in black, while maximum is shown in white.

whereas we determined strong agglomeration spots in the stomach fluid, as indicated by colored circles (Figure 6E,F). For Al_2O_3 nanoparticles, these intense spots disappeared in the intestine, while strong agglomerated spots were still present for the metallic Al^0 nanoparticles (Figure 6H,I). We could not detect aluminum-containing spots in the $AlCl_3$ samples in saliva and stomach fluid, while there were some measurable accumulation spots of aluminum in the intestine fluid which, however, appeared much weaker than in the nanoparticle samples (Figure 6G).

Elements Associated with Aluminum. IBM measurements were used for the analysis of elements associated with the aluminum nanoparticles (Figure 7). We investigated undigested nanoparticle samples as well as digested particles and ionic samples in the intestinal fluid after artificial digestion. μPIXE images visualize the location of aluminum particles and colocalization of the elements P, K, and Ca with Al (Figure 7). The amount of colocalized elements for particles prepared following the artificial digestion was analyzed. The concentration of sulfur on the NP surface was the same for undigested Al and Al_2O_3 particles. This finding reflects the presence of the same amount of albumin in the protein corona formed on the surface of particles after dispersion in BSA-containing fluid. After digestion the amount of sulfur decreased by a factor >10 for both particles. It is concluded that the albumin corona was removed to a large extent during the digestion process, which might be causally linked to the changes of the pH value during digestion. This leads to the recharging of albumin, which has its isoelectric point at a pH value of 4.6. De novo emerged particles deriving from $AlCl_3$ appeared to contain more sulfur than other particulate aluminum species. Precipitation of aluminum ions with proteins, such as mucin or trypsin from the artificial media, or attachment of sulfur-containing ions might explain this behavior. The digested Al and Al_2O_3 as well as de novo formed aluminum particles revealed similar levels of the elements P and Ca. The concentration of these elements increased by a 2 orders of magnitude in case of Al_2O_3 particles. The high amount of these elements for digested particles might result from the attachment of calcium and phosphate ions, which form a calcium phosphate layer on particle surface. Chlorine and potassium increased more in the metallic aluminum particle samples than in the Al_2O_3 samples. Only a small amount of iron and zinc, derived from the digestion fluids, was associated with aluminum after the digestion process.

Discussion. Protein composition in artificial saliva is slightly more complex than BSA used in standard dispersion, but does not contain proteins or salts that are expected to provoke the formation of completely new chemical entities or complexes with altered chemical characteristics. As a result, in artificial

DOI: 10.1021/acs.langmuir.7b02729
Langmuir 2017, 33, 10726–10735

saliva the properties of the nanomaterials do not differ strongly from those of the undigested samples. In our experiments, artificial saliva did not lead to aggregation or dissolution of neither Al^0, nor Al_2O_3 nanoparticles. Also the formation of new particle populations resulting from free ions was not observed for all Al species.

Stomach fluid is characterized by higher ionic strength and a more acidic environment with a pH value in the range of 2.[22] Previous studies detected a general tendency of nanoparticles to aggregate at low pH values due to the electrostatic destabilization, for example in the case of silver[19,21] or silica nanoparticles.[25,34] Previous studies also showed an enhanced ion release from silver[20,21,35] and zinc oxide[34] nanoparticles in gastric fluid. In this study, we were able to prove that these effects are also observable for Al-containing nanoparticles. We found agglomeration by TEM, ToF-SIMS, and SAXS, combined with a disappearance of nanoscaled particles as determined by SP-ICP-MS. We also detected ion release from both particle species in gastric fluid, but to a very low extent, thus excluding predominant dissolution of the particles. We suggest that a small amount of ions is released from the particles and becomes dissolved, without remarkably changing the mean radii of the primary particles. As expected, a slightly higher ion release occurs from the metallic than from the mineral form of Al. Free Al ions can bind to or build complexes with proteins and biological compounds contained in foods, as well as with biological structures of the intestinal tissue.[3,36,37] Recent studies showed that this is not necessarily connected to an increased toxicity in vitro,[21] but that the phenomenon can lead to increased cellular particle uptake depending on the composition of the digestive juices and food components contained therein.[20]

The most remarkable physicochemical changes occurred at the transition from the artificial stomach fluid to the intestinal fluid, which simulates the passage into the duodenum. There, pH increases to 7.5 and bile is added. TEM, SAXS, SP-ICP-MS, and ToF-SIMS showed a reconstitution of the state and particle size previously measured in saliva fluid. This means that all observed Al species, including soluble $AlCl_3$, reach the intestine partly as nanoparticles. ICP-MS showed a decrease of free ions in digested samples for both primary particle species (metallic and mineral oxidized Al), suggesting the formation of complexes or aggregates. Furthermore, a strong decrease of free ions in the $AlCl_3$ solution was detected along with the appearance of nanoscaled structures in the intestinal fluid. ToF-SIMS and μPIXE images also showed agglomerates deriving from $AlCl_3$ samples that were not detectable during the previous digestion steps in saliva and gastric fluid. TEM-pictures show newly emerging, nanoscaled particle-like structures that differ in shape and density from the other particulate aluminum species. ToF-SIMS proved that these aggregates contain aluminum and IBM revealed the colocalization of aluminum with sulfur. The presence of sulfur detected in de novo formed particles supports the assumption that these particles are formed by precipitation of Al-protein-nano-complexes. We thus postulate these structures to be metal–organic particle-like complexes that are predominantly in the nanoscaled range. The differences in density and chemical composition, as compared to the Al^0 and Al_2O_3 particles also used in the study, is the most likely reason why they cannot be detected by SP-ICP-MS.

Furthermore, a calcium phosphate layer was found on the surfaces of all three particulate aluminum species. The formation of this layer could impact significantly on the protein corona formation, the cellular uptake, and the bioavailability of nanoparticles.[38−40]

With the help of SAXS, we observed a particle size distribution with a volume-weighted mean radius of 2.9 nm for the particle population formed de novo. The issue of de novo formation of particles as part of a transition between particulate and ionic species has, up to now, not been in the primary focus of research. Comparable de novo particle formation has also been observed for silver.[41,42] Although soluble compounds precipitate or agglomerate due to changing physicochemical conditions, it is noteworthy that a significant amount of these de novo emerged particles are in the nanoscaled range. Therefore, they might have nanospecific characteristics, including enhanced reactivity and altered uptake. Furthermore, when talking about toxicological analyses of nanomaterials, one should keep in mind that there is a certain balance between dissolved, agglomerated and non-agglomerated nanoparticulate species deriving from the same origin. These conversion processes occur bidirectionally and differ significantly among the multiple biological environments. Up to now, little is known about the two-directional solubilization behavior of metallic nanoparticles. We observed a remarkable change of the chemical state of dissolved aluminum between stomach and small intestine. Figure 8 summarizes possible transitions between free ions, nanoparticles, and agglomerates during the digestion process. Experimental evidence for the scenario drafted in Figure 8 has been presented in this study for aluminum and was similarly observed for silver in previous studies.[20,21,35] Even if de novo formation of nanoscaled particles from other metals like silver has not been experimentally shown in intestinal fluid,

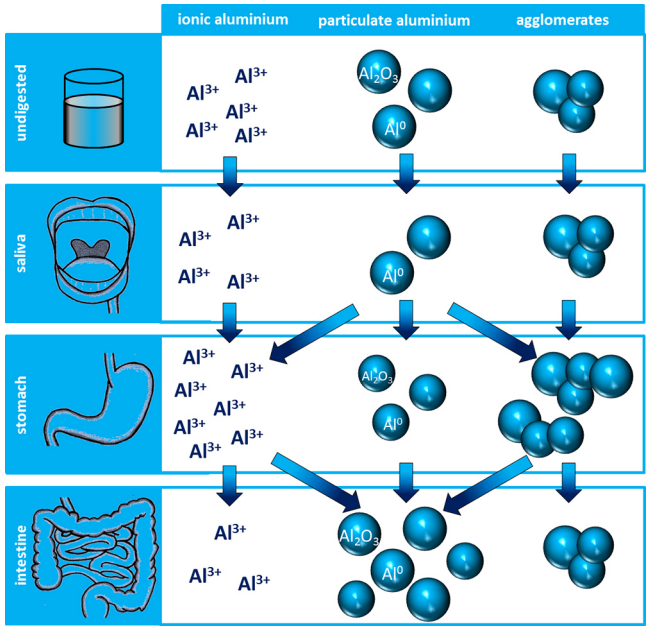

Figure 8. Suggested scheme of aluminum particle dissolution and agglomeration during the artificial digestion process. Samples stay unaffected in artificial saliva but agglomerate in stomach fluid. At the same time, ions are released from particles resulting in partial dissolution. In intestinal fluid, agglomerates tend to deagglomerate into primary particles. In addition, nanoscaled particulate structures are formed de novo from free ions.

DOI: 10.1021/acs.langmuir.7b02729
Langmuir 2017, 33, 10726−10735

physicochemical similarities of the different metals, as well as their shared affinity to biological structures, suggest that de novo formation of nanoparticles might also occur from additional metals following oral uptake of dissolved ions.

Altogether, we used a broad spectrum of methods to characterize the behavior of different aluminum species during an in vitro digestion process. As no single method is capable of capturing all the different physicochemical modifications, it is necessary to use complementary analytical techniques for a systematic characterization of the properties of nanomaterials. Such a strategy will yield comprehensive knowledge to investigate nanomaterials and their fate in relevant biological media and to link these results to their toxicological potential. For this purpose, it is indispensable to take into account the different transitions leading to a mixture of ionic, particulate and agglomerated species from one pristine material.

SUMMARY AND CONCLUSIONS

During the gastrointestinal digestion process, metallic and oxidized aluminum particles undergo physicochemical conversions depending on their biological environment. While staying almost unaffected in saliva, they preferably agglomerate in gastric juice and also slightly release ions into the fluid. In the intestine, these agglomerates tend to deagglomerate into primary particles again, whereas free ions form solid complexes with biological compounds. These complexes can be nanoscaled and differ significantly from primary particles in their size, shape, and density. Particles and dissolved ions can be transformed into each other, and their surface element composition can change. A broad spectrum of methods is required to characterize all these parameters adequately. With respect to this knowledge, toxicological investigations of individual nanoparticle species are only purposeful with regard to a specific biological and chemical environment. By demonstrating the mutual conversion of nanoparticles and dissolved metal ions, the present data underline that it might not be possible to distinguish between particle- and ion-dependent effects in toxicological studies. Careful physicochemical characterization will be essential for proper interpretation of toxicity data.

ASSOCIATED CONTENT

Supporting Information

The Supporting Information is available free of charge on the ACS Publications website at DOI: 10.1021/acs.langmuir.7b02729.

Mean radii of primary Al_2O_3 nanoparticles as a function of particle concentration measured by SAXS (PDF)

AUTHOR INFORMATION

Corresponding Author

*E-mail: Linda.Boehmert@bfr.bund.de. Tel.: +49 30 18412 2042.

ORCID

Claudia Kästner: 0000-0003-3730-7404
Linda Böhmert: 0000-0002-1153-2841
Dajana Lichtenstein: 0000-0002-2699-677X
Andreas F. Thünemann: 0000-0002-9883-6134

Notes

The authors declare no competing financial interest.

ACKNOWLEDGMENTS

This study was funded by the German Research Foundation DFG (Grant Number LA 3411/1-1) and by the French "Agence Nationale de la Recherche" ANR (Project ID ANR-13-IS10-0005) as part of the German-French SolNanoTOX project.

REFERENCES

(1) Willhite, C. C.; Ball, G. L.; McLellan, C. J. Total allowable concentrations of monomeric inorganic aluminum and hydrated aluminum silicates in drinking water. *Crit. Rev. Toxicol.* **2012**, *42* (5), 358−442.

(2) Yokel, R. A.; Florence, R. L. Aluminum bioavailability from the approved food additive leavening agent acidic sodium aluminum phosphate, incorporated into a baked good, is lower than from water. *Toxicology* **2006**, *227* (1−2), 86−93.

(3) Yokel, R. A.; McNamara, P. J. Aluminium toxicokinetics: an updated minireview. *Pharmacol. Toxicol.* **2001**, *88* (4), 159−67.

(4) Lote, C. J.; Saunders, H. Aluminium: gastrointestinal absorption and renal excretion. *Clin. Sci.* **1991**, *81* (3), 289−95.

(5) Exley, C. The toxicity of aluminium in humans. *Morphologie* **2016**, *100* (329), 51−5.

(6) Wagner, W. *Canadian Minerals Yearbook*; Natural Resources Canada: Ottawa, 1999

(7) Savory, J.; Bertholf, R. L.; Wills, M. R. Aluminium toxicity in chronic renal insufficiency. *Clin. Endocrinol. Metab.* **1985**, *14* (3), 681−702.

(8) Walton, J. R. Chronic aluminum intake causes Alzheimer's disease: applying Sir Austin Bradford Hill's causality criteria. *J. Alzheimer's Dis.* **2014**, *40* (4), 765−838.

(9) Darbre, P. D. Underarm antiperspirants/deodorants and breast cancer. *Breast Cancer Res.* **2009**, *11* (Suppl 3), S5.

(10) Greger, J. L. Dietary and other sources of aluminium intake. *Ciba Found. Sympos.* **1992**, *169*, 26−35 ; discussion 35−49..

(11) Yang, Y.; Doudrick, K.; Bi, X.; Hristovski, K.; Herckes, P.; Westerhoff, P.; Kaegi, R. Characterization of food-grade titanium dioxide: the presence of nanosized particles. *Environ. Sci. Technol.* **2014**, *48* (11), 6391−400.

(12) Faust, J. J.; Doudrick, K.; Yang, Y.; Capco, D. G.; Westerhoff, P. A Facile Method for Separating and Enriching Nano and Submicron Particles from Titanium Dioxide Found in Food and Pharmaceutical Products. *PLoS One* **2016**, *11* (10), e0164712.

(13) Golja, V.; Drazic, G.; Lorenzetti, M.; Vidmar, J.; Scancar, J.; Zalaznik, M.; Kalin, M.; Novak, S. Characterisation of food contact non-stick coatings containing TiO2 nanoparticles and study of their possible release into food. *Food Addit. Contam., Part A* **2017**, *34*, 421.

(14) Echegoyen, Y.; Nerin, C. Nanoparticle release from nano-silver antimicrobial food containers. *Food Chem. Toxicol.* **2013**, *62*, 16−22.

(15) Lin, Q. B.; Li, H.; Zhong, H. N.; Zhao, Q.; Xiao, D. H.; Wang, Z. W. Migration of Ti from nano-TiO(2)-polyethylene composite packaging into food simulants. *Food Addit. Contam., Part A* **2014**, *31* (7), 1284−90.

(16) Nel, A.; Xia, T.; Madler, L.; Li, N. Toxic potential of materials at the nanolevel. *Science (Washington, DC, U. S.)* **2006**, *311* (5761), 622−7.

(17) Di Silvio, D.; Rigby, N.; Bajka, B.; Mackie, A.; Baldelli Bombelli, F. Effect of protein corona magnetite nanoparticles derived from bread in vitro digestion on Caco-2 cells morphology and uptake. *Int. J. Biochem. Cell Biol.* **2016**, *75*, 212−22.

(18) Oomen, A. G.; Hack, A.; Minekus, M.; Zeijdner, E.; Cornelis, C.; Schoeters, G.; Verstraete, W.; Van de Wiele, T.; Wragg, J.; Rompelberg, C. J.; Sips, A. J.; Van Wijnen, J. H. Comparison of five in vitro digestion models to study the bioaccessibility of soil contaminants. *Environ. Sci. Technol.* **2002**, *36* (15), 3326−34.

(19) Walczak, A. P.; Fokkink, R.; Peters, R.; Tromp, P.; Herrera Rivera, Z. E.; Rietjens, I. M.; Hendriksen, P. J.; Bouwmeester, H. Behaviour of silver nanoparticles and silver ions in an in vitro human

DOI: 10.1021/acs.langmuir.7b02729
Langmuir 2017, 33, 10726−10735

gastrointestinal digestion model. *Nanotoxicology* **2012**, *7* (7), 1198−210.
(20) Lichtenstein, D.; Ebmeyer, J.; Knappe, P.; Juling, S.; Bohmert, L.; Selve, S.; Niemann, B.; Braeuning, A.; Thunemann, A. F.; Lampen, A. Impact of food components during in vitro digestion of silver nanoparticles on cellular uptake and cytotoxicity in intestinal cells. *Biol. Chem.* **2015**, *396* (11), 1255−64.
(21) Böhmert, L.; Girod, M.; Hansen, U.; Maul, R.; Knappe, P.; Niemann, B.; Weidner, S. M.; Thunemann, A. F.; Lampen, A. Analytically monitored digestion of silver nanoparticles and their toxicity on human intestinal cells. *Nanotoxicology* **2014**, *8* (6), 631−42.
(22) Versantvoort, C. H.; Oomen, A. G.; Van de Kamp, E.; Rompelberg, C. J.; Sips, A. J. Applicability of an in vitro digestion model in assessing the bioaccessibility of mycotoxins from food. *Food Chem. Toxicol.* **2005**, *43* (1), 31−40.
(23) Gerloff, K.; Pereira, D. I.; Faria, N.; Boots, A. W.; Kolling, J.; Forster, I.; Albrecht, C.; Powell, J. J.; Schins, R. P. Influence of simulated gastrointestinal conditions on particle-induced cytotoxicity and interleukin-8 regulation in differentiated and undifferentiated Caco-2 cells. *Nanotoxicology* **2013**, *7* (4), 353−66.
(24) Kästner, C.; Thünemann, A. F. Monitoring the fate of small silver nanoparticles during artificial digestion. *Langmuir* **2016**, *32*, 7383.
(25) Peters, R.; Kramer, E.; Oomen, A. G.; Rivera, Z. E.; Oegema, G.; Tromp, P. C.; Fokkink, R.; Rietveld, A.; Marvin, H. J.; Weigel, S.; Peijnenburg, A. A.; Bouwmeester, H. Presence of nano-sized silica during in vitro digestion of foods containing silica as a food additive. *ACS Nano* **2012**, *6* (3), 2441−51.
(26) Hur, S. J.; Lee, S. Y.; Lee, S. J. Effect of biopolymer encapsulation on the digestibility of lipid and cholesterol oxidation products in beef during in vitro human digestion. *Food Chem.* **2015**, *166*, 254−60.
(27) Kastner, C.; Thunemann, A. F. Catalytic Reduction of 4-Nitrophenol Using Silver Nanoparticles with Adjustable Activity. *Langmuir* **2016**, *32* (29), 7383−91.
(28) Pace, H. E.; Rogers, N. J.; Jarolimek, C.; Coleman, V. A.; Higgins, C. P.; Ranville, J. F. Determining transport efficiency for the purpose of counting and sizing nanoparticles via single particle inductively coupled plasma mass spectrometry. *Anal. Chem.* **2011**, *83* (24), 9361−9.
(29) Lichtenstein, D.; Ebmeyer, J.; Meyer, T.; Behr, A. C.; Kastner, C.; Böhmert, L.; Juling, S.; Niemann, B.; Fahrenson, C.; Selve, S.; Thunemann, A. F.; Meijer, J.; Estrela-Lopis, I.; Braeuning, A.; Lampen, A. It takes more than a coating to get nanoparticles through the intestinal barrier in vitro. *Eur. J. Pharm. Biopharm.* **2017**, *118*, 21.
(30) Jungnickel, H.; Pund, R.; Tentschert, J.; Reichardt, P.; Laux, P.; Harbach, H.; Luch, A. Time-of-flight secondary ion mass spectrometry (ToF-SIMS)-based analysis and imaging of polyethylene microplastics formation during sea surf simulation. *Sci. Total Environ.* **2016**, *563*−*564*, 261−6.
(31) Hsiao, I. L.; Bierkandt, F. S.; Reichardt, P.; Luch, A.; Huang, Y. J.; Jakubowski, N.; Tentschert, J.; Haase, A. Quantification and visualization of cellular uptake of TiO2 and Ag nanoparticles: comparison of different ICP-MS techniques. *J. Nanobiotechnol.* **2016**, *14* (1), 50.
(32) Willhite, C. C.; Karyakina, N. A.; Yokel, R. A.; Yenugadhati, N.; Wisniewski, T. M.; Arnold, I. M.; Momoli, F.; Krewski, D. Systematic review of potential health risks posed by pharmaceutical, occupational and consumer exposures to metallic and nanoscale aluminum, aluminum oxides, aluminum hydroxide and its soluble salts. *Crit. Rev. Toxicol.* **2014**, *44* (Suppl 4), 1−80.
(33) Exley, C. A biogeochemical cycle for aluminium? *J. Inorg. Biochem.* **2003**, *97* (1), 1−7.
(34) McCracken, C.; Zane, A.; Knight, D. A.; Dutta, P. K.; Waldman, W. J. Minimal intestinal epithelial cell toxicity in response to short- and long-term food-relevant inorganic nanoparticle exposure. *Chem. Res. Toxicol.* **2013**, *26* (10), 1514−25.
(35) Liu, J.; Hurt, R. H. Ion release kinetics and particle persistence in aqueous nano-silver colloids. *Environ. Sci. Technol.* **2010**, *44* (6), 2169−75.
(36) Murko, S.; Milacic, R.; Scancar, J. Speciation of Al in human serum by convective-interaction media fast-monolithic chromatography with inductively coupled plasma mass spectrometric detection. *J. Inorg. Biochem.* **2007**, *101* (9), 1234−41.
(37) Ruiperez, F.; Mujika, J. I.; Ugalde, J. M.; Exley, C.; Lopez, X. Pro-oxidant activity of aluminum: promoting the Fenton reaction by reducing Fe(III) to Fe(II). *J. Inorg. Biochem.* **2012**, *117*, 118−23.
(38) Dordelmann, G.; Kozlova, D.; Karczewski, S.; Lizio, R.; Knauer, S.; Epple, M. Calcium phosphate increases the encapsulation efficiency of hydrophilic drugs (proteins, nucleic acids) into poly(D,L-lactide-co-glycolide acid) nanoparticles for intracellular delivery. *J. Mater. Chem. B* **2014**, *2* (41), 7250−7259.
(39) Morgan, T. T.; Muddana, H. S.; Altinoglu, E. I.; Rouse, S. M.; Tabakovic, A.; Tabouillot, T.; Russin, T. J.; Shanmugavelandy, S. S.; Butler, P. J.; Eklund, P. C.; Yun, J. K.; Kester, M.; Adair, J. H. Encapsulation of Organic Molecules in Calcium Phosphate Nanocomposite Particles for Intracellular Imaging and Drug Delivery. *Nano Lett.* **2008**, *8* (12), 4108−4115.
(40) Bertoli, F.; Garry, D.; Monopoli, M. P.; Salvati, A.; Dawson, K. A. The intracellular destiny of the protein corona: a study on its cellular internalization and evolution. *ACS Nano* **2016**, *10* (11), 10471−10479.
(41) Juling, S.; Bachler, G.; von Gotz, N.; Lichtenstein, D.; Bohmert, L.; Niedzwiecka, A.; Selve, S.; Braeuning, A.; Lampen, A. In vivo distribution of nanosilver in the rat: The role of ions and de novo-formed secondary particles. *Food Chem. Toxicol.* **2016**, *97*, 327−335.
(42) Hansen, U.; Thünemann, A. F. Characterization of Silver Nanoparticles in Cell Culture Medium Containing Fetal Bovine Serum. *Langmuir* **2015**, *31* (24), 6842−52.

DOI: 10.1021/acs.langmuir.7b02729
Langmuir 2017, 33, 10726−10735

3.3 Aluminum and aluminum oxide nanomaterial uptake after oral exposure - a comparative study

Benjamin C. Krause[*§], Fabian L. Kriegel[*], Daniel Rosenkranz[*], Nadine Dreiack, Jutta Tentschert, Harald Jungnickel, Pegah Jalili, Valerie Fessard, Peter Laux & Andreas Luch

[*]These authors contributed equally, [§]Corresponding author

This chapter was published online on 14 February 2020 in:

Scientific Reports volume 10, Article number: 2698 (2020)

DOI: https://doi.org/10.1038/s41598-020-59710-z

This publication contains an "author contributions" section to display the individual involvement of the authors.

The supplementary material of the publication can be found in Annex III.

SCIENTIFIC REPORTS
nature research

OPEN

Aluminum and aluminum oxide nanomaterials uptake after oral exposure - a comparative study

Benjamin C. Krause[1,3*], Fabian L. Kriegel[1,3], Daniel Rosenkranz[1,3], Nadine Dreiack[1], Jutta Tentschert[1], Harald Jungnickel[1], Pegah Jalili[2], Valerie Fessard[2], Peter Laux[1] & Andreas Luch[1]

The knowledge about a potential *in vivo* uptake and subsequent toxicological effects of aluminum (Al), especially in the nanoparticulate form, is still limited. This paper focuses on a three day oral gavage study with three different Al species in Sprague Dawley rats. The Al amount was investigated in major organs in order to determine the oral bioavailability and distribution. Al-containing nanoparticles (NMs composed of Al^0 and aluminum oxide (Al_2O_3)) were administered at three different concentrations and soluble aluminum chloride ($AlCl_3 \cdot 6H_2O$) was used as a reference control at one concentration. A microwave assisted acid digestion approach followed by inductively coupled plasma mass spectrometry (ICP-MS) analysis was developed to analyse the Al burden of individual organs. Special attention was paid on how the sample matrix affected the calibration procedure. After 3 days exposure, $AlCl_3 \cdot 6H_2O$ treated animals showed high Al levels in liver and intestine, while upon treatment with Al^0 NMs significant amounts of Al were detected only in the latter. In contrast, following Al_2O_3 NMs treatment, Al was detected in all investigated organs with particular high concentrations in the spleen. A rapid absorption and systemic distribution of all three Al forms tested were found after 3-day oral exposure. The identified differences between Al^0 and Al_2O_3 NMs point out that both, particle shape and surface composition could be key factors for Al biodistribution and accumulation.

Aluminum is one of the most abundant elements on earth and is widely used in many different consumer product applications due to its unique characteristics. As an ubiquitous element, Al occurs in natural sources, e.g. food and drinking water, as well as in food additives, packaging and kitchenware[1,2]. Besides industrial, also agricultural, medical and consumer product uses are known for synthetic alumina, mixed Al silicate and Al oxide NMs. Especially composite materials containing Al show favourable properties when being used as packaging materials for the protection of food against humidity and oxidation and are more and more common[3–6]. Moreover, various Al salts are used in food as additives, e.g. as stabilizers, pH regulators and anti-caking agents[7,8]. As a consequence of modern life style Al-containing materials and substances are of high abundance in the human environment. In our study we could show *de novo* synthesis of Al-containing nanomaterials from ions after induction of a pH shift[9]. Based on this and because of the detection and quantification of Al in biological media is difficult, one should assume at least partial particle concentration in the body after oral uptake of Al. This raises questions about the potential hazard of particulate Al species.

Adverse effects of Al have been repeatedly discussed in the past. Neurodegenerative diseases such as Alzheimer's[10,11] as well as certain bone diseases[12–14] and dialysis dementia[15,16] have been attributed to Al exposure. Although inhalation and dermal uptake of Al may occur, ingestion is mainly responsible for Al organ burden with regard to the public population[17]. Consequently, a tolerable weekly intake (TWI) of 1 mg/kg body weight was implemented by the European Food Safety Authority (EFSA), while a provisional tolerable weekly intake (PTWI) of 2 mg/kg body weight has been set by the Joint FAO/WHO Expert Committee on Food Additives (JECFA). However, both values do not distinguish between ionic and nanoparticulate Al species[18,19], despite the increasing use of Al-containing NMs[20]. Al NMs may change the impact on human health due to their unique

[1]German Federal Institute for Risk Assessment (BfR), Department of Chemical and Product Safety, Max-Dohrn-Straße 8-10, 10589, Berlin, Germany. [2]ANSES, French Agency for Food, Environmental and Occupational Health and Safety, Fougères Laboratory, 10B rue Claude Bourgelat, 35306, Fougères Cedex, France. [3]These authors contributed equally: Benjamin C. Krause, Fabian L. Kriegel and Daniel Rosenkranz. *email: Benjamin-christoph.krause@bfr.bund.de

Methods	Al^0 NM	Al_2O_3 NM
TEM	Primary particle size and shape: 2–50 nm, nearly spherical	Primary particle size and shape: 10 × 20–50 nm, grain-like shape
EELS-TEM	Core-shell structure, thin (2–5 nm) oxide layer	Fully oxidized particle
XRD	Aluminum surface; partially oxidized	Fully oxidized surface
SAXS	Particle radius: >10 nm	Primary particle radius: 7.1 nm Aggregates' radius: >10 nm
SP-ICP-MS	Primary particle size: 54–80 nm	Primary particle size: 50–80 nm
ICP-MS	Ion release: 0.2–0.5% (in 0.05% BSA)	Ion release: 0.2–0.4% (in 0.05% BSA)
ToF-SIMS	Particle-amino acid agglomerates	Particle-amino acid agglomerates; polyoxo-aluminates
IBM, atom number %	Impurities: P (1%); biocorona: S (5%), protein; $Ca_3(PO_4)_2$ coating: P (3%)	Impurities: S (0.2%); biocorona: S (1%), $Ca_3(PO_4)_2$ coating: P (1%)

Table 1. Characterization data for Al^0 and Al_2O_3 NM. Modified from[30].

physico-chemical properties, e.g. their size, high specific surface area, and high reactivity[21–24]. Hence, reliable information on oral uptake and the resulting organ burden of Al-containing NMs is needed. In a recent *in vitro* study, the influence of an artificial digestion process on two different Al NMs and one salt species was examined[9]. This process led to the *de novo* formation of nanoparticles in the artificial intestinal juice for the two NM species and also for the Al salt[9]. *In vivo* studies in rats showed that ionic Al is systemically distributed throughout the organs after oral uptake. High concentrations were found in kidneys, liver, spleen, bones and brain. Al is also highly persistent with half-life times up to 150 days, for example, in the brain[25–28]. On the contrary, little is known about the distribution of particulate Al species, and possible differences between individual Al species.

In this study, we compared Al^0 and Al_2O_3 NMs with an ionic Al species. Oral uptake was investigated by measuring Al concentrations in duodenum and colon samples. Systemic exposure was estimated through analyses of blood, liver, kidney and spleen samples. We carefully examined matrix suppression effects since they may affect the Al levels detected by ICP-MS[29]. For this purpose, a calibration for each organ was compared with the standard aqueous calibration method. Our approach highlights the advantages of matrix-matching in ICP-MS based *in vivo* studies. A reduction of the number of animals needed for a robust analysis combined with low limits of detection were achieved, while at the same time, matrix effects were taken into account.

Results

Characterization of Al and Al_2O_3 NMs. Both, Al^0 and Al_2O_3 NMs have been characterized elsewhere (Table 1)[30]. In brief, the core particle diameter was confirmed to be between 2–50 nm for the nearly spherical Al^0 NMs by transmission electron microscopy (TEM). Al_2O_3 NMs are more rod-shaped with a width mostly around 10 nm and a length that varies between 20–50 nm as determined by TEM. The size distribution showed a broader variance for Al^0 than for Al_2O_3 NMs. Dynamic light scattering (DLS) determined the hydrodynamic diameter in dispersion of 0.05% BSA. For Al^0 NMs, a hydrodynamic diameter of 250 nm was detected, while Al_2O_3 NMs showed a smaller diameter of 180 nm. X-ray diffraction (XRD) and TEM in an element resolved mode demonstrated the difference of the Al^0 and Al_2O_3 NMs composition and especially their surface. While Al^0 NMs had a core-shell structure with Al core and a 2–5 nm oxygen shell, the Al_2O_3 NMs were homogeneously oxidized. An overview about the main characterization data is given in Table 1. An artificial digestion approach showed a decreased solubility coupled to *de novo* formation of Al-containing particles in the nanoscale range occurring in the intestinal fluid compared to the stomach[9].

Matrix-matching. After an in-house validation of the analytical method for digestion, quantification and evaluation of the Al content in the investigated organs, an ANOVA and PCA analysis based on the different treatment groups were performed (see Methods section for details). This step was conducted to exclude the possibility that animals did not correspond to the variation in the overall population. The results of ANOVA and PCA (see Supplementary Table S1 and Supplementary Fig. S1) showed no significant difference among the animals of the different treatment groups.

In order to minimize measurement uncertainties and standard deviation for the quantification, a matrix calibration was carried out for each organ investigated. The calibration points quantified in the different matrices were highly correlated to the data points calculated from the regression curve of each organ (Fig. 1 and Table 2). For each tested organ a calibration linearity between 0.9960 and 0.9997 was achieved.

The F-Test compares the variances of both water and matrix calibration sensitivities. This revealed significant differences between the calibration in water and in the several matrices. It is therefore not possible to use the water calibration without correction factors calculated from the matrix calibration. In order to avoid the preparation of matrix calibration for each day of measurement a daily response factor (DRF) was used. The DRF accounts for day to day ICP-MS sensitivity variations as well as for matrix effects. After the introduction of the DRF, all sensitivities of the matrix calibrations could be correlated to the water calibration of each day to calculate the recovery rate. The intensities for Al in water are considerably higher than those of each matrix used. Thus, the values for recovery depend on the matrix (see Supplementary Fig. S2). These results pointed out the necessity for a matrix-matched calibration, which led to reliable results. The sample intensities were corrected by subtracting the value of averaged microwave blanks (see Eq. (1) in the methods section). In order to avoid performing a matrix calibration curve each day, a matrix calibration was done on one day and the resulting intensities of the samples

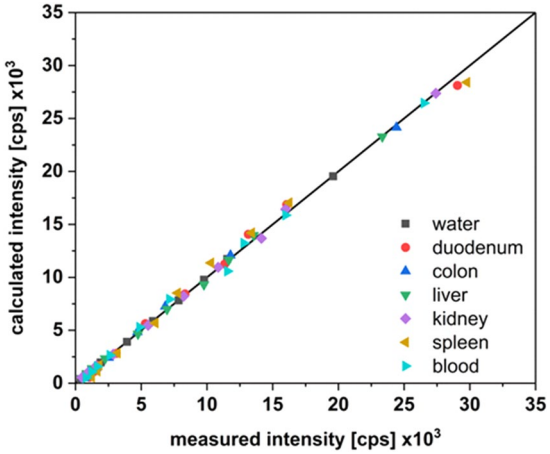

Figure 1. Regression analysis of matrix calibration data. The measured intensities were plotted versus the calculated intensities which were obtained from the regression functions.

Matrix	Linearity (r^2)	Sensitivity [cps $(ng\ g^{-1})^{-1}$]	LOD [µg g^{-1}] organ	LOQ [µg g^{-1}] organ	F-Test*	Recovery [%]
water	0.9994	390.68	0.035	0.042	1	100
duodenum	0.9979	526.35	0.070	0.115	0.13	135
colon	0.9995	483.10	0.466	1.394	0.56	92
liver	0.9996	465.66	0.024	0.049	0.44	96
kidney	0.9997	568.27	0.032	0.082	0.16	122
spleen	0.9959	547.35	0.039	0.082	0.13	96
blood	0.9983	528.93	0.008	0.015	0.20	97

Table 2. Analytical figure of merit. The different matrices (water, duodenum, colon, liver, kidney, spleen and blood) were evaluated based on the quality parameters of the calibration (linearity, sensitivity, limit of detection (LOD), limit of quantification (LOQ), recovery). F-Test was carried out to compare the variance between water and matrix calibration sensitivities. *F-Test: water/matrix; $F \geq 0.99$ for using water calibration only.

were corrected using a DRF (see Eq. (2) in the methods section). We defined the sensitivity of the ICP-MS device as the slope of the calibration curve (Table 2). Therefore, the sensitivity obtained using a water calibration on the day when the samples were analysed was divided by the sensitivity of the water calibration from the day of the matrix calibration (see Eq. (3) in the methods section). Additionally, the recovery of the microwave-assisted digestion was calculated. Considering a factor taking into account these corrections, it was possible to calculate the concentration of Al burden per gram of tissue in a highly robust manner (see Eqs. (4–6) in the methods section). All obtained values were above the LOQ (Fig. 2). Assuming that the data are not equally distributed, through median and average comparison (Table 3), the Wilcoxon sign test was used for statistical analysis of non-normal distributed dependent groups. For each dose group, the distribution of Al concentrations in the organs was examined. The significance levels were corrected according to Holm-Šidàk and an unspecific pairwise comparison was carried out[31]. For almost all comparisons, a significant difference between dose groups and the Al species as well as to the control group at the significance level of 0.05 (one-side) could be observed.

Uptake evaluation. In this study, $AlCl_3{\cdot}6H_2O$ is regarded as a reference substance to determine the uptake of Al ions. According to the mass balance in all investigated organs, ca. 25% of the ionic $AlCl_3{\cdot}6H_2O$ did pass the intestinal barrier (Fig. 2). A similar behaviour was observed for the Al^0 NMs at all three concentrations tested although the total Al content administered with Al^0 NMs was 1.9–7.6-fold higher when compared to $AlCl_3{\cdot}6H_2O$. If the overall uptake of Al was comparable for the Al^0 NM and the salt species, in contrast, a higher overall Al uptake could be observed in animal tissues treated with Al_2O_3 NMs (Fig. 2). It is worth noting that the accumulation of Al in the intestine (washed duodenum and colon) and in systemic organs differed significantly. In contrast to Al^0 treatment, a concentration-dependent increase of intestinal Al was detected after Al_2O_3 administration.

Indeed, in the intestine, a dose-dependent linear increase of the Al fraction was recorded. Figure 2 depicts the fractions of Al found in intestine and systemic organs investigated in this study. The sum of both Al fractions was normalized to 100%.

After administration of Al^0 NMs, the lowest dose of 3.19 mg/rat resulted in the highest concentrations in intestine, both duodenum and colon with concentrations in the range of 1–2 µg/g and of 2–3.5 µg/g respectively (Fig. 3A).

The Al uptake was calculated based on the mass fraction of Al in the compound. The Al concentration was then median normalized to the values found in samples with a 1.68 mg/rat $AlCl_3{\cdot}6H_2O$ exposure (see Eq. (7) in the methods section, for further details see Supplementary Tables S2 and S3). An overview about all investigated

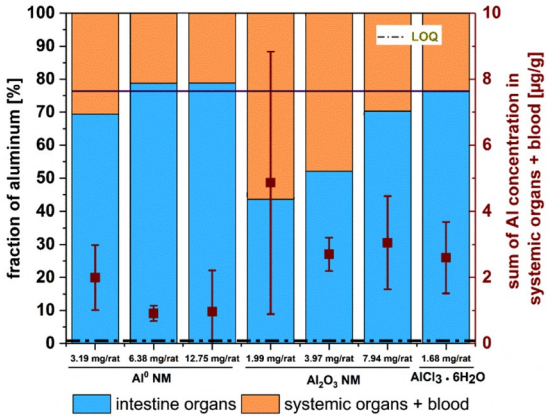

Figure 2. Overall fraction of Al in investigated organs. The intestine (duodenum and colon; blue) and the systemic organs (liver, kidney, spleen) and blood (orange) values [%] are given. The black bar indicates the reference value found for ionic $AlCl_3 \cdot 6H_2O$ fraction [%]. Brown squares indicate the median of the sum of Al concentration in systemic organs and blood [µg/g] and the vertical bars indicate the interquartile ranges.

	∑ all organs			∑ Liver, Kidney, Spleen		
Dose	Median µg/g	Mean µg/g	Skewness	Median µg/g	Mean µg/g	Skewness
Al^0 6.25 mg/kg	8.16	10.21	right skew	2.46	3.29	right skew
Al^0 12.5 mg/kg	3.85	4.88	right skew	0.72	1.30	right skew
Al^0 25 mg/kg	5.79	9.56	right skew	1.22	2.54	right skew
Al_2O_3 6.25 mg/kg	11.16	25.83	right skew	5.01	6.78	right skew
Al_2O_3 12.5 mg/kg	10.08	16.09	right skew	4.81	5.84	right skew
Al_2O_3 25 mg/kg	15.37	19.80	right skew	4.58	5.84	right skew
$AlCl_3 \cdot 6H_2O$ 25 mg/kg	9.38	14.23	right skew	2.33	6.85	right skew

Table 3. Comparison of median and mean for determination of skewness for doses per kg body weight. "All organs" refers to all examined organs.

organs with the Al concentration in µg/g for all eight treatment groups is given in Supplementary Fig. S3. The application of Al^0 NM at the lowest dose resulted in the highest Al concentration in the duodenum. Normalized to the Al concentration found in the same organs following exposure to $AlCl_3 \cdot 6H_2O$, only 85% were detected. A less prominent concentration was determined relatively to the $AlCl_3 \cdot 6H_2O$ for the mid (about 17%) and the high dose (about 11%). A comparable effect was observed in the colon, where the relative amount was about 60% for the lowest dose, 20% for the mid and about 15% for the highest dose (Fig. 3A). Comparing Al^0 NMs and Al_2O_3 NMs, more Al could be detected in the duodenum after Al_2O_3 exposure. However, Al_2O_3 NMs contain only about 62% of the Al content than Al^0 NMs. While no dose dependency was observed in the duodenum, the Al concentration increased dose dependently in the colon. A maximum concentration of 7.7 µg/g organ was observed at the highest dose level (Fig. 3B). Normalized to an ionic $AlCl_3 \cdot 6H_2O$ dose of 1.68 mg Al/rat, the treatment with Al_2O_3 NMs resulted in an Al content of 20–113% in the duodenum and of 45–95% in the colon (Fig. 3B).

After crossing the intestinal barrier, the different Al species were distributed to systemic organs via blood. At the lowest dose of Al^0 NM, Al was detected to a large extent in liver and blood (Fig. 4A), and in the two intestinal sections (Fig. 3A). Compared to $AlCl_3 \cdot 6H_2O$, a lower amount of Al was detected in liver (0.07–0.33-fold of the amount detected for $AlCl_3 \cdot 6H_2O$), while a 8.98–41.45-fold increased uptake was measured in blood for mid and low doses of Al^0 NMs (Fig. 4A).

A similar concentration-dependent behaviour (in respect to the amount given) was observed for Al_2O_3 NMs: the lowest dose showed the highest difference in comparison to the median normalized and fraction-corrected concentration of $AlCl_3 \cdot 6H_2O$. However, the concentration dependency showed a linear decrease (Fig. 4B). Compared to the corresponding values in $AlCl_3 \cdot 6H_2O$ treated animals, the Al content varied between 1.49-fold for the lowest and 0.27-fold for the highest dose (liver). In blood, an almost 390.92-fold increase for the lowest dose and a 89.92-fold increase for the highest dose were observed in comparison to animals treated with $AlCl_3 \cdot 6H_2O$ (Fig. 4B). Al concentrations in liver and blood were found between 1.07 and 1.64 µg/g for Al_2O_3 NMs treated rats, compared to a range between 0.03 and 0.52 µg/g for Al^0 NM treated rats. When comparing Al^0 and Al_2O_3 NMs, the latter one is found up to ten times higher in the blood (Fig. 4).

Since liver is the first organ after intestinal uptake, a significant accumulation of Al was expected. Therefore, we normalized the liver uptake as 100% to show the different uptake and accumulation patterns of Al^0 and Al_2O_3 NMs at various concentrations. With the low and medium Al^0 NM doses, a relatively high concentration of Al was found in the kidney with concentrations of 0.65 and 0.23 µg/g respectively. However, with Al^0 NMs, the

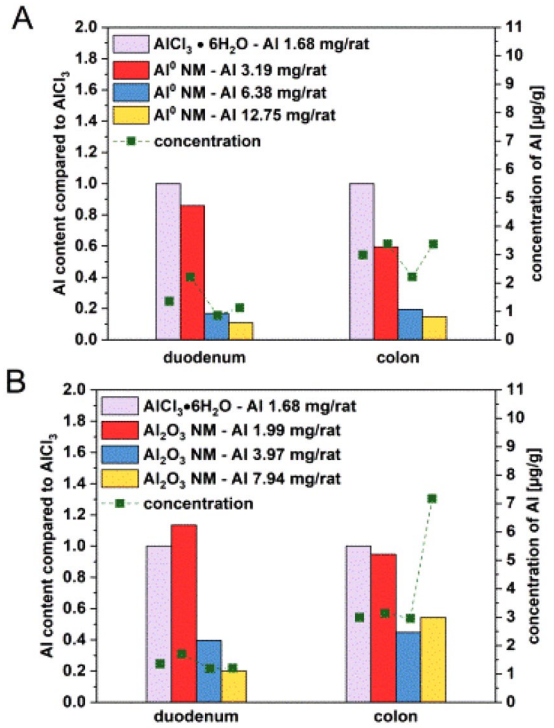

Figure 3. Al concentrations in duodenum and colon after 3 day oral treatment. The organs were collected 3 hours after the last administration of Al^0 NMs (**A**) and Al_2O_3 NMs (**B**). Each bar was normalized on the concentration obtained with $AlCl_3{\cdot}6H_2O$ at 1.7 mg/rat corrected by the corresponding Al content of $AlCl_3{\cdot}6H_2O$ and the applied NM. Green squares display the Al concentration which was found in the organ [µg/g].

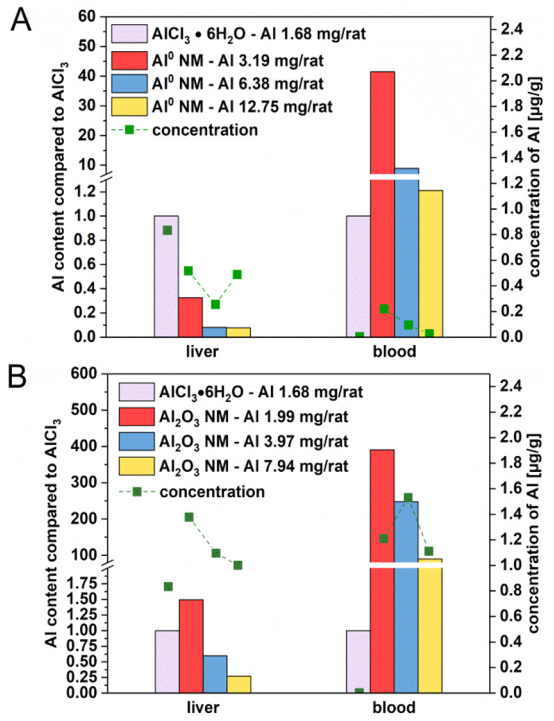

Figure 4. Accumulation of Al in liver and blood after 3 day oral treatment. All organs were collected 3 hours after the last administration of Al^0 NMs (**A**) and Al_2O_3 NMs (**B**). Each bar was normalized on the concentration of 1.7 mg Al/rat. Values were corrected by the corresponding Al content of $AlCl_3{\cdot}6H_2O$ and the applied NM. Green squares display the Al concentration which was found in the organ in [µg/g].

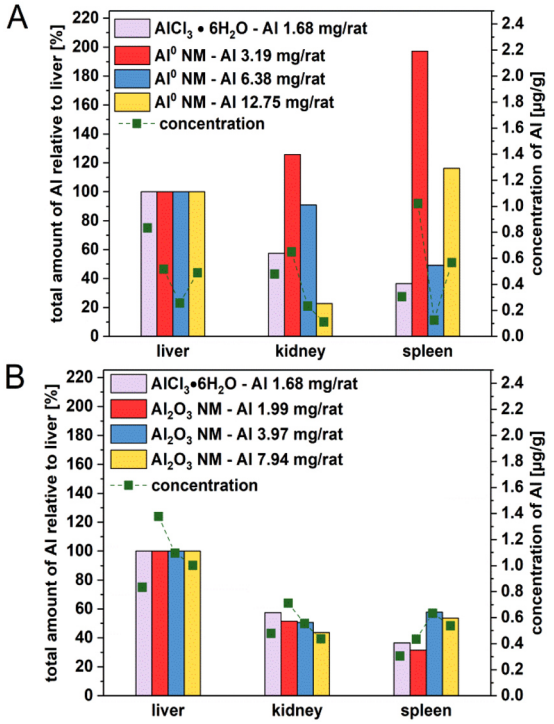

Figure 5. Comparison of the Al content of liver, kidney and spleen after 3 day oral treatment. The organs were collected 3 hours after the last administration of Al^0 NMs (**A**) and Al_2O_3 NMs (**B**). Each bar was normalized on the uptake of the liver in the corresponding treatment group. Green squares display the Al concentration which was found in the respective organ in [µg/g].

maximum Al concentration (1.02 µg/g) was found in the spleen with the lowest treatment dose (Fig. 5A). Al_2O_3 NMs accumulated three times higher in the liver than Al^0 NMs. Following to administration of Al_2O_3 NMs, the Al levels detected in the liver (1.07 to 1.48 µg/g) are the highest among the other systemic organs (Fig. 5B).

Discussion

In the current study we compared the oral bioavailability and distribution of ionic and nanoparticulate Al^0 and Al_2O_3 in rats following a 3-day oral treatment. ICP-MS was used to quantify the Al concentration in duodenum, colon, blood, liver, kidney and spleen to evaluate the biodistribution patterns of the three Al species. Some challenges were faced for the quantification of Al amounts. First, the ubiquitous presence of Al in the tissues hinders the detection of Al that originates from the treatment. The background levels of Al were shown to vary from organ to organ (see Supplementary Fig. S3). For this purpose, a robust calibration methodology was developed where matrix effects were taken into account. Our matrix calibration data clearly indicated the need for matrix correction (see Supplementary Fig. S2). In fact, the calibration in water showed a higher sensitivity compared to all calibrations in matrices. The matrix affects the analyte sensitivity due to signal suppression or enhancement by dissolved salts. Another possible interference especially in high matrix load samples is the deposition of solid matrix on the ICP-MS apertures[32]. After setting up the matrix calibration method, we were able to detect very low concentrations of Al in the tissue samples above the background levels (see Table 2 and Supplementary Fig. S3). However, as daily matrix calibration requires an analytical effort and the recurrent use of animal tissues, the DRF, an established approach in chromatography, was adapted to this study. This approach not only compensates for daily measurement fluctuations but also adjusts the sensitivity of the calibration in water by the calibration with matrix in order to take matrix effects into account. The DRF methodology contributes to achieve the high sensitivity required for a reliable detection of low Al levels by ICP-MS. Consequently, we recommend always testing the influence of sample matrix on the analyte detection. If, as demonstrated in this study, analyte suppression is observed, matrix calibration in combination with the DRF approach is advised for sample analysis.

Following oral administration by gavage with Al^0 NM, Al_2O_3 NM and ionic aluminum, Al levels were detected in all investigated organs and specific differences were highlighted between Al^0 and Al_2O_3 NMs compared to ionic $AlCl_3{\cdot}6H_2O$. These findings are in contrast to a previous inhalation study where, despite high lung burdens of AlOOH NMs, no significant systemic organ burden (brain, liver, and kidney) could be detected[33]. This highlights the importance of the oral uptake route for the overall Al burden in humans.

After gavage the distribution of Al_2O_3 NM between intestine and systemic organs showed significant differences (Fig. 2), while distribution of Al^0 NM was rather comparable to the ionic $AlCl_3{\cdot}6H_2O$. Therefore, NMs with the same metallic component may show different accumulation behaviour in living organisms. We observed a dose-dependent decrease of Al levels in systemic organs with increasing concentrations of Al_2O_3 NM suggesting an impairment of the intestinal barrier function with increasing dose and subsequent accumulation in the

intestine. An explanation could be that the agglomeration state of Al_2O_3 NMs was higher with increasing concentrations. Above a certain size, agglomerates may be less prone to cross the gut-blood barrier. Therefore not only the composition of the NM, but also its agglomeration state may be regarded as a key parameter for oral uptake assessment[34,35]. The results in our study showed that the rod-shaped Al_2O_3 NMs were present in higher concentrations compared to the spherical Al^0 NMs in the organs investigated. These findings were in good accordance with the results of uptake investigations of polystyrene NMs on Caco-2 cells[36]. However, this assumption is not always confirmed[37]. Al^0 NMs might be more easily taken up but also may be excreted faster, whereas the rod shaped structure of Al_2O_3 NMs prevents a fast elimination out of the animal. A similar difference between spherical and rod-shaped NMs was also observed for SiO_2 NM in rats, of which spherical particles were taken up to a higher amount after 2 and 24 h. After 7 days, the rod-shaped particles showed the highest concentrations in the organs[38]. Furthermore, the surface composition might also influence the biokinetic behaviour of the NMs[39]. For Al^0 NM, a core-shell structure with an Al core and a thin Al oxide layer (2–5 nm) due to passivation with oxygen in the manufacturing process has been confirmed by XRD and element-specific TEM. Al^0 NMs were shown to contain 85% Al (Table 1). In contrast, Al_2O_3 is fully oxidized, with a rather homogenous distribution of Al and oxygen on its surface. Recently we showed that the protein corona formed upon contact with cell culture media is less complex for Al^0 NM compared to Al_2O_3 NM[40]. The different surface properties of NMs facilitate interactions with the surrounding environment, thus the NM, thus influencing bioavailability and tissue retention of the NM[30]. Our results highlight that physico-chemical characteristics including composition, shape, aggregation state and surface composition could affect the kinetics of NMs. As shown in an artificial digestion experiment *in vitro*, $AlCl_3{\cdot}6H_2O$ formed efficiently Al-containing salts and particles in the nano range in the artificial small intestine environment. These newly formed nanoparticles which originated from $AlCl_3{\cdot}6H_2O$, showed a low solubility comparable to Al^0 NM[9]. This observation may explain the almost identical uptake behaviour of Al^0 NM and $AlCl_3{\cdot}6H_2O$ in our study. *In vitro* results from intestinal culture models incubated with the different Al species also showed low uptake rates and no major differences between Al^0 and Al_2O_3 NMs and $AlCl_3{\cdot}6H_2O$ accumulation within the cells[40]. In our study, although the distribution pattern was similar between the two NMs, but the Al concentrations differed significantly. We clearly observed that the Al concentrations found in the organs are not correlated to the total amount of Al given by gavage. In fact, although with the lowest amount of Al in the administered dose, $AlCl_3{\cdot}6H_2O$ was clearly taken up to a higher degree in comparison to NMs (1.9–7.6-fold higher depending on the tissue). The increased uptake of $AlCl_3{\cdot}6H_2O$ might be due to a higher permeability of the intestinal barrier for ions versus particles. However, this was not observed during *in vitro* studies[40]. Nevertheless, compared to the larger agglomerates originating from Al^0 and Al_2O_3 NMs, ions are expected to cross the intestinal barrier more easily. It is worth to mention that the application of Al_2O_3 NM with a lower mass fraction of Al than Al^0 NM, led to a higher accumulation of Al in the organs.

Al^0 and Al_2O_3 NM accumulation between the small and the large intestine differed significantly from each other with a higher concentration found in the colon. The difference of pH between duodenum and colon may impact the agglomeration behaviour of the particles. Moreover, the longer retention time in the colon could also favour their uptake leading to an increased Al amount in the colon[9].

After passage of the gut –blood barrier, Al was identified in the blood where it possibly is distributed to the systemic organs through the blood flow. Previous work suggested that ionic Al is able to associate with transferrin and other plasma proteins as well as with low molecular weight fractions (citrate, hydroxide)[1]. In our study the blood concentration of $AlCl_3{\cdot}6H_2O$ was relatively low compared to the 1.2-fold higher burden found for the highest dose of Al^0 NMs. The measured value for Al_2O_3 NMs was even 100 times higher than $AlCl_3{\cdot}6H_2O$ (Fig. 4B). Based on the low solubility of Al^0 and Al_2O_3 NMs determined earlier[9], these results suggests that particulate Al was also transported by blood but probably was better retained in the blood by the formation of a specific protein corona. Especially low molecular weight fractions can circulate between tissue and blood. As $AlCl_3{\cdot}6H_2O$ could potentially interact with low molecular weight proteins, it might reach liver and other organs with a higher efficiency (Fig. 5A, B). In contrast, as shown by protein corona data[40], Al^0 NMs and especially Al_2O_3 NMs might preferentially interact with higher molecular weight plasma proteins, then limiting their access into tissues and possibly enhancing Al half-life in blood. A few studies investigated the bioavailability and biodistribution of Al-containing NMs after oral treatment in mice. Our results after only three days exposure to Al_2O_3 NMs (Fig. 5B) are in good accordance with the biodistribution pattern in liver, kidney and spleen reported after 13 weeks[41]. Another animal study suggested that Al_2O_3 NMs was systemically available since liver and kidney impairments were observed after oral uptake[42].

In conclusion, our *in vivo* study showed a significant uptake of Al from both, Al^0 and Al_2O_3 NMs, following a 3-day oral gavage treatment. Rapid absorption and systemic distribution of Al for all three different forms tested is concluded. Nevertheless, some differences between Al^0 and Al_2O_3 NMs were observed assuming that agglomerate shape and surface composition may play an important role in particle accumulation. In contrast to *in vitro* results from the literature Al_2O_3 NM accumulates to a higher extent in comparison to Al^0 NM in both, intestine and systemic organs. Our findings identify challenges in the extrapolation of NM accumulation, even if the used materials possess a similar chemical composition. An interesting difference to ionic Al was the long retention time of Al levels in blood with Al_2O_3 NMs. The low dose study design challenged conventional ICP-MS approaches. In order to increase the sensitivity and robustness of the technique we conducted a matrix calibration in combination with a DRF, which showed superior performance in terms of sensitivity compared to the standard water calibration method. The applied method also eliminated the influence of day to day variation on the calibration. This method enabled the reliable quantification of all Al organ burdens even in the low µg/g range. Our study successfully showed that a respective matrix matched calibration can easily improve the data quality for the evaluation of low dose studies. The approach of statistical evaluation presented here utilizes a DRF to enable robust data analysis in order to obtain resilient data for risk assessment.

Methods

Materials. Al^0 NMs (mean diameter 18 nm (TEM), 99.9%) and Al_2O_3 NMs (mean diameter 20 nm (TEM), 99+%) were purchased from Ionic Liquids Technologies GmbH (IoLiTec), Heilbronn, Germany. $AlCl_3{\cdot}6H_2O$ and bovine serum albumin (BSA) were bought from Sigma Aldrich. All other chemicals used in this study were reagent grade.

Animals and experimental design. All experiments were in accordance with the ethical recommendations of the Directive 2010/63/EU of the European Parliament and were validated by the Anses ethical committee (COMETH). This study was performed to investigate the biodistribution of Al nanomaterials and served as a preliminary dose-finding study for genotoxicity testing, where the doses administered should represent the maximum tolerated doses according to regulatory guidelines. In fact, according to the OECD guidelines 474 and 489 for the micronucleus and comet assays respectively, it is clearly required that the highest dose should be the maximum tolerated dose for a few repeated administrations and that 2 other lower doses must additionally be tested. The experimental design was chosen to fulfil all the above-mentioned criteria.

Male Sprague-Dawley rats (8–10 weeks old, around 200 g) were purchased from Janvier (Saint Berthevin, France). Rats were housed in conventional cages and had free access to water and food. Temperature and humidity were constant with a light/dark cycle of 12 h/12 h. The animals were treated after at least 5 days of acclimatization. Animals (5 per group) were randomly assigned to one of eight groups (including vehicle controls).

Animals were treated by gavage (9.76 ml/kg) at 0 h, 24 h, and 45 h and sacrificed 3 h after the last administration. Al^0 and Al_2O_3 NMs were given at 6, 12.5 and 25 mg/kg body weight (bw), and $AlCl_3{\cdot}6H_2O$ at 25 mg/kg bw in ultra-pure water (UPW) with 0.05% BSA according to the NanoGenoTox protocol and as previously described[30]. UPW with 0.05% BSA was used as negative control.

Tissue collection and sample preparation. Animals were anesthetized with an intraperitoneal sublethal dose of pentobarbital (60 mg/kg). The following samples were collected: blood, liver, spleen, kidney, duodenum, and colon. The intestinal sections were washed and thoroughly cleaned. A portion of each organ (always a similar part irrespective of treatment) was weighed and rapidly frozen in liquid nitrogen. For the blood samples always 1 ml blood were taken and rapidly frozen in liquid nitrogen. The samples were kept at −80 °C until further processing.

For matrix calibration, a sample of each organ from the controls was spiked with 25 µg/ml of ionic Al. All samples were then digested using a microwave-assisted acid digestion with 69% HNO_3 and 30% H_2O_2 for 30 min at 200°C and 160 bars. The samples were then diluted to a concentration of 500 ng/g. This solution served as stock for the calibration concentrations (1–50 ng/g). All samples were analysed in triplicate.

Data analysis. The PCA and the one-way ANOVA was carried out in Origin 9.1 (OriginLab Corporation, USA). Microsoft Excel (2016) was used for all other calculations including the F-Test, used for correlation of matrix specific calibrations. The organ weights in combination with the treatment groups were used as input vectors for PCA and ANOVA.

ICP-MS measurements. Measurements were performed at a quadrupole ICP mass spectrometer (XSeries 2, Thermo Fisher Scientific GmbH, Dreieich, Germany) equipped with a PFA ST Nebulizer, a quartz cyclonic spray chamber and a 2.5 mm quartz injector (all from Thermo Fisher Scientific) using the following isotopes: ^{27}Al and, as an internal standard, ^{103}Rh. Daily calibrations were performed using ionic standards of Al in a 3.5% HNO_3 solution ranging from 2 to 500 µg/L. Rh as internal standard was added to each sample. The gas flow for the cool gas and the auxiliary gas were set to 14 L/min, and 0.65 L/min respectively. The sample flow rate was 0.4 mL/min. All isotopes were analysed using the collision cell technique at 5 mL/min collision gas flow (93% He and 7% H_2).

Equations. The sample intensities ($\boldsymbol{Int_{Sample}}$) were corrected by subtracting the number of averaged microwave blanks (≤ 10) ($\overline{\boldsymbol{Int}}_{\boldsymbol{Water}}$):

$$\boldsymbol{Int_{corr}} = \boldsymbol{Int_{Sample}} - \overline{\boldsymbol{Int}}_{\boldsymbol{Water}} \tag{1}$$

To determine the $\boldsymbol{DRF}$, the sensitivity on each day was divided by the sensitivity of the matrix adjusted calibration of that day:

$$\boldsymbol{DRF} = \frac{\boldsymbol{sensitivity_{sample\ day}}}{\boldsymbol{sensitivity_{matrix\ calibration\ day}}} \tag{2}$$

DRF was then used to correct the intensity values:

$$\boldsymbol{Int_{sample,\,corr}} = \boldsymbol{Int_{corr}}/\boldsymbol{DRF} \tag{3}$$

Dividing Eq. 1 by Eq. 2 considering the Al sensitivity in the corresponding matrix, the used organ mass ($\boldsymbol{m_{org}}$) and the recovery after the microwave digestion ($\boldsymbol{R_{MW}}$) results in the Al organ burden per gram organ:

$$\boldsymbol{c(Al)} = \left[\left(\left[\boldsymbol{Int_{sample,\,corr}}/\boldsymbol{S_{matrix}}\right]\right)/\boldsymbol{m_{org}}\right]/\boldsymbol{R_{MW}} \tag{4}$$

LOD and LOQ were determined using the blank value method[43]. The data of the control group (5 animals) were used for the determination of the lowest detectable signal. The intensities obtained were converted into concentrations using the matrix calibrations (Table 2). The data for the different groups did not follow a normal distribution. Therefore, median and interquartile ranges (IQR) of the control group for each organ were used to calculate the LOD and LOQ. A 1.5 × IQR corresponds to a standard deviation of 3σ:

$$\boldsymbol{LOD = Median + 1.5 * IQR} \tag{5}$$

$$\boldsymbol{LOQ = Median + 5 * IQR} \tag{6}$$

Al concentrations ($\boldsymbol{c_{Al\ NM}}$) were normalized on the $AlCl_3{\cdot}6H_2O$ concentration ($\boldsymbol{c_{AlCl_3}}$) (Figs. 3 and 4), corrected by the mass fraction of $AlCl_3{\cdot}6H_2O$ per rat ($\boldsymbol{m_{AlCl_3}}$) and the corresponding NM species ($\boldsymbol{m_{Al\ NM}}$):

$$\boldsymbol{median\ normalized\ Al\ concentration} = \frac{\boldsymbol{c_{Al\ NM} * m_{AlCl_3}}}{\boldsymbol{c_{AlCl_3} * m_{Al\ NM}}} \tag{7}$$

Therefore, the term "Al concentration" refers to the concentration of Al measured by ICP-MS. The median normalized Al concentration is only used for subsequent evaluation of Al organ burdens.

Data availability

The ICP-MS data sets can be obtained by the authors upon individual request.

Received: 29 November 2019; Accepted: 3 February 2020;
Published online: 14 February 2020

References

1. Yokel, R. A. & McNamara, P. J. Aluminium toxicokinetics: an updated minireview. *Pharmacol. Toxicol* **88**(4), 159–67 (2001).
2. Tietz, T. *et al.* Aggregated aluminium exposure: risk assessment for the general population. *Archives of Toxicology* **93**(12), 3503–3521 (2019).
3. Zhang, H. *et al.* Aluminium in food and daily dietary intake assessment from 15 food groups in Zhejiang Province, China. *Food Additives & Contaminants: Part B* **9**(2), 73–78 (2016).
4. Stahl, T. *et al.* Migration of aluminum from food contact materials to food—a health risk for consumers? Part I of III: exposure to aluminum, release of aluminum, tolerable weekly intake (TWI), toxicological effects of aluminum, study design, and methods. *Environmental Sciences Europe* **29**(1), 19 (2017).
5. Gupta, V. K., Agarwal, S. & Saleh, T. A. Synthesis and characterization of alumina-coated carbon nanotubes and their application for lead removal. *Journal of Hazardous Materials* **185**(1), 17–23 (2011).
6. Seo, J. *et al.* Hierarchical and Multifunctional Three-Dimensional Network of Carbon Nanotubes for Microfluidic Applications. *Advanced Materials* **24**(15), 1975–1979 (2012).
7. Saiyed, S. M. & Yokel, R. A. Aluminium content of some foods and food products in the USA, with aluminium food additives. *Food Additives and Contaminants* **22**(3), 234–244 (2005).
8. Asimakopoulos, A. G. *et al. Colour Additives for Foods and Beverages*, ed. Scotter, M. United Kingdom: Elsevier Science & Technology. 260 (2015).
9. Sieg, H. *et al.* Impact of an Artificial Digestion Procedure on Aluminum-Containing Nanomaterials. *Langmuir* **33**(40), 10726–10735 (2017).
10. Crapper, D. R., Krishnan, S. S. & Dalton, A. J. Brain Aluminum Distribution in Alzheimers Disease and Experimental Neurofibrillary Degeneration. *Science* **180**(4085), 511–513 (1973).
11. Lukiw, W. J. *et al.* Aluminum in neurological disease - a 36 year multicenter study. *J Alzheimers Dis Parkinsonism*, **8**(6) (2019).
12. Bushinsky, D. A. Bone disease in moderate renal failure: Cause, nature, and prevention. *Annual Review of Medicine* **48**, 167–176 (1997).
13. Crapper McLachlan, D. R. *et al.* Intramuscular desferrioxamine in patients with Alzheimer's disease. *Lancet* **337**(8753), 1304–8 (1991).
14. Rodriguez, J. & Mandalunis, P. M. A Review of Metal Exposure and Its Effects on Bone Health. *J. Toxicol* **2018**, 4854152 (2018).
15. Dunea, G. *et al.* Role of Aluminum in Dialysis Dementia. *Annals of Internal Medicine* **88**(4), 502–504 (1978).
16. Seidowsky, A. *et al.* Aluminic intoxication in chronic hemodialysis. A diagnosis rarely evoked nowadays. Clinical case and review of the literature. *Nephrologie & Therapeutique* **14**(1), 35–41 (2018).
17. Krewski, D. *et al.* Human health risk assessment for aluminium, aluminium oxide, and aluminium hydroxide. *Journal of Toxicology and Environmental Health-Part B-Critical Reviews* **10**, 1–269 (2007).
18. JECFA, *Evaluation of certain food additives and contaminants*. World Health Organization. p. 7–17 (2011).
19. EFSA. Scientific Opinion of the Panel on Food Additives, Flavourings, Processing Aids and Food Contact Materials on a request from European commission on Safety of aluminium from dietary intake. *EFSA Journal* **6**(7), 1–34 (2008).
20. Laux, P. *et al.* Nanomaterials: certain aspects of application, risk assessment and risk communication. *Archives of Toxicology* **92**(1), 121–141 (2018).
21. Moores, A. & Goettmann, F. The plasmon band in noble metal nanoparticles: an introduction to theory and applications. *New Journal of Chemistry* **30**(8), 1121–1132 (2006).
22. Kelly, K. L. *et al.* The optical properties of metal nanoparticles: The influence of size, shape, and dielectric environment. *Journal of Physical Chemistry B* **107**(3), 668–677 (2003).
23. Brown, D. M. *et al.* Size-dependent proinflammatory effects of ultrafine polystyrene particles: A role for surface area and oxidative stress in the enhanced activity of ultrafines. *Toxicology and Applied Pharmacology* **175**(3), 191–199 (2001).
24. Hussain, S. *et al.* Oxidative stress and proinflammatory effects of carbon black and titanium dioxide nanoparticles: Role of particle surface area and internalized amount. *Toxicology* **260**(1–3), 142–149 (2009).
25. Greger, J. L., Chang, M. M. & Macneil, G. G. Tissue Turnover of Aluminum and Ga-67 - Effect of Iron Status. *Proceedings of the Society for Experimental Biology and Medicine* **207**(1), 89–96 (1994).
26. Greger, J. L. & Radzanowski, G. M. Tissue Aluminum Distribution in Growing, Mature and Aging Rats - Relationship to Changes in Gut, Kidney and Bone Metabolism. *Food and Chemical Toxicology* **33**(10), 867–875 (1995).
27. Yokel, R. A. *et al.* Entry, half-life, and desferrioxamine-accelerated clearance of brain aluminum after a single Al-26 exposure. *Toxicological Sciences* **64**(1), 77–82 (2001).

28. Jouhanneau, P. *et al*. Gastrointestinal absorption, tissue retention, and urinary excretion of dietary aluminum in rats determined by using Al-26. *Clinical Chemistry* **43**(6), 1023–1028 (1997).
29. Gerotto, M. *et al*. Interference Effects and Their Control in ICP-MS Analysis of Serum and Saline Solutions. *Microchemical Journal* **51**(1), 73–87 (1995).
30. Krause, B. *et al*. Characterization of aluminum, aluminum oxide and titanium dioxide nanomaterials using a combination of methods for particle surface and size analysis. *Rsc Advances* **8**(26), 14377–14388 (2018).
31. Holm, S. A Simple Sequentially Rejective Multiple Test Procedure. *Scandinavian Journal of Statistics* **6**(2), 65–70 (1979).
32. Chen, X. Matrix effects in inductively coupled plasma mass spectrometry. (1995).
33. Pauluhn, J. Pulmonary Toxicity and Fate of Agglomerated 10 and 40 nm Aluminum Oxyhydroxides following 4-Week Inhalation Exposure of Rats: Toxic Effects are Determined by Agglomerated, not Primary Particle Size. *Toxicological Sciences* **109**(1), 152–167 (2009).
34. des Rieux, A. *et al*. Nanoparticles as potential oral delivery systems of proteins and vaccines: A mechanistic approach. *Journal of Controlled Release* **116**(1), 1–27 (2006).
35. Lundquist, P. & Artursson, P. Oral absorption of peptides and nanoparticles across the human intestine: Opportunities, limitations and studies in human tissues. *Advanced Drug Delivery Reviews* **106**, 256–276 (2016).
36. Banerjee, A. *et al*. Role of nanoparticle size, shape and surface chemistry in oral drug delivery. *Journal of Controlled Release* **238**, 176–185 (2016).
37. Foroozandeh, P. & Aziz, A. A. Insight into Cellular Uptake and Intracellular Trafficking of Nanoparticles. *Nanoscale Research Letters*, **13** (2018).
38. Zhao, Y.T. *et al*. A comparison between sphere and rod nanoparticles regarding their *in vivo* biological behavior and pharmacokinetics. *Scientific Reports* **7** (2017).
39. Fadeel, B. *et al*. Keeping it real: The importance of material characterization in nanotoxicology. *Biochemical and Biophysical Research Communications* **468**(3), 498–503 (2015).
40. Sieg, H. *et al*. Uptake and molecular impact of aluminum-containing nanomaterials on human intestinal caco-2 cells. *Nanotoxicology* **12**(9), 992–1013 (2018).
41. Park, E. J. *et al*. A 13-week repeated-dose oral toxicity and bioaccumulation of aluminum oxide nanoparticles in mice. *Archives of Toxicology* **89**(3), 371–379 (2015).
42. Prabhakar, P. V. *et al*. Oxidative stress induced by aluminum oxide nanomaterials after acute oral treatment in Wistar rats. *J. Appl. Toxicol* **32**(6), 436–45 (2012).
43. Harrington, J. M. *et al*. Validation of a Metallomics Analysis of Placenta Tissue by Inductively-Coupled Plasma Mass Spectrometry. *Biological Trace Element Research* **169**(2), 164–173 (2016).

Acknowledgements

The French-German bilateral project SolNanoTOX was funded by the German Research Foundation (DFG, Project ID: DFG (FKZ LA 3411/1-1 and LA 1177/9-1) and the French National Research Agency (ANR, Project ID: ANR-13-IS10-0005). The BfR provided intramural support SFP1322-642 for F.L.K. and A.L.

Author contributions

V.F., J.T., H.J., P.L. and A.L. designed and supervised the study. B.K., N.D. and P.J. planned the experiments. P.J. performed the *in vivo* study. B.K., F.L.K. and N.D. analysed the ICP-MS samples. F.L.K., B.K. and D.R. evaluated the data and drafted the manuscript. D.R. designed the figures with contributions from B.K. and F.L.K. V.F., P.L., J.T., H.J. and A.L. revised and finalized the manuscript. All authors reviewed and approved the final manuscript.

Competing interests

The authors declare no competing interests.

Additional information

Supplementary information is available for this paper at https://doi.org/10.1038/s41598-020-59710-z.

Correspondence and requests for materials should be addressed to B.C.K.

Reprints and permissions information is available at www.nature.com/reprints.

Publisher's note Springer Nature remains neutral with regard to jurisdictional claims in published maps and institutional affiliations.

4. Discussion

The oral uptake of NPs is a very complex process. As they pass through the various compartments of the gastrointestinal tract, NPs undergo various changes. Both, the constantly changing biological compounds present, which allow particle interactions, and strong changes in pH influence important particle properties such as surface area, agglomeration behavior and solubility. By combining different techniques and approaches, important insights into oral bioavailability and distribution of NPs in tissue can be obtained. One of the basic requirements for almost all NP-related questions is a detailed and comprehensive characterization of NPs. The following section discusses this relationship in more detail.

4.1 Characterization of Al and Al_2O_3 NPs

Since the specific properties of NPs depend on their physicochemical characteristics, which in turn influence their toxicity as well as their behavior and interactions with the environment, conclusions about NPs are not possible without their detailed characterization. There are many different techniques for the analysis and characterization of NPs. However, most of these techniques can usually only determine very specific properties of the NPs. So far, there is no universal technique available that can analyze all important particle parameters. As a result, it is necessary to use a combination of different techniques to cover as many parameters as possible. The respective advantages and disadvantages of the individual techniques must be considered. In this thesis the advantages of complementary techniques are demonstrated. Furthermore, a guideline for the characterization of different parameters such as size, surface area and solubility was developed (see chapter 3.1).

One of the most frequently investigated properties for risk and toxicological assessment is the size [128]. One reason for this is that most NP definitions are related to the size of the NPs. In addition, the size is responsible for various nanoparticle-specific properties such as increased reactivity and changed optical properties. Different sizing techniques determine various types of particle size. For example the hydrodynamic diameter, describes the effective diameter in the solution containing all H_2O molecules present in its hydration sphere [202]. Frequently used techniques are DLS and NTA, which on the one hand can give fast indications for particle size, size distribution and hydrodynamic diameter, but on the other hand quickly reach their

limits for more complex and polydisperse samples. Especially DLS with its intensity-weighted data will emphasize the larger fractions of polydisperse samples. Therefore, often other sizing techniques are used to obtain a more comprehensive characterization of NPs.

Another possibility of size characterization is the focus on the particle core without considering surrounding molecules or interactions on its surface. The so-called primary particle size can be determined by different techniques, like TEM, SEM or SAXS. Like for other techniques, advantages and disadvantages of these techniques need to be considered when choosing the appropriate techniques for a given problem. TEM can only measure dried samples, which makes it impractical for *in situ* measurements and does not allow measurements of particles in biological fluids. Furthermore, the drying process can influence the agglomeration behavior of the NPs. Although image analysis software exists [203], irregular shaped particles are difficult to interpret and therefore require manual evaluation. This leads to a time-consuming procedure, which is often considered statistically weak, as only a partial section of the sample can be examined [203]. Nevertheless, TEM is often considered the gold standard of size characterization techniques because the imaging method can determine both the size and shape of the particles very accurately. In addition, chemical information on the composition of NPs can be obtained with appropriate extensions of the TEM (EDX, EELS). Compared to TEM, SAXS can analyze a broader variety of different sample types and easily used for *in situ* measurements. However, SAXS requires some information on the sample, for example the shape from complementary techniques like TEM (see chapter 3.1). It therefore points out the benefit of using complementary techniques for NP characterization.

Another interesting technique for primary particle size determination is SP-ICP-MS. Since ICP-MS, in contrast to classical TEM and SAXS, represents an element-specific technique, the differentiation of NPs from proteins is much easier. In addition, NP mixtures of different elemental composition can be analyzed consecutively. Also, an indication of the ionic content of the specific element can be achieved, which gives further information about the solubility of NPs.

The obtained results describe the different principles of size determination techniques and

highlight the advantages of using complementary techniques for the verification of the results whenever possible (see chapter 3.1).

Particle surface is a further important characteristic when investigating NPs, as it impacts the solubility of NPs in complex media. For its analysis mostly X-ray and electron-based techniques like XRD and TEM are used to gather information on the surface (see chapter 3.1). XRD not only confirmed a thin aluminum oxide layer on the metallic Al^0 NPs, but also proved differences between the surface of Al^0 and Al_2O_3 NPs. These differences could be confirmed and visualized by TEM in combination with EELS. Based on these results, a different solubility of both Al-containing NPs was expected, as the thin aluminum oxide layer is much more likely broken up and may release Al ions. Compared to Al_2O_3 bulk material the respective NPs should still show a higher solubility, as due to their high specific surface area, much more Al ions are present at the surface.

An additional property, which influences the solubility of NPs, is particle composition. Besides the described techniques for surface investigation, ICP-MS can be applied for the determination of unknown as well as for confirmation of a known particle composition. ICP-MS is very commonly used due to its high sensitivity which is beneficial when small samples with low concentrations must be analyzed. Furthermore, it is element-specific, in contrast to other characterizing techniques like DLS, NTA or SAXS and TEM without elemental additions. Its multi-element analysis allows not only a fast determination of NP composition but is also capable of the detection of impurities of the NPs which may alter their behavior and the toxicity of a NP.

For Al, the oral uptake route is the most relevant [54]. Since Al is ubiquitous in the human environment, a high uptake also via food occurs, resulting in regular exceeding of the tolerable intake values [43]. Hence, the investigation of the Al solubility behavior after oral uptake is of paramount importance. The solubility of NPs is a crucial parameter for characterization and risk assessment. It is strongly pH dependent, where low or high pH values result in a higher solubility than neutral ones [127, 204]. During the characterization, the solubility of amphoteric Al was investigated (see chapter 3.1). At pH values close to many biological environments, a very low solubility of both, Al^0 and Al_2O_3 NPs, was detected. However, in an acidic environment, like the stomach, the solubility is expected to be higher. On the other

hand, the intestine with its more neutral or slightly basic pH values was expected to lead to lower solubility. It must be considered, that due to the complex mixture of enzymes, proteins, and salts, the dissolution behavior of the NPs can still differ significantly from the one observed for the pristine NPs (see chapter 3.1).

In biological samples, where complex matrices are present, the elucidation of particle-biological samples interactions is very important to draw conclusions on NP solubility. Two techniques were used to investigate different aspects of these interactions (see chapter 3.1). Using ion beam microscopy (IBM), an increased adsorption of calcium and phosphorus could be observed in the aluminum-containing NPs in cell culture medium. It is suspected that calcium and phosphorus ions form a calcium phosphate layer on the particle surface because calcium phosphate has a high affinity to the corona proteins of the NPs. With ToF-SIMS further particle interactions could be shown. Especially interactions of the two Al NPs with different amino acids proved that Al^0 and Al_2O_3 behave differently in biological environments such as cell culture media.

The physicochemical characterization of Al and Al_2O_3 NPs (as carried out in chapter 3.1) is the basis for further *in vitro* and *in vivo* experimentations. It allows the prediction and understanding of particle interactions and enables the explanation of mode of actions. Different effects, such as solubility behavior and particle-medium interactions can be explained and included in the evaluation of the *in vitro* results. These effects can be further attributed to analyzed properties like surface, shape and agglomeration behavior. Furthermore, it became evident how important it is to use more than one technique to determine physicochemical characterization parameters to verify results. In the context of oral uptake of Al-containing NPs, it remains to be clarified in further investigations how an acidic pH value affects their solubility in the stomach. The investigation of oral uptake of NPs is a specific problem that will be examined in more detail in the context of this thesis. Changing environments and complex matrices alter certain properties of the particles. To understand the uptake and related modes of actions, these changes have to be characterized separately and should be included in the evaluation. One possibility to investigate NPs after oral uptake is the use of an artificial digestion system, which was applied in the following. The *in vitro*

digestion approach offers the advantage to analytically assess the NPs whilst on passage through the different sections of the digestive system.

4.2 Fate of Al^0 and Al_2O_3 NPs – *in vitro* simulation of oral uptake

The oral uptake of NP is followed by the passage thorugh compartments with changing chemical compositions. Al-containing NPs may get modified whilst on route, resulting in dissolution, agglomeration or deagglomeration which might also impact on the bioavailability of the Al species. Eventually, those NPs reaching the intestine differ from the NPs present in the stomach. The absorption in the intestine is dependent on the solubility of the NPs, which is related to size, shape and chemical composition. However, also additional factors may change the dissolution behavior of NPs, like surface coating, protein corona composition and the biological compounds present.

Different approaches where developed and tested to mimic the conditions present in the gastrointestinal tract. More simple systems only consider the pH values and use buffered solutions to analyze the behavior of test substances [205]. More physiological relevant approaches also consider salts, digestion enzymes, proteins, bile extract and sometimes even food components [206, 207]. Such complex systems allow monitoring of NP changes during transit through the gastrointestinal tract while also giving information on the subsequent biological interactions of NPs present in the intestine. Since the biological interactions of NPs are very dependent on the solubility, both, ionic and particulate forms should be investigated.

In this thesis, an artificial digestion approach mimicking three different compartments of the oral uptake route, was applied for three different Al species. Metallic Al^0 and Al_2O_3 with similar size were used as particulate species while $AlCl_3$ was used as an ionic control for comparison. The three compartments modeled were the mouth with artificial saliva, the stomach with artificial gastric juice and the intestine with artificial intestinal fluid. With the methods discussed (see chapter 3.1), differences in solubility, size, shape, element attachment, agglomeration behavior, and stability were characterized using elemental analysis, SAXS, TEM, SP-ICP-MS, IBM, and ToF-SIMS. Special focus was given to the analysis of variations between the two particulate species and to the ionic control (see chapter 3.2).

The composition of artificial saliva is the least complex of the three tested fluids representing the digestion compartments. It is comparable to the BSA solution used for the standard dispersion of the NPs. It is not expected that the proteins, salts and compounds of the artificial saliva should change metals or metal oxides, especially given the short incubation time of 5 min. In addition, the pH, which greatly influences solubility, is nearly neutral (about 6.4), resulting in almost no dissolution of Al (as discussed in chapter 3.1). As a result, the characterization of the Al NPs in the saliva does not differ much compared to the undigested NPs after the standard dispersion (see chapter 3.1 and 3.2). Neither agglomeration, nor dissolution of the two Al-containing NPs was detectable in artificial saliva. To verify the result, several of the methods discussed in chapter 3.1, like TEM, SAXS and SP-ICP-MS, were applied additionally. Neither imaging (TEM) nor counting (SAXS, SP-ICP-MS) techniques detected the *de novo* formation of NPs which might originate from free ions in the solution.

Since this artificial digestion approach is a consecutive model, as a next step the artificial gastric fluid is added to the artificial saliva containing the NPs. The mixture gets more complex with additional proteins, enzymes and salts. Additionally, the pH is adjusted to approximately two. Based on literature on silver and silica NPs, an agglomeration of the Al NPs was expected [208, 209]. One explanation could be the electrostatic destabilization based on the low pH values in gastric fluids. For more soluble NPs like silver and zinc oxide, there was also an increased ion release shown in artificial gastric fluid [207, 210]. Both, the agglomeration and the increased ion release was also detected for Al-containing NPs (see chapter 3.2). The techniques used in chapter 3.1, TEM and SAXS, again showed comparable results for agglomeration of the NPs, which was also confirmed by ToF-SIMS. Analysis by SP-ICP-MS, gave supportive evidence, demonstrating the disappearance of nanoscaled particles up to 200 nm. The conventional ICP-MS detected ion release for both Al-containing NPs. Compared to the ion release in the BSA dispersion solutions discussed in chapter 3.1, the dissolution was significantly higher. However, compared to soluble NPs like ZnO, the ion release was much lower. Therefore the solubility of Al-containing NPs in artificial gastric fluid seems to be of lesser importance for the bioavailability [210]. Considering the unalike characteristics for Al and Al_2O_3 NPs (as determined in chapter 3.1), a difference in the capacity to release ions in

artificial gastric fluid. Indeed, Al NPs released more Al than Al_2O_3 NPs. Based on the TEM measurements (see chapter 3.1), the core-shell-structure of Al NPs seems to be more affected by the acidic environment than the fully oxidized Al_2O_3 NPs. For free Al ions it is well established that they readily bind to or even form complexes with proteins or other chemically suitable compounds if available (e.g. food or biological compounds in the intestine) [35, 211, 212]. While this is not necessarily associated with increased toxicity [208], it has been shown that increased cellular particle uptake can occur based on the composition of the artificial fluids and the compounds they contain [207].

As a final step of the digestion approach, artificial intestinal fluid is added. Various compounds like salts, enzymes and bile extract are added and also the pH was adjusted to 7.5. All techniques that were used for particle size and agglomeration state determination, namely TEM, SAXS, SP-ICP-MS and ToF-SIMS, showed comparable results to the previously measured data in saliva. These findings suggest that the three observed Al species, Al and Al_2O_3 NPs as well as the ionic $AlCl_3$, partly occur in nanoparticulate form in the intestine. Analysis by ICP-MS demonstrated a significant decrease in the amount of free Al ions, not only for the two NP species, but also for the ionic $AlCl_3$. ToF-SIMS revealed the formation of different complexes of the two Al-containing NP species in cell culture medium (see chapter 3.1), which has a similar pH value and a broad variety of biological compounds present and therefore resembles artificial intestinal juice partly. In addition, for ionic $AlCl_3$ nanoscaled structures were discovered in the intestinal fluid. TEM measurements indicated nanoscaled particle-like structures with varying shapes and densities compared to the two particulate species Al and Al_2O_3. These findings were confirmed by ToF-SIMS. With this complementary technique agglomerates derived from $AlCl_3$ samples were also detected that were not present in the saliva or the gastric fluid. Furthermore, the technique also confirmed that the detected agglomerates contain Al, while IBM showed colocalization of Al with sulfur. The detected sulfur supports the working hypothesis, that these particles originate from precipitation of Al with proteins in the nanoscale range. The *de novo* formation of particles in the intestinal fluid was demonstrated experimentally for different Al species (see chapter 3.2). Taking both the physicochemical similarities of different metals and also their affinity to biological compounds

into consideration, it is tempting to speculate that also other metals might form *de novo* particles under similar conditions.

The *de novo* formed Al-protein structures were not detectable by SP-ICP-MS. The detection limit of the SP-ICP-MS for Al is between 50-80 nm, depending on the complexity of the matrix and the ionic background present. SAXS showed a particle size distribution with a volume-weighted mean radius of 2.9 nm for the particle population formed *de novo* [134]. The primary particle size is therefore much lower than the detection limit of the SP-ICP-MS in this digestion approach. This finding clearly demonstrates that the use of complementary techniques is crucial to enable a comprehensive and thorough characterization, especially when complex samples and matrices are involved.

The characterization of NPs along the oral uptake route is key to identify and understand the fate and changes NPs undergo when in contact with biological material. That data should also help to gain more insight into the toxicological potential of NPs. The most important discovery was the finding that the applied Al species underwent different conformational transitions resulting in a mixture of ionic, particulate and agglomerated species (see chapter 3.2). The mutual conversion of NPs and dissolved ions can complicate the attribution of toxicological effects to particles or ions. While the *in vitro* approach can provide information on the solubility, agglomeration, conversion and new formation of NPs and ions in the gastrointestinal tract, important parameters such as oral bioavailability or tissue distribution cannot adequately be addressed with this basic system. Therefore, an *in vivo* study was performed to elucidate whether the observed physio-chemical differences between Al and Al_2O_3 NP found (see chapters 3.1 and 3.2) would result in e.g. diverse tissue distribution pattern after oral uptake.

4.3 Oral bioavailability and distribution of Al and Al_2O_3 NPs *in vivo*

For the evaluation of the oral uptake of NPs, the oral bioavailability and the distribution in systemic organs are of major importance. With its high abundance and attributed adverse effects, Al is a relevant element for investigation of the oral uptake. Although an extensive characterization of Al and Al_2O_3 NPs (see chapter 3.1) as well as a discussion of their fate and transformation (see chapter 3.2) was carried out, that data is insufficient to allow for an extrapolation with respect to oral bioavailability and systemic distribution. In order to get a

better understanding, a three-day oral gavage study on Sprague Dawley rats was conducted (see chapter 3.3). ICP-MS was used to analyze the Al content of selected organs. That this technique can be successfully employed to determine the ion release in NP dispersions and for measuring the dissolution of Al and Al_2O_3 NPs during the three artificial digestion steps was already demonstrated (see chapter 3.1 and 3.2). However, the complexity of the matrix plays a key role for ICP-MS measurements. *In vivo*, the matrix differs for every organ, and therefore needs to be considered for a reliable quantification of Al amounts in the investigated organs. The matrix can influence the analyte detection by either suppression or enhancement of the signal. Hence, particular attention was paid on how the sample matrix affects the calibration procedure during this *in vivo* study (see chapter 3.3).

The three Al species applied in the *in vivo* study were extensively characterized and discussed (see chapters 3.1 and 3.2). Tissue distribution of the three species were evaluated by quantification of Al in duodenum, colon, blood, liver, kidney and spleen. Due to the ubiquitous presence of Al causing a high background level in the tissues of the animals the quantification of Al amounts was challenging and new approach needed to be implemented. To overcome this hurdle, a robust calibration methodology considering matrix effects was developed. While the calibration in water showed higher sensitivity compared to matrix calibrations, the matrix affected the analyte sensitivity by signal depression, indicating the necessity for a matrix correction. High matrix load samples can also cause interferences by deposition of solid matrix on the ICP-MS apertures [213]. By using the developed matrix calibration, it was possible to detect and quantify even very low Al concentrations in tissue samples and distinguish them from the background. The disadvantages of a matrix calibration are a high analytical effort and an increased number of animals. Therefore, a daily response factor (DRF) was introduced for this study. This allows correcting daily measurement fluctuations as well as matrix effects which arise from the biological samples. The results led to the recommendation to use a matrix calibration in combination with a DRF in case of matrix interferences to reduce the analytical effort and still obtain reliable results.

One key discovery of this study was the finding that Al is bioavailable and distributes in organs after oral exposure. For the three Al species tested (Al, Al_2O_3 and ionic $AlCl_3$), Al was detected

in all investigated organs (see chapter 3.3). In contrast, a previous inhalation study showed no significant systemic organ burden despite high lung burdens [214]. Another interesting observation were specific differences in the distribution between Al and Al_2O_3 NPs compared to the ionic $AlCl_3$. This may not be so surprising given the results of characterization and artificial digestion behavior (see chapters 3.1 and 3.2).

The distribution of Al NPs between intestine and systemic organs after gavage was rather comparable to the ionic $AlCl_3$ control. Al_2O_3 NPs on the other hand differed significantly in their distribution. These results are an indication that NP with the same metallic component can nevertheless have a different agglomeration behavior *in vivo*. In addition, a dose-dependent decrease of Al levels in systemic organs was observed for increased Al_2O_3 NP concentrations. A possible explanation can be an impairment of the intestinal barrier function, leading to accumulation of the NPs in the intestine. Based on characterization results of Al and Al_2O_3 NPs (chapter 3.1) agglomeration behavior, different agglomeration states of both particle species could be one reason for the different uptake and distribution in the intestine. Therefore, the agglomeration state should be considered for oral uptake assessment [215, 216].

Shape seems to be another key parameter for distribution of NPs in tissue. Despite their same nominal particle size, Al and Al_2O_3 NPs showed a difference in shape when analyzed by TEM (see chapter 3.1). While Al NPs were almost spherical, Al_2O_3 NPs were more rod-like. During the *in vivo* study, higher concentrations of the rod-shaped Al_2O_3 NPs compared to the spherical Al NPs were detected in the investigated organs. This fits nicely with the literature, were studies addressing the uptake of polystyrene NPs in Caco-2 cells showed a comparable behavior [217], but this is not always confirmed [218]. The shape may also affect the time required for uptake as well as excretion of the NPs, which could explain the lower Al concentrations found for Al NPs treated rats after three days. An *in vivo* study on SiO_2 NPs showed higher concentrations of spherical particles after 2 and 24 h, but higher concentrations for rod-shaped NPs after 7 days [219].

Another important parameter is surface composition, which was already extensively investigated (see chapter 3.1). With TEM and XRD, the differences between Al and Al_2O_3 NPs

in their surface composition were revealed. Element-specific TEM determined the core-shell structure of Al NPs demonstrating an Al core and a thin Al oxide layer of 2-5 nm due to passivation in the manufacturing process. Al_2O_3 NPs showed a fully oxidized structure with a rather homogenous looking Al and oxygen distribution on the surface. An *in vitro* study with the same Al species showed that the formed protein corona in cell culture medium for Al is less complex than for Al_2O_3 NP [220]. Different interactions of the surface with the environment influence bioavailability and tissue retention of NPs.

Ionic $AlCl_3$ showed a comparable uptake behavior to Al NPs. The investigations of the *de novo* particle formation revealed a comparable low solubility of these new formed structures (see chapter 3.2), which could be a reason for the almost identical uptake behavior of Al NPs and ionic $AlCl_3$. Additional *in vitro* results from intestinal culture models incubated with the different Al species suggested no major differences between Al and Al_2O_3 NPs and ionic $AlCl_3$ [220]. In the *in vivo* study however, only the distribution pattern between Al and Al_2O_3 NPs was similar while significant differences in the Al concentrations were detected (chapter 3.3). This highlights the limitations of *in vitro* studies, as the uptake process is much more complex and influenced by different processes occurring in living organisms, thus still needing *in vivo* studies to a certain degree.

When considering the mass fraction of Al in the different species, it became apparent that ionic $AlCl_3$ with the lowest mass fraction three species tested was taken up to a higher degree than both particulate forms. This finding could be explained by higher permeability of the intestinal barrier for ions compared to particles. With larger agglomerates of NPs, the crossing of particles gets more and more unlikely. However, when comparing both NP species, Al_2O_3 NPs, which have a lower mass fraction of Al than Al NPs, led to higher Al accumulation in the organs.

The duodenum and colon are part of the small and large intestine, but the Al accumulation of both particulate Al species differed significantly. Based on the results obtained during the artificial digestion approach (see chapter 3.2), one can expect a different behavior of the two particulate forms at different pH values. While the duodenum forms the transition from the stomach to the small intestine, the colon is a part of the large intestine. Therefore, the pH in

the duodenum is still acidic, whereas it is already in the alkaline range in the colon. In the artificial digestion simulation (chapter 3.2), pH differences led to a significant change in agglomeration behavior.

Besides the intestinal and other organs, the element concentration in blood is an interesting parameter when evaluating the bioavailability and distribution of NPs. Especially for Al it is known, that it can associate with transferrin and other plasma proteins or low molecular weight fractions [35]. Interestingly, the ionic $AlCl_3$ showed the lowest concentrations of all three Al species in the conducted *in vivo* study (see chapter 3.3). While for the highest dose of Al NPs the concentration was only slightly higher, it was up to 100 times higher for Al_2O_3 NPs. Relating these findings to the already discussed low solubility of Al and Al_2O_3 NPs at nearly neutral pH (see chapters 3.1 and 3.2), it can be assumed, that also particulate Al was transported by blood. However, due to specific protein corona formation, it may be retained longer in the blood.

In summary, a rapid absorption and distribution of Al for all the species tested was determined after three-day oral gavage. Data for composition, shape, surface composition and agglomeration state suggested that those parameters influence the uptake of similar sized NPs. Furthermore, an important difference between Al and Al_2O_3 uptake in the investigated organs was detected, which is contrary to *in vitro* uptake studies in intestinal and hepatic cell lines. This challenges extrapolation of NP behavior based only on one or few physicochemical parameters.

In addition, also a calibration approach was developed and implemented to enable reliable detection of low concentrations of Al in complex matrices that are challenged with high background interferences.

5. Conclusion and Outlook

Any testing of the toxicological potential of NPs should be accompanied by a comprehensive characterization of NPs in different states, from dispersion to the *in vitro* environment. The first part of this thesis therefore dealt with the exemplary characterization of two NP, one metallic and one metal oxide, of similar size. Using a wide range of complementary analytical methods, key parameters such as particle size, surface area and composition were determined in detail and confirmed. The dissolution represents one of the most important determinants of NP toxicity, since it gives insight into their behavior in the respective biological environment. Dissolution investigation of Al NPs revealed a very low dissolution rate and a small percentage of ion release at neutral pH. In-depth investigations of the surface of both, Al and Al_2O_3 NPs, identified a significant difference in the extent of oxidation and surface composition. Al NPs showed a core-shell structure with an only few nm thick Al oxide layer, while Al_2O_3 NPs were fully oxidized with a rather homogenous distribution of Al and oxygen. This key finding gave a first hint for the differences between both similar composed particles and led to the working hypothesis, that also the behavior and fate after oral exposure would differ significantly. This was confirmed by XRD and EELS measurements, highlighting the benefit of using different techniques to obtain reliable results. ToF-SIMS measurements revealed further differences between Al and Al_2O_3 NPs. Both NPs showed a different complexation in biological media. Al NPs formed complexes with amino acids, while Al_2O_3 NPs mostly showed polyoxo-complexes out of two or more Al_2O_3 molecules. The obtained results demonstrated that all applied methods had their own specific advantages. The application of combined techniques as presented here enables a better prediction of the solubility behavior of NPs. The results from the first part of this thesis underline the necessity to distinguish between various forms of Al. As demonstrated, the different species of Al can be absorbed, distributed differently and also undergo altered reactions. I*n vitro* models can simulate important properties, for example the biological surrounding or the pH, to gain more insights in the processes occurring after oral exposure. An artificial digestion approach was therefore applied in the second part of this thesis, to identify potential differences in physicochemical properties with regard to different compartments of the gastrointestinal tract.

The oral uptake route is the most relevant for Al. Within the gastrointestinal tract, NPs can be subject to various changes that alter their bioavailability, distribution and interactions with the environment. Therefore, the second part of this thesis focused on the investigation of NPs at different steps of the oral uptake by simulating the gastrointestinal tract with the help of an artificial digestion approach. Three different compartments of the oral uptake route, saliva, stomach and intestine, were simulated and separately investigated. Almost no effects were observed in saliva, most likely due to the nearly neutral pH value and the short time of passage. In the gastric fluid, both Al and Al_2O_3 NPs agglomerated while also showing a higher ion release compared to saliva. The intestine lead to a deagglomeration of the formed agglomerates from gastric fluid. In addition, ions released from the Al species formed solid complexes with biological compounds. While these complexes proved to be nanoscaled, they showed differences in size, shape and density, compared to the primary Al NPs applied at the beginning of the artificial digestion. The unknown identity of this new formed nanoscaled fraction could lead to a facilitated uptake in the organism. Due to their tendency to bind to different proteins, exchange reactions with essential proteins in the body would also be conceivable. Another key finding was the fact that particles and dissolved ions can be converted into each other. During these transformations, their surface composition can change. Once again, the broad spectrum of methods applied proved valuable for comprehensive characterization and determination of all the observed effects. The results also indicate that toxicological studies of NP species are only meaningful when the chemical and biological environment is considered. The proof of the mutual conversion of particles and ions also suggests that it may not always be possible to differentiate between particle- and ion-dependent effects in toxicological studies. For an appropriate interpretation of toxicological data, a comprehensive physicochemical characterization will be mandatory. As expected from the results of the first part of this thesis, *in vitro* investigations of the different Al species applied also showed significant differences between each other. Even processes, like *de novo* particle formation, occurred that were not predictable by the characterization results. The need to verify these differences *in vivo* was further strengthened, so that an *in vivo* study was conducted in the last part of this thesis.

Oral bioavailability and distribution are very complex processes and cannot be fully investigated *in vitro*. The third part of this thesis therefore aimed to gain insights into these processes by conducting an *in vivo* study. After a three-day oral gavage treatment, both, Al and Al_2O_3 NPs, were significantly absorbed. For all three Al species a rapid absorption and distribution in the investigated organs could be demonstrated. However, some differences between Al and Al_2O_3 NPs were found, indicating that shape, agglomeration behavior and surface composition have an influence on particle accumulation. While in in vitro experiments no differences in the uptake of Al and Al_2O_3 could be shown, higher amounts of Al were found in the investigated organs and blood in animals treated with Al_2O_3 NPs. These differences suggest a complication when extrapolating NP accumulation, even for similar chemical composed materials. Regarding the ionic $AlCl_3$ control, there was an interesting difference in blood retention time, which led to increased Al levels in the blood for Al_2O_3 NPs. In addition to the already known difficulties in the determination of Al in biological samples, the low-dose design of the study led to further challenges for ICP-MS detection. In order to reduce the number of animals for biokinetic studies, a matrix calibration approach was developed. The approach improved the sensitivity and robustness of the method. Combined with a DRF, a superior performance compared to standard water calibration was achieved. At the same time, this approach also eliminated day to day variations on the calibration. This resulted in a reliable quantification of all Al organ burdens even in the low µg/g range. With the results of the third part of this thesis, an improvement of data quality for evaluation of low dose studies could be demonstrated. Using a DRF for data evaluation enabled robust data evaluation. In parallel, significant differences in oral bioavailability and the distribution of the two NPs in blood and organs were detected.

Currently, the recommended limit for aluminum release from food does not take into account the differentiation of various forms of aluminum, e.g., ions, micro- and nanomaterials. Future analytical investigations on aluminum-containing NPs should not only consider the widely used Al_2O_3 but also metallic Al NPs and include their interaction with the corresponding ions.

The results of all three parts of this thesis, the characterization (chapter 3.1), the artificial digestion simulation (chapter 3.2) and the oral bioavailability and distribution investigations

in vivo (chapter 3.3) strengthen the assumption, that physicochemical characteristics like composition, shape, aggregation state and surface composition affect the kinetics of NPs significantly. While it is not possible to classify different types of NPs only by their size, further physicochemical characteristics need to be taken into account in order to facilitate the prediction of NP behavior. Specific scenarios, for example the oral uptake of NPs, need their own characterization approach considering the respective chemical and biological environments.

In conclusion a distinction must be made between different forms of Al, such as ionic or nanoparticulate species when:

- Evaluating Al toxicity after oral intake
- Establishing reference values
- Planning future toxicological studies

The solubility of NPs should be considered as an important endpoint in NP risk assessment and needs to be analyzed by appropriate methods.

6. Literature

1. Krewski, D., et al., *Human health risk assessment for aluminium, aluminium oxide, and aluminium hydroxide.* Journal of Toxicology and Environmental Health-Part B-Critical Reviews, 2007. **10**: p. 1-269.
2. McLachlan, R., et al., *Micro Reform -- Impacts on Firms: Aluminium Case Study*. 1998: Industry Commission.
3. Hind, A.R., S.K. Bhargava, and S.C. Grocott, *The surface chemistry of Bayer process solids: a review.* Colloids and Surfaces a-Physicochemical and Engineering Aspects, 1999. **146**(1-3): p. 359-374.
4. Totten, G.E. and D.S. MacKenzie, *Handbook of aluminum*. 2003, New York; Basel: M. Dekker.
5. Committee, T.G.A.R., *Global Aluminium Recycling: A Cornerstone of Sustainable Development*. 2009, International Aluminium Institute.
6. Association, T.A., *Aluminum: The Element of Sustainability*. 2011.
7. IAI. *Primary Aluminium Production in 2018*. 2019 [cited 2019 8th august]; Available from: http://www.world-aluminium.org/statistics/#map.
8. Lyle, J.P., D.A. Granger, and R.E. Sanders, *Aluminum Alloys*, in *Ullmann's Encyclopedia of Industrial Chemistry*. 2000.
9. Davis, J.R., *Aluminum and Aluminum Alloys*. 1993: ASM International.
10. Lumley, R.N., *Fundamentals of aluminium metallurgy: Production, processing and applications*. 2010. 1-843.
11. Mortensen, A., *Concise Encyclopedia of Composite Materials*. 2006: Elsevier Science.
12. Ceramic Society of Japan, T., *Advanced Ceramic Technologies & Products*. 2012.
13. Armarego, W. and C. Chai, *Purification of Laboratory Chemicals*. 2009: Butterworth-Heinemann.
14. Supp, E., *How to produce methanol from coal*. 1990, Berlin; New York: Springer-Verlag.
15. Ertl, G., H. Knözinger, and J. Weitkamp, *Preparation of Solid Catalysts*. 2008: Wiley.
16. Helmboldt, O., et al., *Aluminum Compounds, Inorganic*, in *Ullmann's Encyclopedia of Industrial Chemistry*. 2007.
17. Gupta, R.K., et al., *Adjuvant properties of aluminum and calcium compounds.* Pharm Biotechnol, 1995. **6**: p. 229-48.
18. Singh, M., *Vaccine Adjuvants and Delivery Systems*. 2007: Wiley.
19. Galbraith, A., et al., *Fundamentals of Pharmacology: A Text for Nurses and Health Professionals*. 1999, Harlow: Pearson Education The Limited.
20. Papich, M.G., *Saunders Handbook of Veterinary Drugs: Small and Large Animal*. 2015: Elsevier Health Sciences.
21. Ryan, R.S.M. and W.H. Organization, *WHO Model Formulary, 2004*. 2004: World Health Organization.
22. Gupta, R.K., *Aluminum compounds as vaccine adjuvants.* Advanced Drug Delivery Reviews, 1998. **32**(3): p. 155-172.
23. Winter, R., *A Consumerýs Dictionary of Household, Yard and Office Chemicals: Complete Information About Harmful and Desirable Chemicals Found in Everyday Home Products, Yard Poisons, and Office Polluters*. 2007: iUniverse.
24. Brown, W.G., *Reductions by Lithium Aluminum Hydride*, in *Organic Reactions*. 2011. p. 469-510.
25. Gerrans, G.C., P. Hartmann-Petersen, and R. Hartmann-Petersen, *Sasol Encyclopaedia of Science and Technology*. 2004: New Africa Education.
26. Witt, M. and H.W. Roesky, *Organoaluminum chemistry at the forefront of research and development.* Current Science, 2000. **78**(4): p. 410-430.

27. EFSA, *Scientific Opinion of the Panel on Food Additives, Flavourings, Processing Aids and Food Contact Materials on a request from European commission on Safety of aluminium from dietary intake.* EFSA Journal, 2008. **6**(7): p. 1-34.
28. COT, *Committee on toxicity of chemicals in food, consumer products and the environment (COT) - Statement on the potential risks from aluminium in the infant diet.* 2013.
29. JECFA, *Safety evaluation of certain food additives and contaminants prepared by the Seventy-fourth meeting of the Joint FAO/WHO Expert Committee on Food Additives*. Vol. 65. 2012: WHO.
30. Yokel, R.A., et al., *Aluminum citrate uptake by immortalized brain endothelial cells: implications for its blood-brain barrier transport.* Brain Research, 2002. **930**(1-2): p. 101-110.
31. Yokel, R.A., *Brain uptake, retention, and efflux of aluminum and manganese.* Environmental Health Perspectives, 2002. **110**: p. 699-704.
32. Crisponi, G., et al., *Chelating agents for human diseases related to aluminium overload.* Coordination Chemistry Reviews, 2012. **256**(1-2): p. 89-104.
33. Azik, F.M., et al., *A different interaction between parathyroid hormone, calcitriol and serum aluminum in chronic kidney disease; a pilot study.* International Urology and Nephrology, 2011. **43**(2): p. 467-470.
34. Malluche, H.H. and M.C. Faugere, *Aluminum - Toxin or Innocent Bystander in Renal Osteodystrophy.* American Journal of Kidney Diseases, 1985. **6**(5): p. 336-341.
35. Yokel, R.A. and P.J. McNamara, *Aluminium toxicokinetics: An updated MiniReview.* Pharmacology & Toxicology, 2001. **88**(4): p. 159-167.
36. Mujika, J.I., et al., *A QM/MM study of the complexes formed by aluminum and iron with serum transferrin at neutral and acidic pH.* Journal of Inorganic Biochemistry, 2011. **105**(11): p. 1446-1456.
37. Priest, N.D., *The biological behaviour and bioavailability of aluminium in man, with special reference to studies employing aluminium-26 as a tracer: review and study update.* J Environ Monit, 2004. **6**(5): p. 375-403.
38. Wu, X., et al., *The effects of glutamate and citrate on absorption and distribution of aluminum in rats.* Biol Trace Elem Res, 2012. **148**(1): p. 83-90.
39. Poirier, J., et al., *Double-blind, vehicle-controlled randomized twelve-month neurodevelopmental toxicity study of common aluminum salts in the rat.* Neuroscience, 2011. **193**: p. 338-62.
40. EFSA, *Statement of EFSA on the Evaluation of a new study related to the bioavailability of aluminium in food.* EFSA Journal, 2011. **9**(5): p. 2157.
41. Mujika, J.I., J.M. Ugalde, and X. Lopez, *Aluminum speciation in biological environments. The deprotonation of free and aluminum bound citrate in aqueous solution.* Phys Chem Chem Phys, 2012. **14**(36): p. 12465-75.
42. Crisponi, G. and V.M. Nurchi, *Thermodynamic remarks on chelating ligands for aluminium related diseases.* J Inorg Biochem, 2011. **105**(11): p. 1518-22.
43. SCHEER (Scientific Committee on Health, E.a.E.R., *Final Opinion on tolerable intake of aluminium with regards to adapting the migration limits for aluminium in toys*. 2017.
44. Draelos, Z.D., *Antiperspirants and the hyperhidrosis patient.* Dermatologic Therapy, 2001. **14**(3): p. 220-224.
45. Flarend, R., et al., *A preliminary study of the dermal absorption of aluminium from antiperspirants using aluminium-26.* Food and Chemical Toxicology, 2001. **39**(2): p. 163-168.
46. de Ligt, R., et al., *Assessment of Dermal Absorption of Aluminum from a Representative Antiperspirant Formulation Using a (26) Al Microtracer Approach.* Clin Transl Sci, 2018. **11**(6): p. 573-581.

47. Mayeux, G., E. Xhauflaire-Uhoda, and G.E. Piérard, *Patterns of aluminum hydroxychloride deposition onto the skin.* Skin Research and Technology, 2012. **18**(1): p. 64-69.
48. Willhite, C.C., et al., *Systematic review of potential health risks posed by pharmaceutical, occupational and consumer exposures to metallic and nanoscale aluminum, aluminum oxides, aluminum hydroxide and its soluble salts.* Crit Rev Toxicol, 2014. **44 Suppl 4**: p. 1-80.
49. Yanagishita, T., et al., *Histological localization of aluminum in topical aluminum chloride treatment for palmar hyperhidrosis.* Journal of Dermatological Science, 2012. **67**(1): p. 69-71.
50. Bartsch, N., *Polymer additives, contaminants and non-intentionally added substances in consumer products: Combined migration, permeation and toxicity analyses in skin*. 2019, Freie Universität Berlin: Berlin, Germany.
51. Pineau, A., et al., *In vitro study of percutaneous absorption of aluminum from antiperspirants through human skin in the Franz diffusion cell.* J Inorg Biochem, 2012. **110**: p. 21-6.
52. Guillard, O., et al., *Hyperaluminemia in a woman using an aluminum-containing antiperspirant for 4 years.* The American Journal of Medicine, 2004. **117**(12): p. 956-959.
53. Robert, A.Y., *Aluminum in Food – The Nature and Contribution of Food Additives.* 2012.
54. Tietz, T., et al., *Aggregated aluminium exposure: risk assessment for the general population.* Archives of Toxicology, 2019. **93**(12): p. 3503-3521.
55. ATSDR, *Toxicological profile for Aluminum*, P.H.S. U.S. Department of Health and Human Services, Editor. 2008, Agency for Toxic Substances and Disease Registry: Atlanta, GA.
56. Ganrot, P.O., *Metabolism and possible health effects of aluminum.* Environ Health Perspect, 1986. **65**: p. 363-441.
57. Flaherty, D.K., *Chapter 24 - Vaccines in Theory and Practice*, in *Immunology for Pharmacy*. 2012, Mosby: Saint Louis. p. 189-196.
58. Glenny, A.T., *The antigenic value of toxoid precipitated by potassium alum.* J. Pathol. Bacteriol., 1926. **29**: p. 38-45.
59. Frey, A., M.R. Neutra, and F.A. Robey, *Peptomer aluminum oxide nanoparticle conjugates as systemic and mucosal vaccine candidates: Synthesis and characterization of a conjugate derived from the C4 domain of HIV-1(MN) gp120.* Bioconjugate Chemistry, 1997. **8**(3): p. 424-433.
60. Rimaniol, A.-C., et al., *Aluminum hydroxide adjuvant induces macrophage differentiation towards a specialized antigen-presenting cell type.* Vaccine, 2004. **22**(23): p. 3127-3135.
61. Verdier, F., et al., *Aluminium assay and evaluation of the local reaction at several time points after intramuscular administration of aluminium containing vaccines in the Cynomolgus monkey.* Vaccine, 2005. **23**(11): p. 1359-1367.
62. Flarend, R.E., et al., *In vivo absorption of aluminium-containing vaccine adjuvants using 26Al.* Vaccine, 1997. **15**(12): p. 1314-1318.
63. Hem, S.L. and J.L. White, *Structure and properties of aluminum-containing adjuvants.* Pharm Biotechnol, 1995. **6**: p. 249-76.
64. Shirodkar, S., et al., *Aluminum compounds used as adjuvants in vaccines.* Pharm Res, 1990. **7**(12): p. 1282-8.
65. Darbre, P.D., *Underarm cosmetics are a cause of breast cancer.* Eur J Cancer Prev, 2001. **10**(5): p. 389-93.
66. Exley, C., et al., *Aluminium in human breast tissue.* J Inorg Biochem, 2007. **101**(9): p. 1344-6.
67. Romanowicz-Makowska, H., et al., *Concentration of cadmium, nickel and aluminium in female breast cancer.* Pol J Pathol, 2011. **62**(4): p. 257-61.
68. Mannello, F., et al., *Analysis of aluminium content and iron homeostasis in nipple aspirate fluids from healthy women and breast cancer-affected patients.* J Appl Toxicol, 2011. **31**(3): p. 262-9.

69. Oneda, S., et al., *Chronic toxicity and tumorigenicity study of aluminum potassium sulfate in B6C3F1 mice.* In Vivo, 1994. **8**(3): p. 271-8.
70. Fakri, S., A. Al-Azzawi, and N. Al-Tawil, *Antiperspirant use as a risk factor for breast cancer in Iraq.* East Mediterr Health J, 2006. **12**(3-4): p. 478-82.
71. Mirick, D.K., S. Davis, and D.B. Thomas, *Antiperspirant use and the risk of breast cancer.* J Natl Cancer Inst, 2002. **94**(20): p. 1578-80.
72. Ogoshi, K., et al., *Accumulation of aluminum in cancers of the liver, stomach, duodenum and mammary glands of rats.* J Trace Elem Electrolytes Health Dis, 1994. **8**(1): p. 27-31.
73. Romaniuk, A., et al., *Heavy metals effect on breast cancer progression.* J Occup Med Toxicol, 2017. **12**: p. 32.
74. Candy, J.M., et al., *Aluminium accumulation in relation to senile plaque and neurofibrillary tangle formation in the brains of patients with renal failure.* J Neurol Sci, 1992. **107**(2): p. 210-8.
75. Parkinson, I.S., M.K. Ward, and D.N.S. Kerr, *Dialysis Encephalopathy, Bone-Disease and Anemia - the Aluminum Intoxication Syndrome during Regular Hemodialysis.* Journal of Clinical Pathology, 1981. **34**(11): p. 1285-1294.
76. Walton, J.R., *Aluminum in hippocampal neurons from humans with Alzheimer's disease.* Neurotoxicology, 2006. **27**(3): p. 385-94.
77. BfR, *Keine Alzheimer-Gefahr durch Aluminium aus Bedarfsgegenständen - Aktualisierte gesundheitliche Bewertung Nr. 033/2007 des BfR vom 22. Juli 2007*. 2007.
78. IPCS, *Environmental Health Criteria 194 – Aluminium*, I.P.o.C. Safety., Editor. 1997.
79. Oteiza, P.I., et al., *Aluminum accumulation and neurotoxicity in Swiss-Webster mice after long-term dietary exposure to aluminum and citrate.* Metabolism, 1993. **42**(10): p. 1296-300.
80. Golub, M.S., et al., *Effects of dietary aluminum excess and manganese deficiency on neurobehavioral endpoints in adult mice.* Toxicol Appl Pharmacol, 1992. **112**(1): p. 154-60.
81. Golub, M.S. and C.L. Keen, *Effects of dietary aluminum on pubertal mice.* Neurotoxicol Teratol, 1999. **21**(5): p. 595-602.
82. Sorenson, J.R., et al., *Aluminum in the environment and human health.* Environ Health Perspect, 1974. **8**: p. 3-95.
83. Rodelsperger, K., et al., *Potential Health Risks from the Use of Fibrous Mineral Absorption Granulates.* British Journal of Industrial Medicine, 1987. **44**(5): p. 337-343.
84. Cao, H.B., et al., *Exposure and risk assessment for aluminium and heavy metals in Puerh tea.* Science of the Total Environment, 2010. **408**(14): p. 2777-2784.
85. Flaten, T.P., *Aluminium in tea - concentrations, speciation and bioavailability.* Coordination Chemistry Reviews, 2002. **228**(2): p. 385-395.
86. Dabeka, R., et al., *Lead, cadmium and aluminum in Canadian infant formulae, oral electrolytes and glucose solutions.* Food Additives and Contaminants Part a-Chemistry Analysis Control Exposure & Risk Assessment, 2011. **28**(6): p. 744-753.
87. Al-Ashmawy, M.A.M., *Prevalence and Public Health Significance of Aluminum Residues in Milk and Some Dairy Products.* Journal of Food Science, 2011. **76**(3): p. T73-T76.
88. Arnich, N., et al., *Dietary exposure to trace elements and health risk assessment in the 2nd French Total Diet Study.* Food and Chemical Toxicology, 2012. **50**(7): p. 2432-2449.
89. Millour, S., et al., *Pb, Hg, Cd, As, Sb and Al levels in foodstuffs from the 2nd French total diet study.* Food Chemistry, 2011. **126**(4): p. 1787-1799.
90. Ranau, R., J. Oehlenschlager, and H. Steinhart, *Aluminium levels of fish fillets baked and grilled in aluminium foil.* Food Chemistry, 2001. **73**(1): p. 1-6.

91. Mckinnon, A.J., R.W. Cattrall, and G.R. Scollary, *Aluminum in Wine - Its Measurement and Identification of Major Sources.* American Journal of Enology and Viticulture, 1992. **43**(2): p. 166-170.
92. EFSA, *Dietary exposure to aluminium-containing food additives.* EFSA Supporting Publications, 2013. **10**(4): p. 411E.
93. Afriyie-Gyawu, E., et al., *Chronic toxicological evaluation of dietary NovaSil clay in Sprague-Dawley rats.* Food Addit Contam, 2005. **22**(3): p. 259-69.
94. Wiles, M., et al., *Toxicological evaluation and metal bioavailability in pregnant rats following exposure to clay minerals in the diet.* J Toxicol Environ Health A, 2004. **67**(11): p. 863-74.
95. Bolle, F., et al., *Tea brewed in traditional metallic teapots as a significant source of lead, nickel and other chemical elements.* Food Additives and Contaminants Part a-Chemistry Analysis Control Exposure & Risk Assessment, 2011. **28**(9): p. 1287-1293.
96. Demont, M., et al., *Migration of 18 trace elements from ceramic food contact material: Influence of pigment, pH, nature of acid and temperature.* Food and Chemical Toxicology, 2012. **50**(3-4): p. 734-743.
97. Bohrer, D., et al., *Influence of the glass packing on the contamination of pharmaceutical products by aluminium. Part II: Amino acids for parenteral nutrition.* Journal of Trace Elements in Medicine and Biology, 2001. **15**(2-3): p. 103-108.
98. Verbeken, G., et al., *Potential release of aluminum and other metals by food-grade aluminum foil used for skin allograft cryo preservation.* Cell and Tissue Banking, 2011. **12**(3): p. 241-246.
99. Exley, C., et al., *Aluminum in tobacco and cannabis and smoking-related disease.* American Journal of Medicine, 2006. **119**(3).
100. Perl, D.P. and P.F. Good, *Uptake of aluminium into central nervous system along nasal-olfactory pathways.* Lancet, 1987. **1**(8540): p. 1028.
101. Divine, K.K., et al., *Quantitative particle-induced X-ray emission imaging of rat olfactory epithelium applied to the permeability of rat epithelium to inhaled aluminum.* Chem Res Toxicol, 1999. **12**(7): p. 575-81.
102. Exley, C., et al., *Aluminum toxicokinetics.* J Toxicol Environ Health, 1996. **48**(6): p. 569-84.
103. Friesen, M.S., R.A. Purssell, and R.D. Gair, *Aluminum toxicity following IV use of oral methadone solution.* Clin Toxicol (Phila), 2006. **44**(3): p. 307-14.
104. Da Silva, E., et al., *Aluminium and strontium in calcium supplements and antacids: a concern to haemodialysis patients?* Food Addit Contam Part A Chem Anal Control Expo Risk Assess, 2010. **27**(10): p. 1405-14.
105. Mudge, D.W., et al., *Do aluminium-based phosphate binders continue to have a role in contemporary nephrology practice?* BMC Nephrol, 2011. **12**: p. 20.
106. Cardenas, O., et al., *[Aluminium in chronic renal replacement therapy patients undergoing haemodialysis in two renal units in Bogota].* Rev Salud Publica (Bogota), 2010. **12**(4): p. 669-81.
107. Gault, P.M., K.R. Allen, and K.E. Newton, *Plasma aluminium: a redundant test for patients on dialysis?* Ann Clin Biochem, 2005. **42**(Pt 1): p. 51-4.
108. HealthCanada. *Aluminum chloride, aluminum nitrate, aluminum sulfate. Priority Substances List Assessment Report. Follow-up to the State of Science Report 2000.* 2010; Available from: https://www.canada.ca/en/environment-climate-change/services/canadian-environmental-protection-act-registry/publications/aluminum-salts-final-content/chapter-2-3.html#toc4.
109. Frankowski, M., et al., *Determination of aluminium in groundwater samples by GF-AAS, ICP-AES, ICP-MS and modelling of inorganic aluminium complexes.* Environmental Monitoring and Assessment, 2011. **182**(1-4): p. 71-84.

110. Ohno, K., et al., *Exposure assessment of metal intakes from drinking water relative to those from total diet in Japan.* Water Science and Technology, 2010. **62**(11): p. 2694-2701.
111. Horikoshi, S. and N. Serpone, *Microwaves in Nanoparticle Synthesis: Fundamentals and Applications*. 2013: Wiley.
112. Mihindukulasuriya, S.D.F. and L.T. Lim, *Nanotechnology development in food packaging: A review.* Trends in Food Science & Technology, 2014. **40**(2): p. 149-167.
113. Montazer, M. and T. Harifi, *New Approaches and Future Aspects of Antibacterial Food Packaging: From Nanoparticles Coating to Nanofibers and Nanocomposites, with Foresight to Address the Regulatory Uncertainty.* Food Packaging, 2017. **7**: p. 533-565.
114. Lotti, C., et al., *Rheological, mechanical and transport properties of blown films of high density polyethylene nanocomposites.* European Polymer Journal, 2008. **44**(5): p. 1346-1357.
115. Adame, D. and G.W. Beall, *Direct measurement of the constrained polymer region in polyamide/clay nanocomposites and the implications for gas diffusion.* Applied Clay Science, 2009. **42**(3): p. 545-552.
116. Gutiérrez, T.J., A.G. Ponce, and V.A. Alvarez, *Nano-clays from natural and modified montmorillonite with and without added blueberry extract for active and intelligent food nanopackaging materials.* Materials Chemistry and Physics, 2017. **194**: p. 283-292.
117. Greger, J.L., *Dietary and other sources of aluminium intake.* Ciba Found Symp, 1992. **169**: p. 26-35; discussion 35-49.
118. Yang, Y., et al., *Characterization of Food-Grade Titanium Dioxide: The Presence of Nanosized Particles.* Environmental Science & Technology, 2014. **48**(11): p. 6391-6400.
119. Faust, J.J., et al., *A Facile Method for Separating and Enriching Nano and Submicron Particles from Titanium Dioxide Found in Food and Pharmaceutical Products.* PLoS One, 2016. **11**(10): p. e0164712.
120. Echegoyen, Y. and C. Nerin, *Nanoparticle release from nano-silver antimicrobial food containers.* Food Chem Toxicol, 2013. **62**: p. 16-22.
121. Golja, V., et al., *Characterisation of food contact non-stick coatings containing TiO2 nanoparticles and study of their possible release into food.* Food Addit Contam Part A Chem Anal Control Expo Risk Assess, 2017. **34**(3): p. 421-433.
122. Laux, P., et al., *Nanomaterials: certain aspects of application, risk assessment and risk communication.* Archives of Toxicology, 2018. **92**(1): p. 121-141.
123. Bott, J., A. Störmer, and R. Franz, *Migration of nanoparticles from plastic packaging materials containing carbon black into foodstuffs.* Food Additives & Contaminants: Part A, 2014. **31**(10): p. 1769-1782.
124. Thanh, N.T.K., N. Maclean, and S. Mahiddine, *Mechanisms of Nucleation and Growth of Nanoparticles in Solution.* Chemical Reviews, 2014. **114**(15): p. 7610-7630.
125. NIOSH, *Current strategies for engineering controls in nanomaterial production and downstream handling processes*, C.f.D.C.a.P. U.S. Department of Health and Human Services, National Institute for Occupational Safety and Health, Editor. 2013, National Institute for Occupational Safety and Health: Cincinnati, OH.
126. Mourdikoudis, S., R.M. Pallares, and N.T.K. Thanh, *Characterization techniques for nanoparticles: comparison and complementarity upon studying nanoparticle properties.* Nanoscale, 2018. **10**(27): p. 12871-12934.
127. Krause, B., et al., *Characterization of aluminum, aluminum oxide and titanium dioxide nanomaterials using a combination of methods for particle surface and size analysis.* Rsc Advances, 2018. **8**(26): p. 14377-14388.
128. Stefaniak, A.B., et al., *Nanoscale reference materials for environmental, health and safety measurements: needs, gaps and opportunities.* Nanotoxicology, 2013. **7**(8): p. 1325-37.

129. Hassellov, M., et al., *Nanoparticle analysis and characterization methodologies in environmental risk assessment of engineered nanoparticles.* Ecotoxicology, 2008. **17**(5): p. 344-61.
130. Tiede, K., et al., *Detection and characterization of engineered nanoparticles in food and the environment.* Food Addit Contam Part A Chem Anal Control Expo Risk Assess, 2008. **25**(7): p. 795-821.
131. Wilschefski, S.C. and M.R. Baxter, *Inductively Coupled Plasma Mass Spectrometry: Introduction to Analytical Aspects.* The Clinical biochemist. Reviews, 2019. **40**(3): p. 115-133.
132. Pace, H.E., et al., *Determining Transport Efficiency for the Purpose of Counting and Sizing Nanoparticles via Single Particle Inductively Coupled Plasma Mass Spectrometry (vol 83, pg 9361, 2011).* Analytical Chemistry, 2012. **84**(10): p. 4633-4633.
133. Lee, S., et al., *Nanoparticle Size Detection Limits by Single Particle ICP-MS for 40 Elements.* Environmental Science & Technology, 2014. **48**(17): p. 10291-10300.
134. Sieg, H., et al., *Impact of an Artificial Digestion Procedure on Aluminum-Containing Nanomaterials.* Langmuir, 2017. **33**(40): p. 10726-10735.
135. Cornelis, G. and M. Hassellöv, *A signal deconvolution method to discriminate smaller nanoparticles in single particle ICP-MS.* Journal of Analytical Atomic Spectrometry, 2014. **29**(1): p. 134-144.
136. Donovan, A.R., et al., *Single particle ICP-MS characterization of titanium dioxide, silver, and gold nanoparticles during drinking water treatment.* Chemosphere, 2016. **144**: p. 148-153.
137. Stefaniak, A.B., *Principal Metrics and Instrumentation for Characterization of Engineered Nanomaterials*, in *Metrology and Standardization of Nanotechnology*. 2017. p. 151-174.
138. Wang, S. and M.V. Johnston, *Airborne nanoparticle characterization with a digital ion trap–reflectron time of flight mass spectrometer.* International Journal of Mass Spectrometry, 2006. **258**(1): p. 50-57.
139. Njuguna, J. and S. Sachse, *5 - Measurement and sampling techniques for characterization of airborne nanoparticles released from nano-enhanced products*, in *Health and Environmental Safety of Nanomaterials*, J. Njuguna, K. Pielichowski, and H. Zhu, Editors. 2014, Woodhead Publishing. p. 78-111.
140. Ma, Z., et al., *New developments in particle characterization by laser diffraction: size and shape.* Powder Technology, 2000. **111**(1): p. 66-78.
141. Krueger, K.M., et al., *Characterization of Nanocrystalline CdSe by Size Exclusion Chromatography.* Analytical Chemistry, 2005. **77**(11): p. 3511-3515.
142. Minelli, C., et al., *Measuring the size and density of nanoparticles by centrifugal sedimentation and flotation.* Analytical Methods, 2018. **10**(15): p. 1725-1732.
143. Hoo, C.M., et al., *A comparison of atomic force microscopy (AFM) and dynamic light scattering (DLS) methods to characterize nanoparticle size distributions.* Journal of Nanoparticle Research, 2008. **10**(1): p. 89-96.
144. Powers, K.W., et al., *Research strategies for safety evaluation of nanomaterials. Part VI. Characterization of nanoscale particles for toxicological evaluation.* Toxicol Sci, 2006. **90**(2): p. 296-303.
145. Keller, A., et al., *Surface science with nanosized particles in a carrier gas.* Journal of Vacuum Science & Technology A, 2001. **19**(1): p. 1-8.
146. LeBouf, R.F., et al., *Measuring surface area of airborne titanium dioxide powder agglomerates: relationships between gas adsorption, diffusion and mobility-based methods.* Journal of Nanoparticle Research, 2011. **13**(12): p. 7029-7039.

147. Weibel, A., et al., *The Big Problem of Small Particles: A Comparison of Methods for Determination of Particle Size in Nanocrystalline Anatase Powders.* Chemistry of Materials, 2005. **17**(9): p. 2378-2385.
148. Brunauer, S., P.H. Emmett, and E. Teller, *Adsorption of Gases in Multimolecular Layers.* Journal of the American Chemical Society, 1938. **60**(2): p. 309-319.
149. Kaszuba, M., et al., *High-concentration zeta potential measurements using light-scattering techniques.* Philosophical transactions. Series A, Mathematical, physical, and engineering sciences, 2010. **368**(1927): p. 4439-4451.
150. IUPAC, *Compendium of Chemical Terminology*. 2nd ed. (the "Gold Book") ed. 1997, Oxford: Blackwell Scientific Publications.
151. Kennedy, A.J., et al., *Fractionating nanosilver: importance for determining toxicity to aquatic test organisms.* Environ Sci Technol, 2010. **44**(24): p. 9571-7.
152. Holbrook, R.D., et al., *Trophic transfer of nanoparticles in a simplified invertebrate food web.* Nature Nanotechnology, 2008. **3**(6): p. 352-355.
153. Holt, B.D., K.N. Dahl, and M.F. Islam, *Quantification of Uptake and Localization of Bovine Serum Albumin-Stabilized Single-Wall Carbon Nanotubes in Different Human Cell Types.* Small, 2011. **7**(16): p. 2348-2355.
154. Nichols, J.W. and Y.H. Bae, *Odyssey of a cancer nanoparticle: From injection site to site of action.* Nano Today, 2012. **7**(6): p. 606-618.
155. Abdolahpur Monikh, F., et al., *Method for Extraction and Quantification of Metal-Based Nanoparticles in Biological Media: Number-Based Biodistribution and Bioconcentration.* Environmental Science & Technology, 2019. **53**(2): p. 946-953.
156. von der Kammer, F., et al., *Analysis of engineered nanomaterials in complex matrices (environment and biota): General considerations and conceptual case studies.* Environmental Toxicology and Chemistry, 2012. **31**(1): p. 32-49.
157. Laux, P., et al., *Challenges in characterizing the environmental fate and effects of carbon nanotubes and inorganic nanomaterials in aquatic systems.* Environmental Science: Nano, 2018. **5**(1): p. 48-63.
158. Urban, D.A., et al., *Plasmonic nanoparticles and their characterization in physiological fluids.* Colloids Surf B Biointerfaces, 2016. **137**: p. 39-49.
159. Oberdörster, G., E. Oberdörster, and J. Oberdörster, *Nanotoxicology: An Emerging Discipline Evolving from Studies of Ultrafine Particles.* Environmental Health Perspectives, 2005. **113**(7): p. 823-839.
160. Wagner, S., et al., *First steps towards a generic sample preparation scheme for inorganic engineered nanoparticles in a complex matrix for detection, characterization, and quantification by asymmetric flow-field flow fractionation coupled to multi-angle light scattering and ICP-MS.* Journal of Analytical Atomic Spectrometry, 2015. **30**(6): p. 1286-1296.
161. Philippe, A., et al., *Extraction and characterization methods for titanium dioxide nanoparticles from commercialized sunscreens.* Environmental Science: Nano, 2018. **5**(1): p. 191-202.
162. Molnar, I.L., et al., *Method for Obtaining Silver Nanoparticle Concentrations within a Porous Medium via Synchrotron X-ray Computed Microtomography.* Environmental Science & Technology, 2014. **48**(2): p. 1114-1122.
163. Drobne, D., et al., *The Biological Fate of Silver Nanoparticles from a Methodological Perspective.* Materials, 2018. **11**(6).
164. Szakal, C., et al., *Measurement of Nanomaterials in Foods: Integrative Consideration of Challenges and Future Prospects.* ACS Nano, 2014. **8**(4): p. 3128-3135.
165. Vanhaecke, F., *ICP–MS.* Analytical and Bioanalytical Chemistry, 2002. **372**(1): p. 20-21.

166. Milne, J.L.S., et al., *Cryo-electron microscopy – a primer for the non-microscopist.* The FEBS Journal, 2013. **280**(1): p. 28-45.
167. McDonald, K.L., *A review of high-pressure freezing preparation techniques for correlative light and electron microscopy of the same cells and tissues.* Journal of Microscopy, 2009. **235**(3): p. 273-281.
168. Abdolahpur Monikh, F., et al., *Analytical approaches for characterizing and quantifying engineered nanoparticles in biological matrices from an (eco)toxicological perspective: old challenges, new methods and techniques.* Science of The Total Environment, 2019. **660**: p. 1283-1293.
169. Zvyagin, A.V., et al., *Imaging of zinc oxide nanoparticle penetration in human skin in vitro and in vivo.* J Biomed Opt, 2008. **13**(6): p. 064031.
170. Garcia, C.P., et al., *Detection of silver nanoparticles inside marine diatom Thalassiosira pseudonana by electron microscopy and focused ion beam.* PLoS One, 2014. **9**(5): p. e96078.
171. Yang, X., et al., *Silver nanoparticle behavior, uptake, and toxicity in Caenorhabditis elegans: effects of natural organic matter.* Environ Sci Technol, 2014. **48**(6): p. 3486-95.
172. Moger, J., B.D. Johnston, and C.R. Tyler, *Imaging metal oxide nanoparticles in biological structures with CARS microscopy.* Opt Express, 2008. **16**(5): p. 3408-19.
173. van den Broek, B., et al., *Parallel nanometric 3D tracking of intracellular gold nanorods using multifocal two-photon microscopy.* Nano Lett, 2013. **13**(3): p. 980-6.
174. Mock, J.J., et al., *Shape effects in plasmon resonance of individual colloidal silver nanoparticles.* The Journal of Chemical Physics, 2002. **116**(15): p. 6755-6759.
175. Liu, M., et al., *Dark-field microscopy in imaging of plasmon resonant nanoparticles.* Colloids and Surfaces B: Biointerfaces, 2014. **124**: p. 111-117.
176. Bohme, S., et al., *Quantification of Al2O3 nanoparticles in human cell lines applying inductively coupled plasma mass spectrometry (neb-ICP-MS, LA-ICP-MS) and flow cytometry-based methods.* Journal of Nanoparticle Research, 2014. **16**(9).
177. Hsiao, I.L., et al., *Quantification and visualization of cellular uptake of TiO2 and Ag nanoparticles: comparison of different ICP-MS techniques.* Journal of Nanobiotechnology, 2016. **14**.
178. Van Malderen, S.J.M., et al., *Three-Dimensional Reconstruction of the Tissue-Specific Multielemental Distribution within Ceriodaphnia dubia via Multimodal Registration Using Laser Ablation ICP-Mass Spectrometry and X-ray Spectroscopic Techniques.* Analytical Chemistry, 2017. **89**(7): p. 4161-4168.
179. Li, Q., et al., *Imaging gold nanoparticles in mouse liver by laser ablation inductively coupled plasma mass spectrometry.* Scientific Reports, 2017. **7**(1): p. 2965.
180. Böhme, S., et al., *Exploring LA-ICP-MS as a quantitative imaging technique to study nanoparticle uptake in Daphnia magna and zebrafish (Danio rerio) embryos.* Analytical and Bioanalytical Chemistry, 2015. **407**(18): p. 5477-5485.
181. Petersen, E.J., et al., *Quantification of Carbon Nanotubes in Environmental Matrices: Current Capabilities, Case Studies, and Future Prospects.* Environmental Science & Technology, 2016. **50**(9): p. 4587-4605.
182. Loeschner, K., et al., *Detection and characterization of silver nanoparticles in chicken meat by asymmetric flow field flow fractionation with detection by conventional or single particle ICP-MS.* Analytical and Bioanalytical Chemistry, 2013. **405**(25): p. 8185-8195.
183. Sotebier, C.A., et al., *Sample loss in asymmetric flow field-flow fractionation coupled to inductively coupled plasma-mass spectrometry of silver nanoparticles.* Journal of Analytical Atomic Spectrometry, 2015. **30**(10): p. 2214-2222.

184. Mudalige, T.K., et al., *Simple Functionalization Strategies for Enhancing Nanoparticle Separation and Recovery with Asymmetric Flow Field Flow Fractionation.* Analytical Chemistry, 2015. **87**(3): p. 1764-1772.
185. Cascio, C., et al., *Detection, quantification and derivation of number size distribution of silver nanoparticles in antimicrobial consumer products.* Journal of Analytical Atomic Spectrometry, 2015. **30**(6): p. 1255-1265.
186. Katsumiti, A., et al., *Mechanisms of Toxicity of Ag Nanoparticles in Comparison to Bulk and Ionic Ag on Mussel Hemocytes and Gill Cells.* PloS one, 2015. **10**(6): p. e0129039-e0129039.
187. Reed, R.B., et al., *Solubility of nano-zinc oxide in environmentally and biologically important matrices.* Environmental toxicology and chemistry, 2012. **31**(1): p. 93-99.
188. Jiang, J., et al., *Does Nanoparticle Activity Depend upon Size and Crystal Phase?* Nanotoxicology, 2008. **2**(1): p. 33-42.
189. Sharifi, S., et al., *Toxicity of nanomaterials.* Chemical Society Reviews, 2012. **41**(6): p. 2323-2343.
190. Halliwell, B. and J.M.C. Gutteridge, *Free Radicals in Biology and Medicine*. 5 ed. 2015, Oxford: Oxford University Press. 944.
191. Dalle-Donne, I., et al., *S-glutathionylation in protein redox regulation.* Free Radic Biol Med, 2007. **43**(6): p. 883-98.
192. Aillon, K.L., et al., *Effects of nanomaterial physicochemical properties on in vivo toxicity.* Adv Drug Deliv Rev, 2009. **61**(6): p. 457-66.
193. Powers, K.W., et al., *Characterization of the size, shape, and state of dispersion of nanoparticles for toxicological studies.* Nanotoxicology, 2007. **1**(1): p. 42-51.
194. Lovrić, J., et al., *Differences in subcellular distribution and toxicity of green and red emitting CdTe quantum dots.* J Mol Med (Berl), 2005. **83**(5): p. 377-85.
195. Aggarwal, P., et al., *Nanoparticle interaction with plasma proteins as it relates to particle biodistribution, biocompatibility and therapeutic efficacy.* Adv Drug Deliv Rev, 2009. **61**(6): p. 428-37.
196. Verma, A. and F. Stellacci, *Effect of surface properties on nanoparticle-cell interactions.* Small, 2010. **6**(1): p. 12-21.
197. Champion, J.A. and S. Mitragotri, *Role of target geometry in phagocytosis.* Proceedings of the National Academy of Sciences of the United States of America, 2006. **103**(13): p. 4930.
198. Hoshino, A., et al., *Physicochemical Properties and Cellular Toxicity of Nanocrystal Quantum Dots Depend on Their Surface Modification.* Nano Letters, 2004. **4**(11): p. 2163-2169.
199. Goodman, C.M., et al., *Toxicity of gold nanoparticles functionalized with cationic and anionic side chains.* Bioconjug Chem, 2004. **15**(4): p. 897-900.
200. Harper, S., et al., *In vivo biodistribution and toxicity depends on nanomaterial composition, size, surface functionalisation and route of exposure.* Journal of Experimental Nanoscience, 2008. **3**(3): p. 195-206.
201. Griffitt, R.J., et al., *Effects of particle composition and species on toxicity of metallic nanomaterials in aquatic organisms.* Environ Toxicol Chem, 2008. **27**(9): p. 1972-8.
202. Atkins, P.W. and J. De Paula, *Atkins' Physical chemistry*. 2006, Oxford; New York: Oxford University Press.
203. De Temmerman, P.J., et al., *Quantitative characterization of agglomerates and aggregates of pyrogenic and precipitated amorphous silica nanomaterials by transmission electron microscopy.* Journal of Nanobiotechnology, 2012. **10**.
204. Avramescu, M.L., et al., *Influence of pH, particle size and crystal form on dissolution behaviour of engineered nanomaterials.* Environmental Science and Pollution Research, 2017. **24**(2): p. 1553-1564.

205. Oomen, A.G., et al., *Comparison of Five In Vitro Digestion Models To Study the Bioaccessibility of Soil Contaminants.* Environmental Science & Technology, 2002. **36**(15): p. 3326-3334.
206. Walczak, A.P., et al., *Behaviour of silver nanoparticles and silver ions in an in vitro human gastrointestinal digestion model.* Nanotoxicology, 2013. **7**(7): p. 1198-210.
207. Lichtenstein, D., et al., *Impact of food components during in vitro digestion of silver nanoparticles on cellular uptake and cytotoxicity in intestinal cells.* Biol Chem, 2015. **396**(11): p. 1255-64.
208. Bohmert, L., et al., *Analytically monitored digestion of silver nanoparticles and their toxicity on human intestinal cells.* Nanotoxicology, 2014. **8**(6): p. 631-642.
209. Peters, R., et al., *Presence of nano-sized silica during in vitro digestion of foods containing silica as a food additive.* ACS Nano, 2012. **6**(3): p. 2441-51.
210. Voss, L., et al., *Environmental Impact of ZnO Nanoparticles Evaluated by in Vitro Simulated Digestion.* ACS Applied Nano Materials, 2020. **3**(1): p. 724-733.
211. Ruiperez, F., et al., *Pro-oxidant activity of aluminum: promoting the Fenton reaction by reducing Fe(III) to Fe(II).* J Inorg Biochem, 2012. **117**: p. 118-23.
212. Murko, S., R. Milacic, and J. Scancar, *Speciation of Al in human serum by convective-interaction media fast-monolithic chromatography with inductively coupled plasma mass spectrometric detection.* J Inorg Biochem, 2007. **101**(9): p. 1234-41.
213. Chen, X., *Matrix effects in inductively coupled plasma mass spectrometry*. 1995.
214. Pauluhn, J., *Pulmonary toxicity and fate of agglomerated 10 and 40 nm aluminum oxyhydroxides following 4-week inhalation exposure of rats: toxic effects are determined by agglomerated, not primary particle size.* Toxicol Sci, 2009. **109**(1): p. 152-67.
215. des Rieux, A., et al., *Nanoparticles as potential oral delivery systems of proteins and vaccines: A mechanistic approach.* Journal of Controlled Release, 2006. **116**(1): p. 1-27.
216. Lundquist, P. and P. Artursson, *Oral absorption of peptides and nanoparticles across the human intestine: Opportunities, limitations and studies in human tissues.* Advanced Drug Delivery Reviews, 2016. **106**: p. 256-276.
217. Banerjee, A., et al., *Role of nanoparticle size, shape and surface chemistry in oral drug delivery.* Journal of Controlled Release, 2016. **238**: p. 176-185.
218. Foroozandeh, P. and A.A. Aziz, *Insight into Cellular Uptake and Intracellular Trafficking of Nanoparticles.* Nanoscale Research Letters, 2018. **13**.
219. Zhao, Y.T., et al., *A comparison between sphere and rod nanoparticles regarding their in vivo biological behavior and pharmacokinetics.* Scientific Reports, 2017. **7**.
220. Sieg, H., et al., *Uptake and molecular impact of aluminum-containing nanomaterials on human intestinal caco-2 cells.* Nanotoxicology, 2018. **12**(9): p. 992-1013.

7. List of publications

B. Krause, T. Meyer, H. Sieg, C. Kastner, P. Reichardt, J. Tentschert, H. Jungnickel, I. Estrela-Lopis, A. Burel, S. Chevance, F. Gauffre, P. Jalili, J. Meijer, L. Bohmert, A. Braeuning, F. Thunemann, F. Emmerling, V. Fessard, P. Laux, A. Lampen and A. Luch, Characterization of aluminum, aluminum oxide and titanium dioxide nanomaterials using a combination of methods for particle surface and size analysis, *Rsc Adv*, 2018, **8**, 14377-14388.

H. Sieg, C. Kastner, **B. Krause**, T. Meyer, A. Burel, L. Bohmert, D. Lichtenstein, H. Jungnickel, J. Tentschert, P. Laux, A. Braeuning, I. Estrela-Lopis, F. Gauffre, V. Fessard, J. Meijer, A. Luch, A. F. Thunemann and A. Lampen, Impact of an Artificial Digestion Procedure on Aluminum-Containing Nanomaterials, *Langmuir*, 2017, **33**, 10726-10735.

B.C. Krause, F.L. Kriegel, D. Rosenkranz, N. Dreiack, J. Tentschert, H. Jungnickel, P. Jalili, V. Fessard, P. Laux and A. Luch, Aluminum and aluminum oxide nanomaterials uptake after oral exposure - a comparative study. *Sci Rep* 2020, **10,** 2698.

A. Haase, N. Dommershausen, M. Schulz, R. Landsiedel, P. Reichardt, **B. C. Krause**, J. Tentschert and A. Luch, Genotoxicity testing of different surface-functionalized SiO2, ZrO2 and silver nanomaterials in 3D human bronchial models, *Arch Toxicol*, 2017, **91**, 3991-4007.

P. Jalili, N. Gueniche, R. Lanceleur, A. Burel, M.-T. Lavault, H. Sieg, L. Böhmert, T. Meyer, **B.-C. Krause**, A. Lampen, I. Estrela-Lopis, P. Laux, A. Luch, K. Hogeveen and V. Fessard, Investigation of the in vitro genotoxicity of two rutile TiO2 nanomaterials in human intestinal and hepatic cells and evaluation of their interference with toxicity assays, *NanoImpact*, 2018, **11**, 69-81.

H. Sieg, C. Braeuning, B. M. Kunz, H. Daher, C. Kastner, **B. C. Krause**, T. Meyer, P. Jalili, K. Hogeveen, L. Bohmert, D. Lichtenstein, A. Burel, S. Chevance, H. Jungnickel, J. Tentschert, P. Laux, A. Braeuning, F. Gauffre, V. Fessard, J. Meijer, I. Estrela-Lopis, A. F. Thunemann, A. Luch and A. Lampen, Uptake and molecular impact of aluminum-containing nanomaterials on human intestinal caco-2 cells, *Nanotoxicology*, 2018, **12**, 992-1013.

T. Meyer, T. Venus, H. Sieg, L. Böhmert, B. M. Kunz, **B. Krause**, P. Jalili, K. Hogeveen, S. Chevance, F. Gauffre, A. Burel, H. Jungnickel, J. Tentschert, P. Laux, A. Luch, A. Braeuning, A. Lampen, V. Fessard, J.

Meijer and I. Estrela-Lopis, Simultaneous Quantification and Visualization of Titanium Dioxide Nanomaterial Uptake at the Single Cell Level in an In Vitro Model of the Human Small Intestine, *Small Methods*, 2019, **3**, 1800540.

F.L. Kriegel, **B.-C. Krause**, P. Reichardt, A.V. Singh, J. Tentschert, P. Laux, H. Jungnickel, and A. Luch, The Vitamin A and D Exposure of Cells Affects the Intracellular Uptake of Aluminum Nanomaterials and Its Agglomeration Behavior: A Chemo-Analytic Investigation. *Int. J. Mol. Sci.* 2020, ***21***, 1278.

Y.U. Hachenberger, D. Rosenkranz, F.L. Kriegel, **B. Krause**, R. Matschaß, P. Reichardt, J. Tentschert, P. Laux, N. Jakubowski, U. Panne, and A. Luch, Tackling Complex Analytical Tasks: An ISO/TS-Based Validation Approach for Hydrodynamic Chromatography Single Particle Inductively Coupled Plasma Mass Spectrometry. *Materials* 2020, ***13***, 1447.

A. Bannuscher, B. Hellack, A. Bahl, J. Laloy, H. Herman, M. S. Stan, A. Dinischiotu, A. Giusti, **B.-C. Krause**, J. Tentschert, M. Roșu, C. Balta, A. Hermenean, M. Wiemann, A. Luch and A. Haase, Metabolomics profiling to investigate nanomaterial toxicity *in vitro* and *in vivo*, Nanotoxicology, 2020

Annex I

Characterization of aluminum, aluminum oxide and titanium dioxide nanomaterials using a combination of methods for particle surface and size analysis

B. Krause*[a], T. Meyer[b], H. Sieg[c], C. Kästner[d], P. Reichardt[a], J. Tentschert[a], H. Jungnickel[a], I. Estrela-Lopis[b], A. Burel[e], S. Chevance[f], F. Gauffre[f], P. Jalili[g], J. Meijer[h], L. Boehmert[c], A. Braeuning[c], A. F. Thünemann[d], V. Fessard[g], P. Laux[a], A. Lampen[c] and A. Luch[a]

[a] German Federal Institute for Risk Assessment (BfR), Department of Chemical and Product Safety, Max-Dohrn-Straße 8-10, 10589 Berlin, Germany
[b] Institute of Medical Physics and Biophysics, University of Leipzig, Härtelstrasse 16-18, 04275 Leipzig, Germany
[c] German Federal Institute for Risk Assessment (BfR), Department of Food Safety, Max-Dohrn-Straße 8-10, 10589 Berlin, Germany
[d] Federal Institute for Materials Research and Testing (BAM), Unter den Eichen 87, 12205 Berlin, Germany
[e] MRIC TEM BIOSIT, Université de Rennes 1, 2 av pro Leon Bernard, France
[f] Institut des Sciences Chimiques de Rennes, UMR-CNRS 6226, Université de Rennes 1, France
[g] ANSES, French Agency for Food, Environmental and Occupational Health Safety, Fougères Laboratory, 10B rue Claude Bourgelat, 35306, Fougères Cedex, France

Supporting Information

Figure S1: NTA averaged distributions

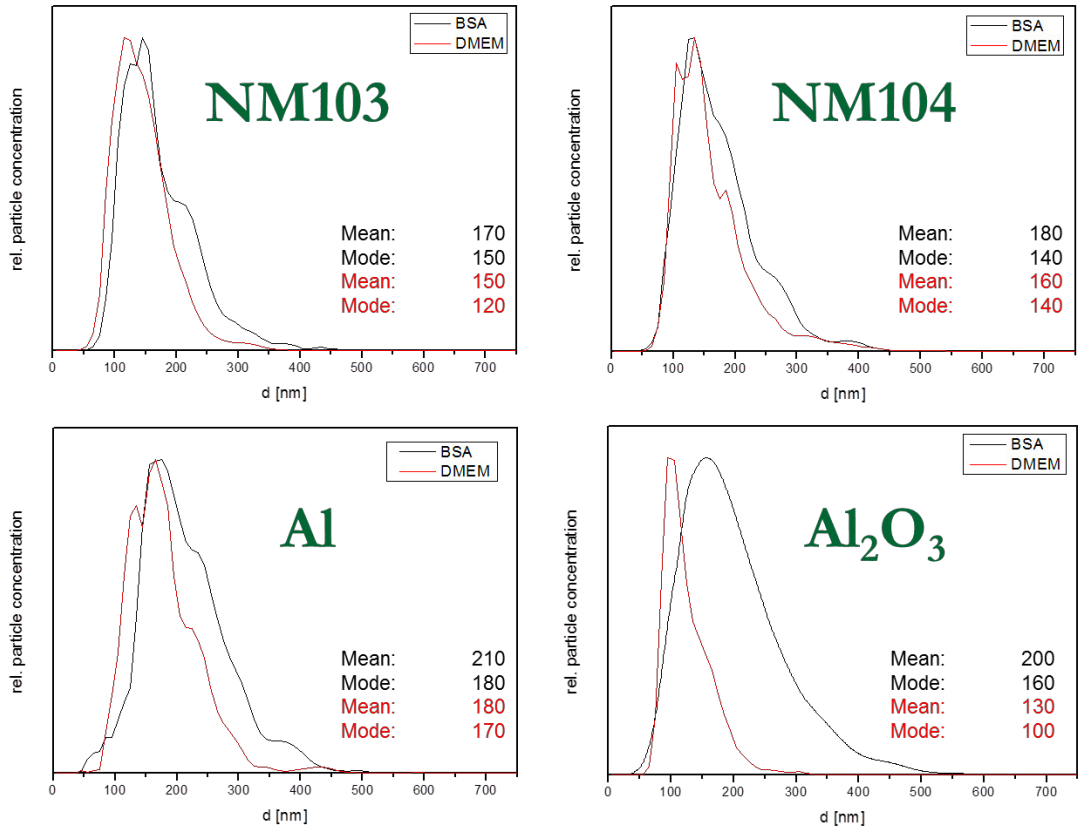

Figure S1: Averaged size distributions of NM103, NM104, Al and Al_2O_3 recorded by NTA. Y-axis: Relative particle concentration; x-axis: hydrodynamic diameter. Black: NMs prepared after Nanogenotox protocol; red: size distribution of NMs under cell culture conditions. BSA: bovine serum albumin; DMEM: Dulbecco's modified eagle medium.

Table S1: Number size distributions by calculation from DLS data

Table S1 Number size distribution with standard deviation (SD) of Al^0, Al_2O_3, NM103 and NM104 NMs in different media calculated based on the intensity size distribution data determined by dynamic light scattering (DLS). All results represent the average of six repeats. BSA: bovine serum albumin; DMEM: Dulbecco's modified eagle medium; FCS: fetal calf serum

	DLS measurements and comparison	
	Lab 1 (Malvern) Number-based size [nm]	Lab 2 (Brookhaven) Number-based size [nm]
	Stock solution (0.05 % BSA in H_2O)	
Al^0 NM	240 ± 10	120 ± 30
Al_2O_3 NM	110 ± 10	80 ± 40
NM103	140 ± 10	250 ± 90
NM104	100 ± 10	200 ± 50
	DMEM (with 10 % FCS)	
Al^0 NM	160 ± 10	80 ± 10
Al_2O_3 NM	10 ± 1	110 ± 70
NM103	110 ± 10	90 ± 10
NM104	110 ± 10	110 ± 10

The size and size distribution of NMs in number-based DLS measurement mode is interesting for a better comparison with other number-based techniques. To compare DLS data to number-based NTA

data, a calculation based on the refractive index and the absorption of the used NMs is possible. While both size distributions are correct, some assumptions need to be taken into account:

a. The involvement of the Mie scattering for the more complicated scattering process for particles much smaller than the wavelength of illuminating light (633 nm for Zetasizer ZS, 640 nm for ZetaPALS)
b. Known optical properties of the investigated NMs
c. good raw data quality (broader distributions or high polydispersity can significantly influence the transition from intensity-based to number based distributions)

In our case, we decided to use the intensity-based distribution only, as there are no assumptions needed compared to the transformation into number-based distributions.

Figure S2: TEM measurement of TiO_2 NMs in DMEM

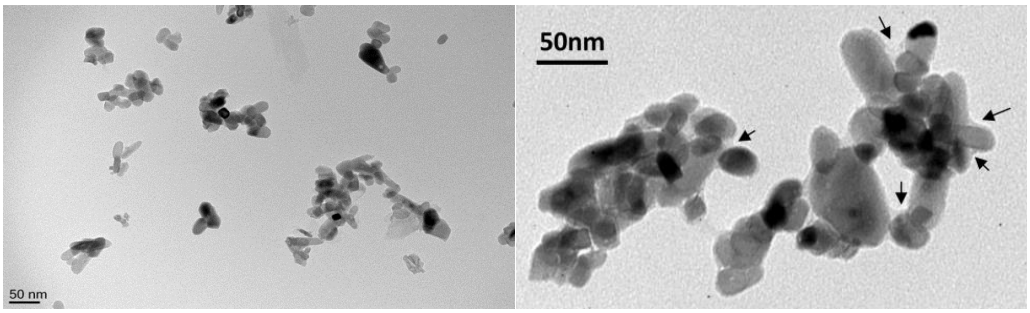

Figure S2: TEM observation of TiO_2 NMs in BSA (left) and DMEM (right) achieved at 80 kV (0.8 g L^{-1}). Arrows show protein deposition.

Figure S3 – S5: SAXS curves fitted with Monte Carlo based data evaluation

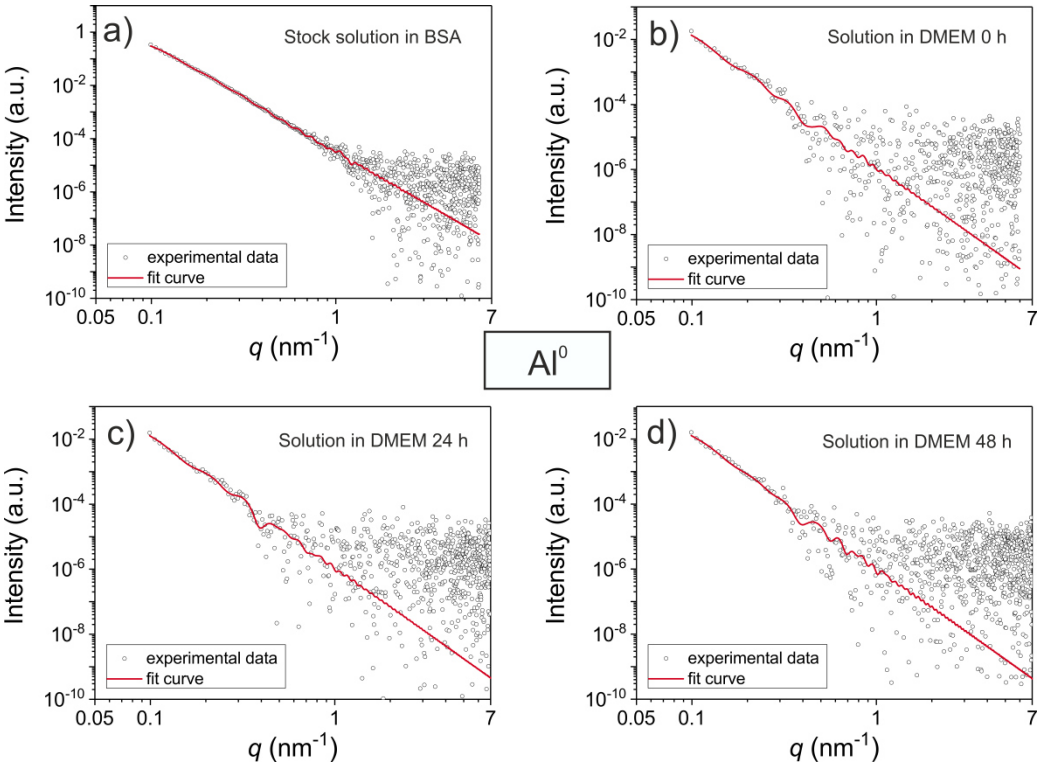

Figure S3: Measured SAXS curves (black circles) of Al NM in (a) stock solution (BSA), (b) directly after addition in DMEM, (c) after 24 h in DMEM and (d) after 48 h in DMEM. The measured data are fitted with a Monte Carlo based data evaluation (red solid lines).

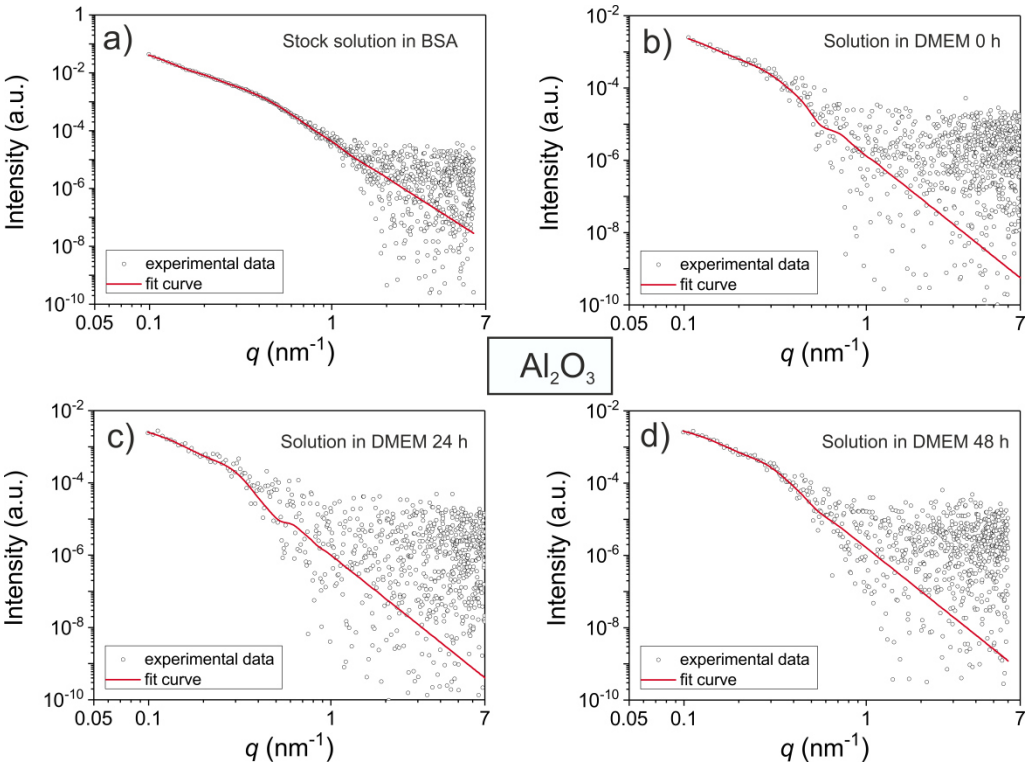

Figure S4: Measured SAXS curves (black circles) of Al_2O_3 NM in (a) stock solution (BSA), (b) directly after addition in DMEM, (c) after 24 h in DMEM and (d) after 48 h in DMEM. The measured data are fitted with a Monte Carlo based data evaluation (red solid lines).

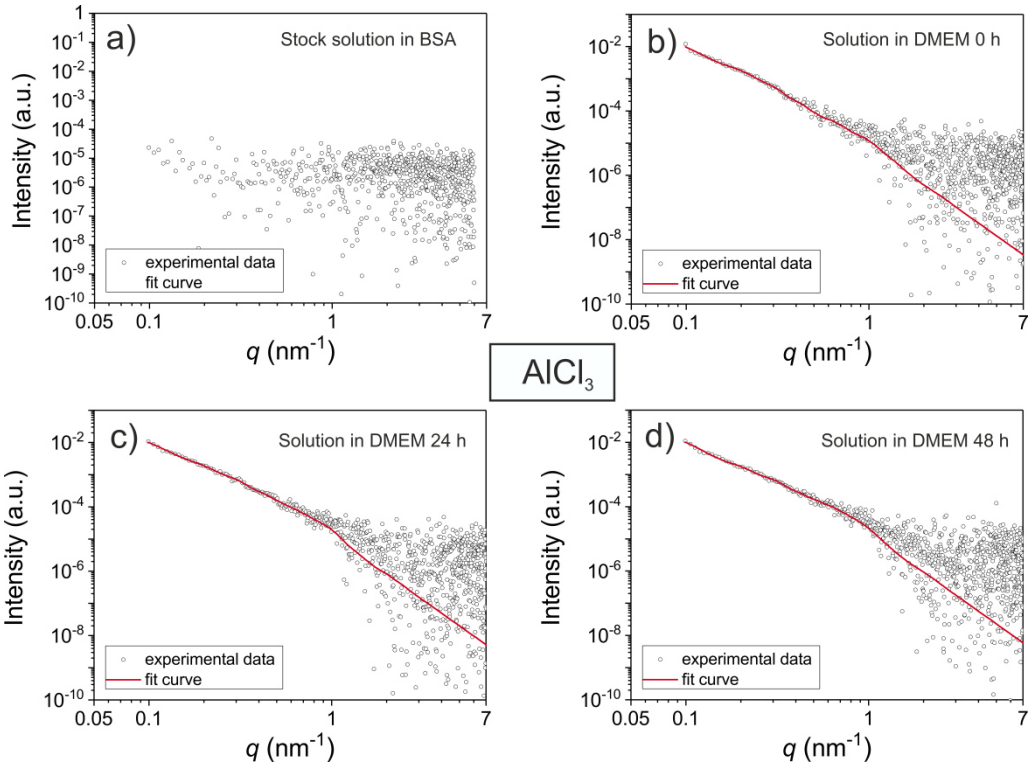

Figure S5: Measured SAXS curves (black circles) of $AlCl_3$ in (a) aqueous stock solution (b) directly after addition in DMEM, (c) after 24 h in DMEM and (d) after 48 h in DMEM. The measured data are fitted with a Monte Carlo based data evaluation (red solid lines).

Figure S6: Impurities of used NMs determined by IBM

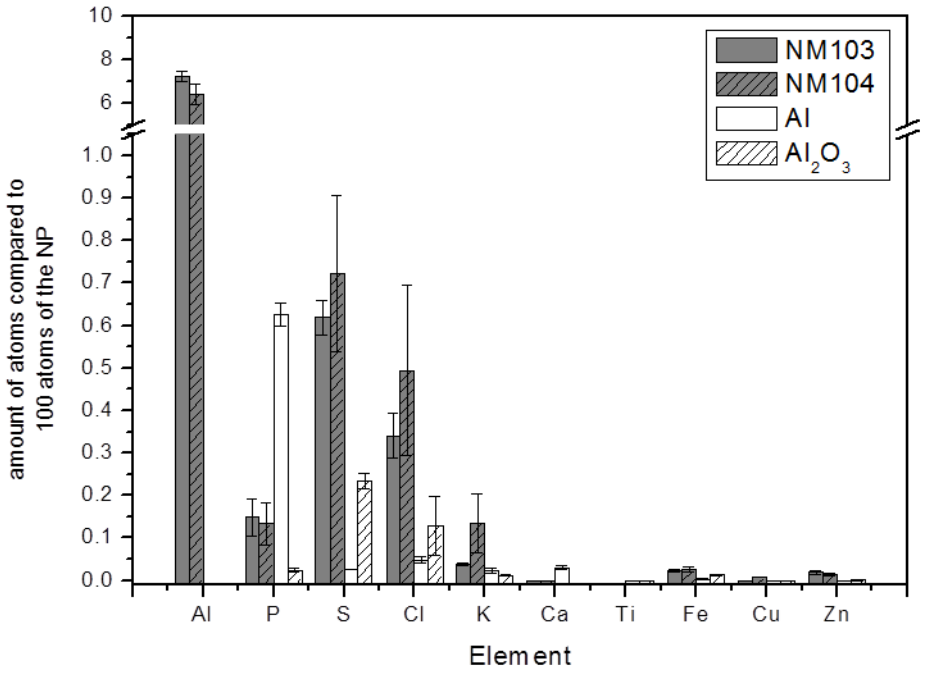

Figure S6: Impurities associated to the NMs as purchased. The impurities are given in number of atoms compared to one hundred atoms of the NMs. In case of TiO_2 titanium isn't shown as well as in case of aluminum containing materials aluminum isn't displayed in the graph.

Figure S7: Aluminum aqua complexes at different pH values

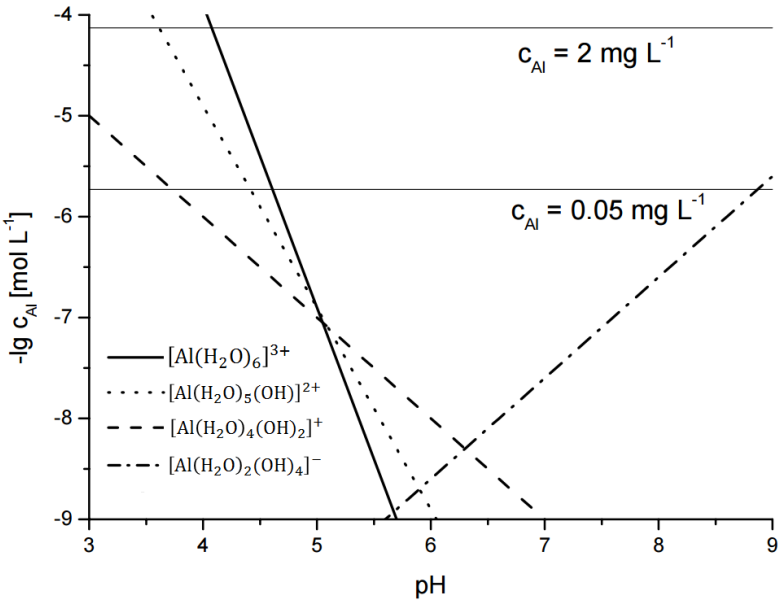

Figure S7: Solubility of Al^{3+} function of pH in equilibrium with $Al(OH)_{3(s)}$, solubility product of $Al(OH)_3$ $KS=10^{-33.9}$ (modified according to Sigg & Stumm 1989) [1].

Figure S8: CRM surface investigations

CRM was applied to study the organic constituents on the surface of the NMs. Figure S8 shows the average Raman spectra of TiO_2 NMs extracted from their spectral images based on the intensity distribution of E_g band of rutile phase, 450 cm^{-1} [2]. The spectra were weighted to integral intensity of NM phonon bands.

For both particles, four main peaks are observable. The peak around 1000 cm^{-1} is a double peak consisting of 988 cm^{-1} induced by ring stretching and 1006 cm^{-1} attributed to ring deformation. These peaks indicate the presence of an aromatic ring structure associated with the particle surface. The region from 1500 to 1700 represents an overlap of different possible structures, e.g. cyclic compounds, double bounds and amide bands [3]. The high variety of possible structures makes clear assignments complicated [3]. The CH_2/CH_3 vibration modes were detected in the region from 2850 to 3000 cm^{-1} attributed to symmetrical and asymmetric CH_2 and CH_3 stretching vibrations and at 1450 cm^{-1} related to $\delta(CH_2)$ and asymmetric $\delta(CH_3)$ deformations [3]. These bands can be associated with aliphatic compounds. The Raman spectra of the hydrophobic NM103 revealed a higher concentration of organic surfactants and aromatic compounds on their surface compared to NM104 NMs.

Both NMs exhibit decreased signals of aromatic and aliphatic compounds on their surface after the treatment with ultra-sonic compared to particles without ultra-sonication. This reveals a loss of organic compounds during the ultra-sonication step.

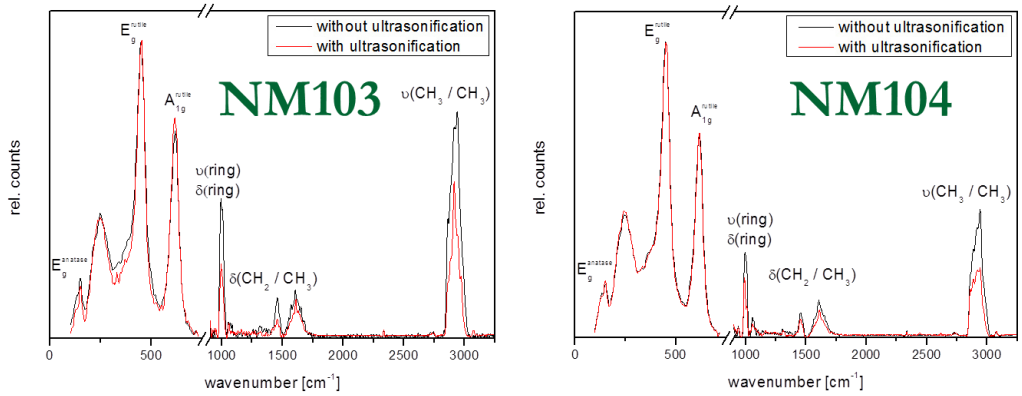

Figure S8: Raman spectra of NMs without and with ultra-sonic treatment. For better visualization, the regions between 900 and 3250 cm^{-1} in both graphs were multiplied by a scaling factor of ten.

Figure S9: Colocalization pattern by IBM

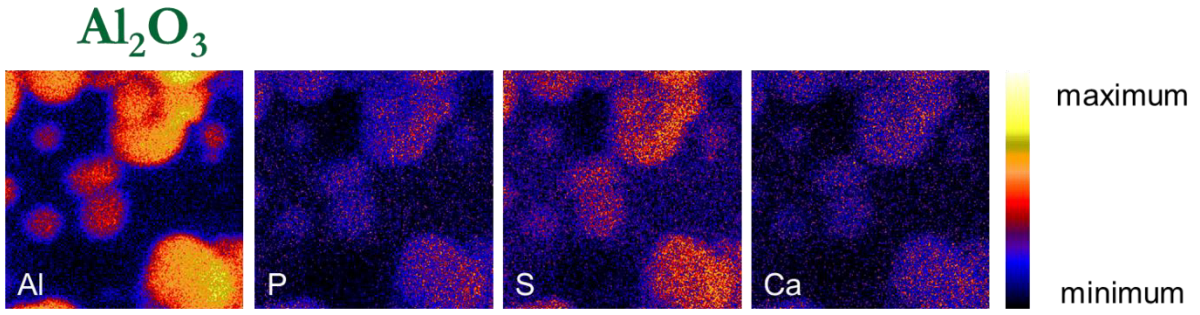

Figure S9: IBM element maps of Al_2O_3 and as purchased only diluted in mpH_2O. The images exhibiting colocalization pattern of the different elements. An area of 50 x 50 µm² is displayed. The color code is as follows: white represents highest concentration and black the lowest concentration.

Figure S10: Influence of different proteins detected by CRM

The bands associated with CH_2/CH_3 vibration modes exhibit the same extent of intensity decrease for both TiO_2 NMs comparing BSA and DMEM conditions as observed by element analysis (Figure S10). Furthermore, the analysis of phonon bands revealed that the crystal structure of both TiO_2 NMs was not affected during the particle preparation process.

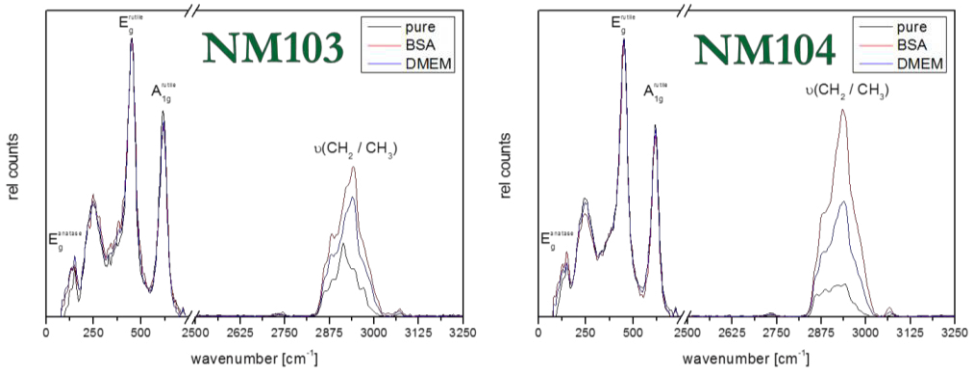

Figure S10: CRM spectra represent the modifications during the preparation process for NM103 (left) and NM104 (right). Pure: particles as purchased; BSA: albumin-coated particles (NanoGenoTOX protocol); DMEM: albumin-coated particles dispersed in DMEM. For better visualization, the regions between 2500 and 3250 cm^{-1} in both graphs were multiplied by a scaling factor of five.

Figure S11 – 14: ToF-SIMS measurements of Al and Al_2O_3 NMs in DMEM

In stock dispersion the albumin concentration is 0.5mg/ml. In DMEM containing FBS the albumin content is about 2mg/ml and about 2.7-4mg/ml other not more specified proteins are included. In addition, the dilution into DMEM was done out of stock dispersion, which already contains 0.5 mg/ml albumin. Using a dilution factor of about 25, 0.02 mg/ml from the BSA stock dispersion, as well as 2

mg/ml albumin and 2.7-4 mg/ml other proteins results in an about 10-times higher protein concentration of DMEM compared to BSA.

Figure S11 shows the distribution of all nanoparticle agglomerates for aluminum nanoparticles and all the different chemical entities (polyoxo-aluminum complex, aluminum-(III)-serine, leucine aluminate and phenylalanine aluminate) separated for each chemical species. All chemical species are clearly separated from each other and located in different areas of the image as specific single agglomerates, which do not co-locate with each other. Figure S12 shows the magnified area, where predominantly Al_2O_3 NMs (shown in purple) agglomerates are located. In these areas of the DMEM with Al_2O_3 NMs single agglomerates, which do not co-localize, made of different chemical entities can be found. Figure S13 shows a magnified area, where larger agglomerates can be found, which largely consist of polyoxo-aluminum complexes and aluminum-(III)-serine. Figure S14 shows a magnification of one of the agglomerate areas. Here regions can be spotted, where polyoxo-aluminum complexes (depicted in blue) and aluminum-(III)-serine (depicted in green) co-localize (see red circles) and areas, where phenylalanine aluminate (depicted in orange) and aluminum-(III)-serine (depicted in green) co-localize (orange circles) as well as areas, where Al_2O_3 NMs (depicted in purple) and aluminum-(III)-serine (depicted in green) co-localize in the same location. These areas may be agglomerates, where a beginning mineralization combines different chemical entities in larger agglomerates.

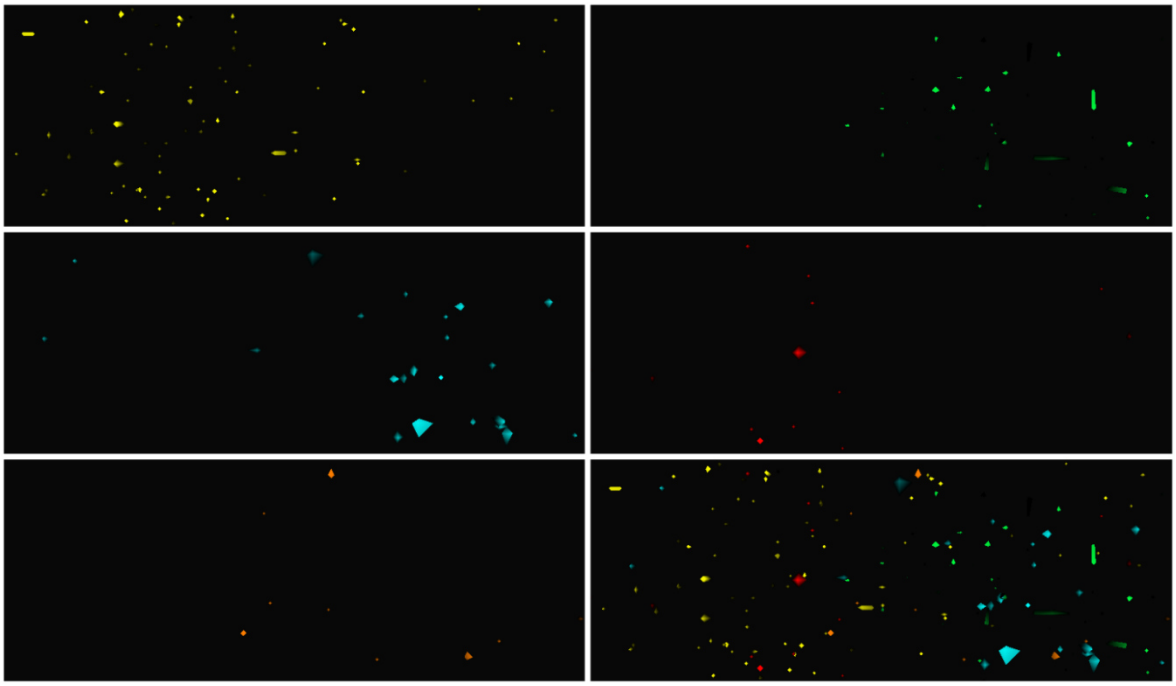

Figure S11: ToF-SIMS reconstructed ion images (90 µm x 30 µm) of Al NMs agglomerates of different chemical entities from DMEM; yellow: Al NMs (a), green: aluminum-(III)-serine (b); orange: phenylalanine aluminate (e); red: leucine aluminate (d); blue: polyoxo-aluminum complex (c). (f) shows an overlay of all ions. In the overlay picture, all chemical entities are separated from each other and do not co-localize.

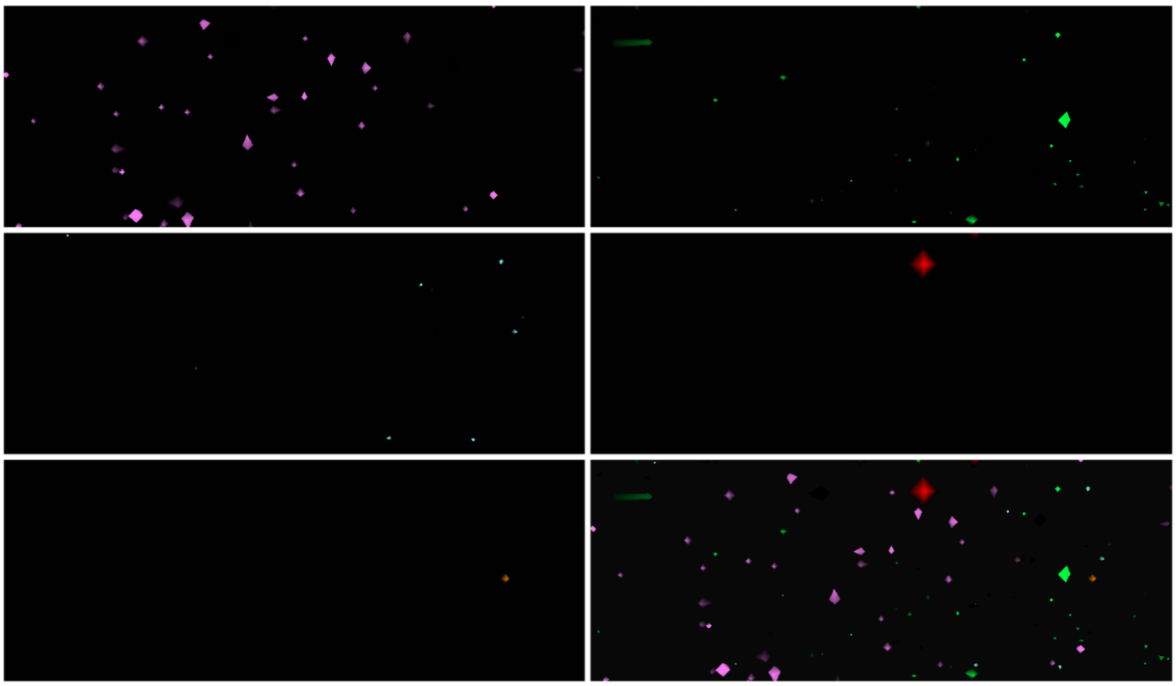

Figure S12: ToF-SIMS reconstructed ion images (90 µm x 30 µm) of Al_2O_3 NMs agglomerates of different chemical entities from DMEM; purple: Al_2O_3 NMs (a), green: aluminum-(III)-serine (b); orange: phenylalanine aluminate (e); red: leucine aluminate (d); blue: polyoxo-aluminum complex (c). (f) shows an overlay of all ions. In the overlay picture, all chemical entities are separated from each other and do not co-localize.

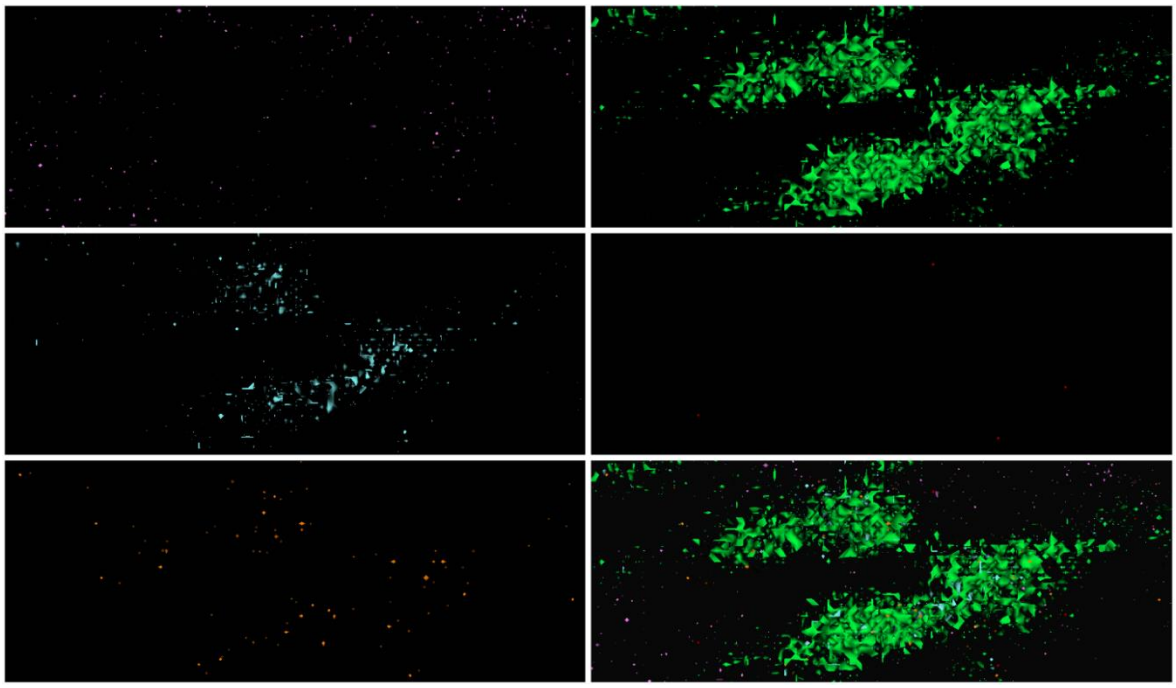

Figure S13: ToF-SIMS reconstructed ion images (90 µm x 30 µm) of Al_2O_3 NMs agglomerates of different chemical entities from DMEM; purple: Al_2O_3 NMs (a), green: aluminum-(III)-serine (b); orange: phenylalanine aluminate (e); red: leucine aluminate (d); blue: polyoxo-aluminum complex (c). (f) shows an overlay of all ions. In the overlay picture, specific areas are visible, where predominantly polyoxo-aluminum complex and aluminum-(III)-serine co-localize in larger agglomerate areas.

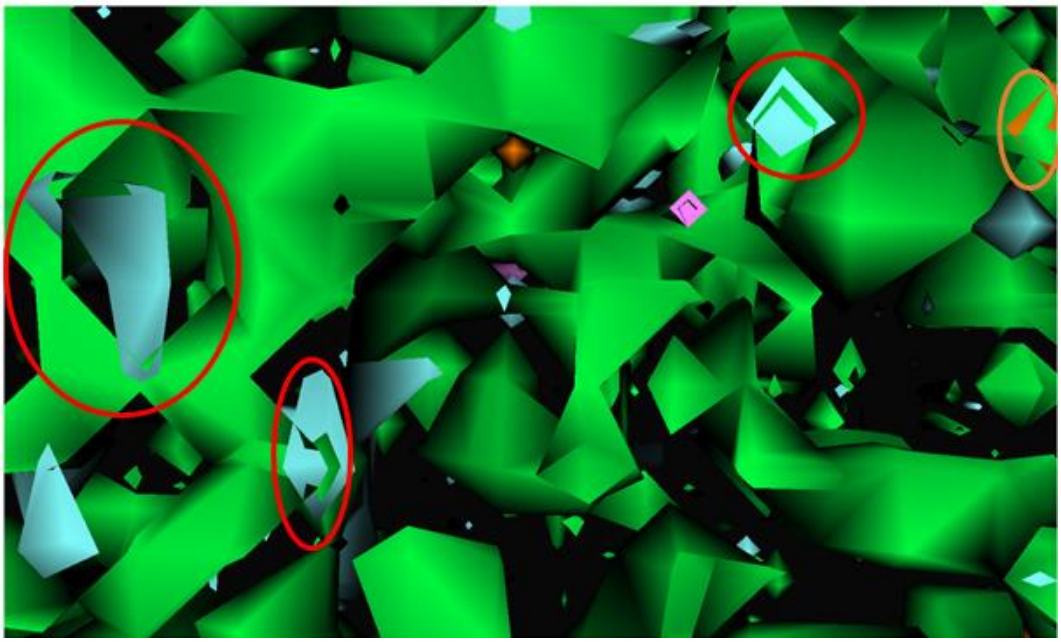

Figure S14: ToF-SIMS reconstructed ion images (20 µm x 10 µm) of Al_2O_3 NMs agglomerates of different chemical entities from DMEM; purple: Al_2O_3 NMs, green: aluminum-(III)-serine; orange: phenylalanine aluminate; red: leucine aluminate; blue: polyoxo-aluminum complex. The picture shows an overlay of all ions. Here specific areas are visible, where polyoxo-aluminum complex (blue) and aluminum-(III)-serine (green) co-localize (see red circles) and areas, where phenylalanine aluminate (orange) and aluminum-(III)-serine (green) co-localize (orange circles) as well as areas, where Al_2O_3 NMs (purple) and aluminum-(III)-serine (green) co-localize in the same location.

Figure S15 – 18: ToF-SIMS measurements of TiO_2 NMs in DMEM

ToF-SIMS was used to visualize TiO_2 NM103 and TiO_2 NM104 as well as nanoparticle agglomerates in DMEM to assess the chemical composition of the nanoparticle agglomerates. The analyses revealed nanoparticle-specific agglomerates, consisting of $TiOH^+$ amino acid complexes TiO_2 amino acid complexes were identified previously as one possible absorption mechanism and it was shown that there was selective absorption of serine on TiO_2 surfaces in benthic microbial fuel cells [4]. Also, adsorption of phenylalanine could already be observed on TiO_2 nanoparticles [5].

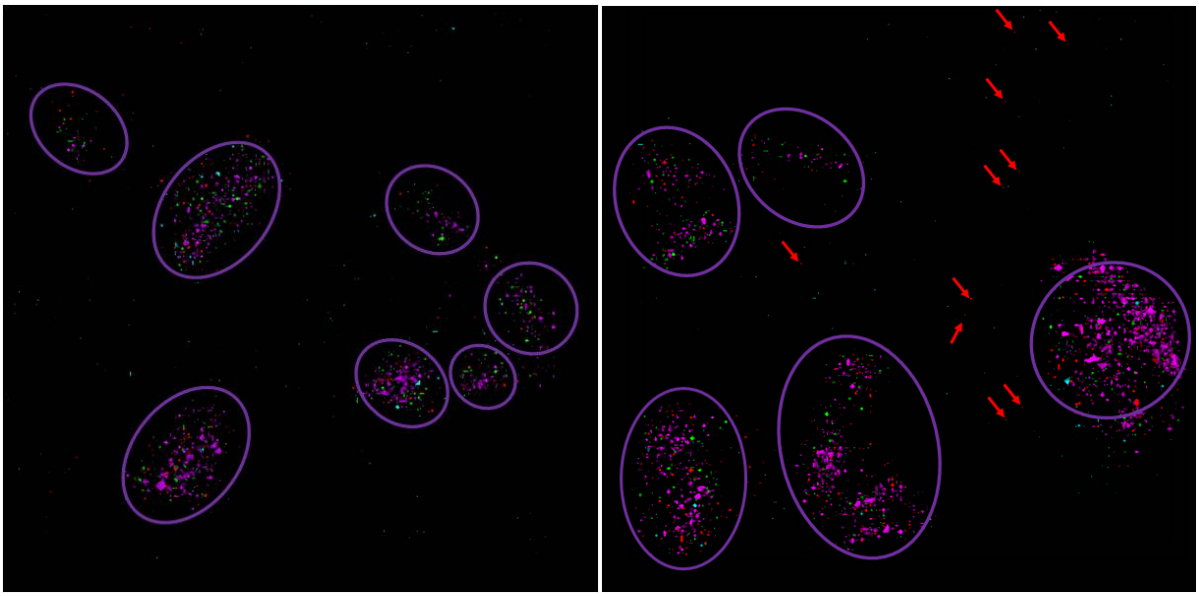

Figure S15: Left: ToF-SIMS reconstructed ion overlay image (500 µm x 500 µm) of TiO_2 NM 103 (left) and NM104 (right) agglomerates of different chemical entities from a DMEM solution; green: TiO_2 NM, blue: $TiOH^+$-serine; purple: $TiOH^+$ -leucine; red: $TiOH^+$ -phenylalanine complex. Purple circles show areas where agglomerates accumulate. Red arrows show single $TiOH^+$-phenylalanine aggregates outside of purple circle areas.

Figure S15 shows the ToF-SIMS image for TiO_2 NM103 (left) and TiO_2 NM104 (right). Larger agglomerate areas (purple circles in Figure S15, left and right), where $TiOH^+$-leucine complexes are present in higher amounts, can be distinguished from areas with predominantly smaller NM agglomerates, made predominantly of $TiOH^+$-serine in Figure S15 (left) showing TiO_2 NM103 while in Figure S15 (right), in addition to $TiOH^+$-serine, $TiOH^+$-phenylalanine aggregates can also be found (see red arrows Figure S15 (right) and Figure S18). For further information about the distribution of all NM agglomerates for TiO_2 NM103 and TiO_2 NM104 and all the different chemical entities ($TiOH^+$-serine, $TiOH^+$-leucine, $TiOH^+$-phenylalanine) separated for each chemical species, see Figures S14 and S15. All chemical species are clearly separated from each other and located in different areas of the image as specific single agglomerates, which do not co-locate with each other.

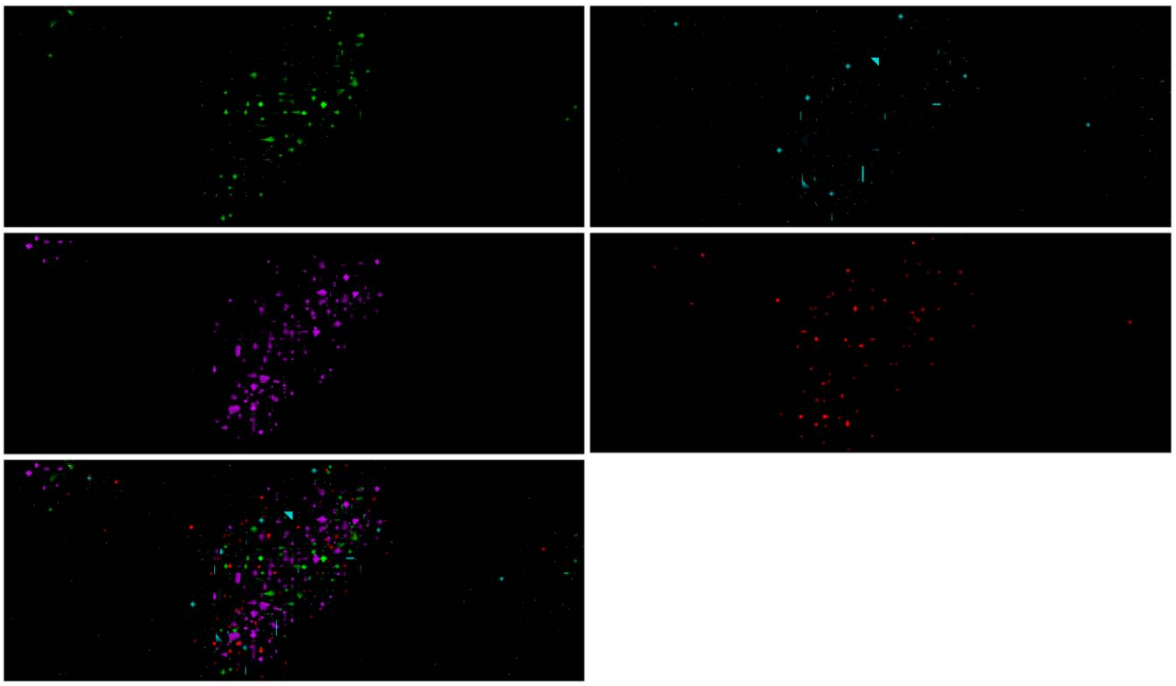

Figure S16: ToF-SIMS reconstructed ion images (90 µm x 30 µm) of TiO_2 NM-103 NMs agglomerates of different chemical entities from DMEM; green: TiO_2 NM (NM-103) (a), blue: $TiOH^+$-serine (b); purple: $TiOH^+$ -leucine (c); red: $TiOH^+$ -phenylalanine (d); (e) shows an overlay of all ions. In the overlay picture, all chemical entities are separated from each other and do not co-localize.

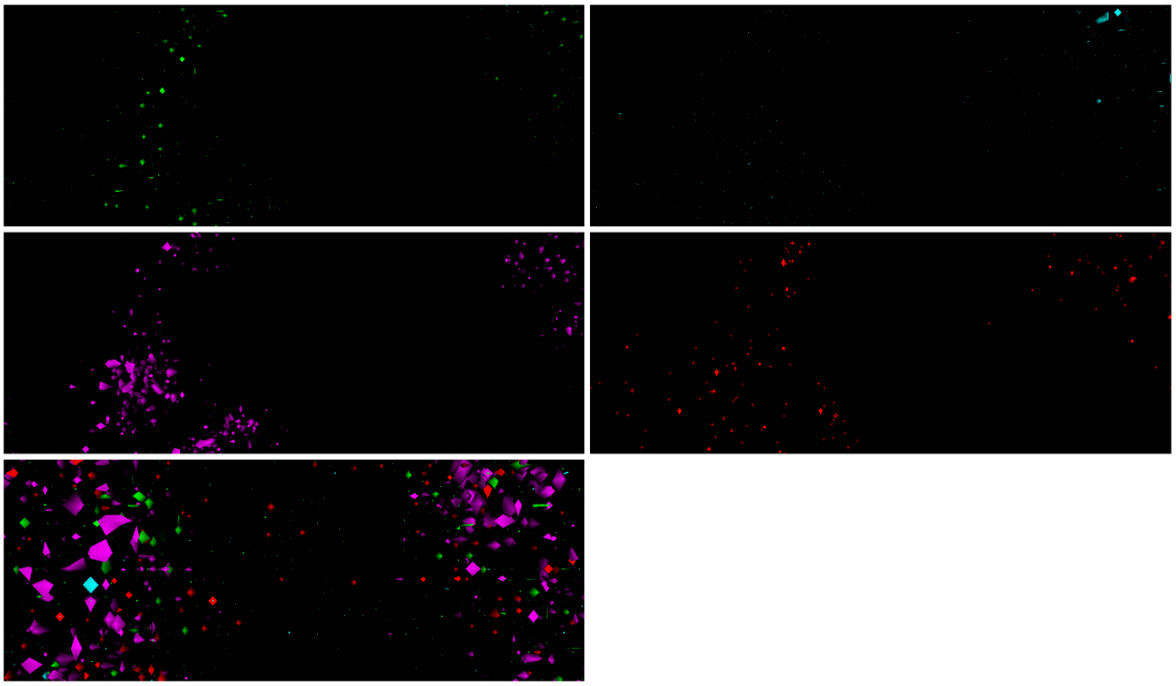

Figure S17: ToF-SIMS reconstructed ion images (90 µm x 30 µm) of TiO_2 NM-104 NMs agglomerates of different chemical entities from DMEM; green: TiO_2 NM (NM-104) (a), blue: $TiOH^+$-serine (b); purple: $TiOH^+$ -leucine (c); red: $TiOH^+$ -phenylalanine (d); (e) shows an overlay of all ions. In the overlay picture, all chemical entities are separated from each other and do not co-localize.

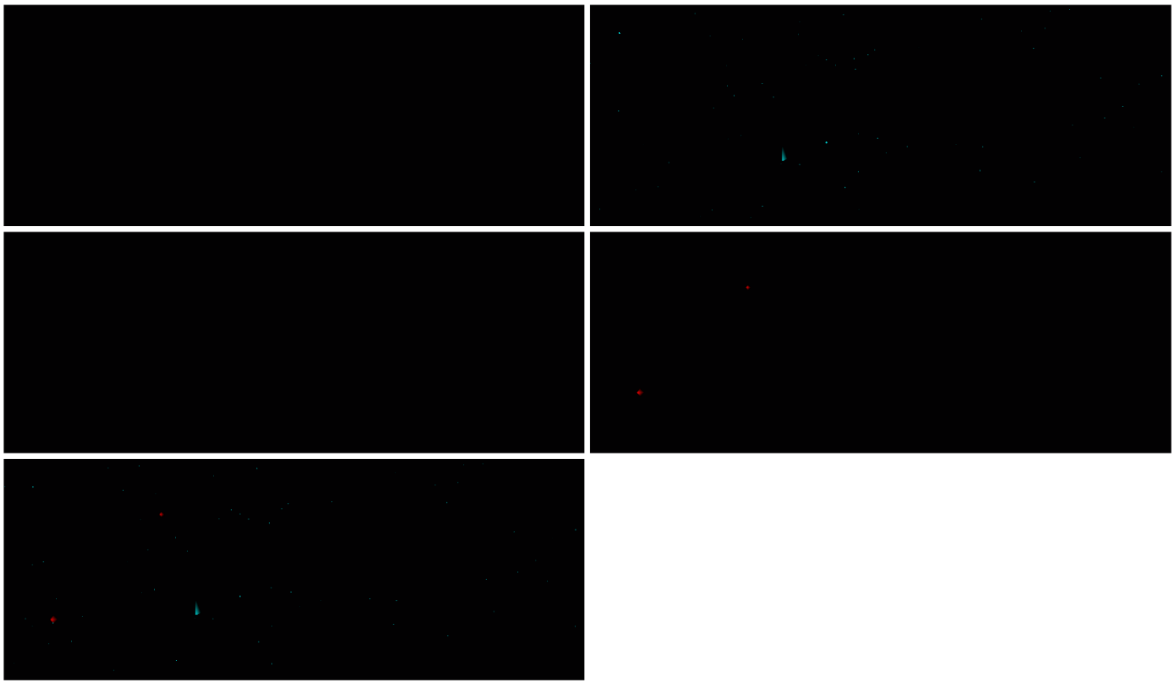

Figure S18: ToF-SIMS reconstructed ion images (90 µm x 30 µm) of TiO_2 NM-104 NMs agglomerates of different chemical entities from DMEM from an area where no agglomerate concentrations were observed; green: TiO_2 NM (NM-104) (a), blue: $TiOH^+$-serine (b); purple: $TiOH^+$ -leucine (c); red: $TiOH^+$ -phenylalanine (d); (e) shows an overlay of all ions. In the overlay picture, all chemical entities are separated from each other and do not co-localize.

[1] L.S. Sigg, W., Aquatische Chemie, Verlag der Fachvereine, Zürich, 1989.
[2] T. Mazza, E. Barborini, P. Piseri, P. Milani, D. Cattaneo, A. Li Bassi, C.E. Bottani, C. Ducati, Raman spectroscopy characterization of TiO2 rutile nanocrystals, Phys Rev B 75(4) (2007).
[3] Z. Movasaghi, S. Rehman, I.U. Rehman, Raman spectroscopy of biological tissues, Appl Spectrosc Rev 42(5) (2007) 493-541.
[4] Y.L. Zhao, C.H. Wang, Y. Zhai, R.Q. Zhang, M.A. Van Hove, Selective adsorption of L-serine functional groups on the anatase TiO2(101) surface in benthic microbial fuel cells, Phys Chem Chem Phys 16(38) (2014) 20806-20817.
[5] A.G. Thomas, W.R. Flavell, C.P. Chatwin, A.R. Kumarasinghe, S.M. Rayner, P.F. Kirkham, D. Tsoutsou, T.K. Johal, S. Patel, Adsorption of phenylalanine on single crystal rutile TiO2(110) surface, Surf Sci 601(18) (2007) 3828-3832.

Annex II

Supporting Information

Impact of an artificial digestion procedure on aluminum-containing nanomaterials

Holger Sieg[1], Claudia Kästner[3], Benjamin Krause[2], Thomas Meyer[4], Agnès Burel[5], Linda Böhmert[1], Dajana Lichtenstein[1], Harald Jungnickel[2], Jutta Tentschert[2], Peter Laux[2], Albert Braeuning[1], Irina Estrela-Lopis[4], Fabienne Gauffre[5], Valérie Fessard[6], Jan Meijer[7], Andreas Luch[2], Andreas F. Thünemann[3] and Alfonso Lampen[1]

[1] German Federal Institute for Risk Assessment, Max-Dohrn-Straße 8-10, 10589 Berlin, Department of Food Safety

[2] German Federal Institute for Risk Assessment, Max-Dohrn-Straße 8-10, 10589 Berlin, Department of Chemical and Product Safety

[3] Bundesanstalt für Materialforschung und -prüfung (BAM), Unter den Eichen 87, 12205 Berlin

[4] Institute of Medical Physics and Biophysics, Leipzig University, Härtelstrasse 16-18, 04275 Leipzig, Germany

[5] Institut des Sciences Chimiques de Rennes, UMR-CNRS 6226, Université de Rennes 1, France

[6] ANSES, French Agency for Food, Environmental and Occupational Health and Safety, Fougères Laboratory, Toxicology of contaminants unit, 10B rue Claude Bourgelat, 35306, Fougères Cedex, France

[7] Felix Bloch Institute for Solid State Physics, Leipzig University, Linnéstraße 5, 04103 Leipzig, Germany

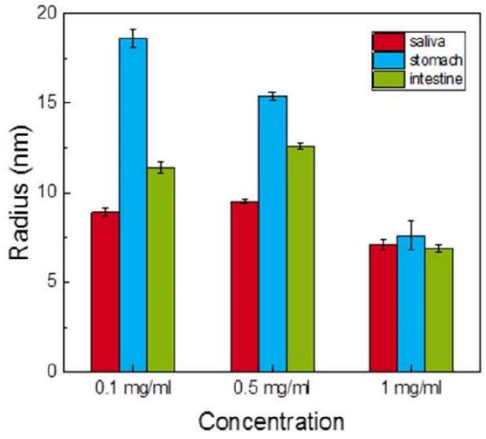

Supplementary Figure 1: Mean radii of the primary Al_2O_3 nanoparticles according to the three digestion steps as a function of the particle concentration. Mean values were calculated by using a lognormal distribution function.

Annex III

Aluminum and aluminum oxide nanomaterials uptake after oral exposure - a comparative study

Benjamin C. Krause (Benjamin-christoph.krause@bfr.bund.de)*[#1]

Fabian L. Kriegel (Fabian.kriegel@bfr.bund.de)[#1]

Daniel Rosenkranz (Daniel.rosenkranz@bfr.bund.de) [#1]

Nadine Dreiack (Nadine.dreiack@bfr.bund.de)[1]

Jutta Tentschert (Jutta.tentschert@bfr.bund.de)[1]

Harald Jungnickel (Harald.jungnickel@bfr.bund.de)[1]

Pegah Jalili (jalilipegah@gmail.com)[2]

Valerie Fessard (Valerie.fessard@anses.fr)[2]

Peter Laux (Peter.laux@bfr.bund)[1]

Andreas Luch (Andreas.luch@bfr.bund.de)[1]

[1]*German Federal Institute for Risk Assessment (BfR), Department of Chemical and Product Safety, Max-Dohrn-Straße 8-10, 10589 Berlin, Germany.*

[2]*ANSES, French Agency for Food, Environmental and Occupational Health and Safety, Fougères Laboratory, 10B rue Claude Bourgelat, 35306, Fougères Cedex, France.*

[#]= Authors contributed equally

[*]= Corresponding author

Supplement

Supplementary Table S1: One-way ANOVA for organ weights based on the different treatment groups.

Group	N Analysis	Mean [mg]	Standard deviation[mg]	SE of Mean [mg]	
1	5	1512	570	255	
2	5	1634	375	168	
3	5	1614	329	147	
4	5	1533	391	175	
5	5	1442	252	112	
6	4	1358	534	267	
7	5	1462	404	181	
8	5	1526	396	177	
	DF	**Sum of Square [mg²]**	**Mean Square [mg]**	**F Value**	**Prob>F**
Model	7	261943	37420	0.219	0.978
Error	31	5292160	170715		
Total	38	5554110			

1: control; 2: Al 6.25 mg/kg bw; 3: Al 12.5 mg/kg bw; 4: Al 25 mg/kg bw; 5: Al_2O_3 6.25 mg/kg bw; 6: Al_2O_3 12.5 mg/kg bw; 7: Al_2O_3 25 mg/kg bw; 8: $AlCl_3 \cdot 6H_2O$ 25 mg/kg bw; no significant difference for $p \leq 0.05$.

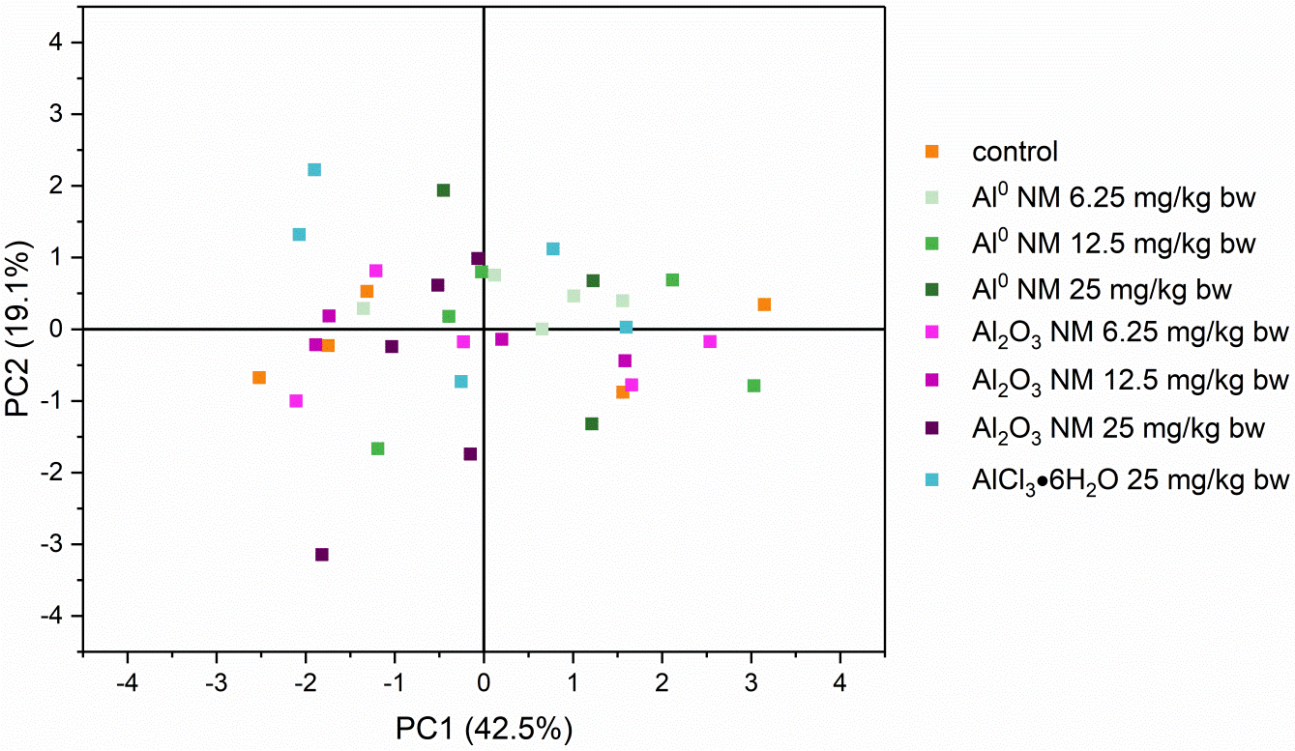

Supplementary Fig. S1: Principal Component Analysis for organ weights based on different treatment groups.

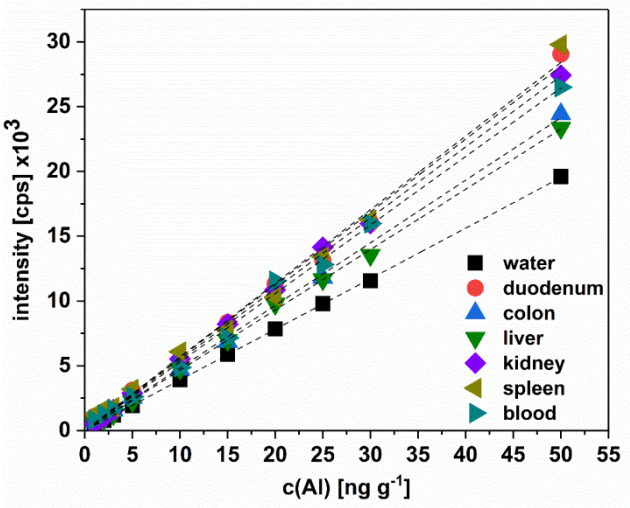

Supplementary Fig. S2: Calibration curves for matrices investigated in this study.

Supplementary Table S2: Data normalization for Al concentration. The example was calculated for liver according to the equation 7.

	dose per day [mg/kg bw]	total given Al amount per rat [mg]	Al concentrations per gram liver [µg/g]	normalized to total given Al amount [‰]	normalized to 1.7 mg/kg $AlCl_3 \cdot 6H_2O$ [%]
	6.25	3.19	0.52	0.16	32.65
Al^0 NM	12.5	6.38	0.26	0.04	8.16
	25	12.75	0.49	0.04	8.16
	6.25	1.99	1.48	0.74	151.02
Al_2O_3 NM	12.5	3.97	1.17	0.29	59.18
	25	7.94	1.07	0.13	26.53
$AlCl_3 \cdot 6H_2O$	25	1.68	0.83	0.49	100

Supplementary Table S3: Data normalization for Al concentration. The example was calculated for the duodenum according to the equation 7.

	dose per day [mg/kg bw]	total given Al amount per rat [mg]	Al concentrations per gram duodenum [µg/g]	normalized to total given Al amount [‰]	normalized to 1.7 mg/kg $AlCl_3 \cdot 6H_2O$ [%]
	6.25	3.19	2.21	0.69	85.19
Al^0 NM	12.5	6.38	0.86	0.13	16.05
	25	12.75	1.13	0.09	11.11
	6.25	1.99	1.82	0.91	112.35
Al_2O_3-NM	12.5	3.97	1.27	0.32	39.51
	25	7.94	1.29	0.16	19.75
$AlCl_3 \cdot 6H_2O$	25	1.68	1.36	0.81	100

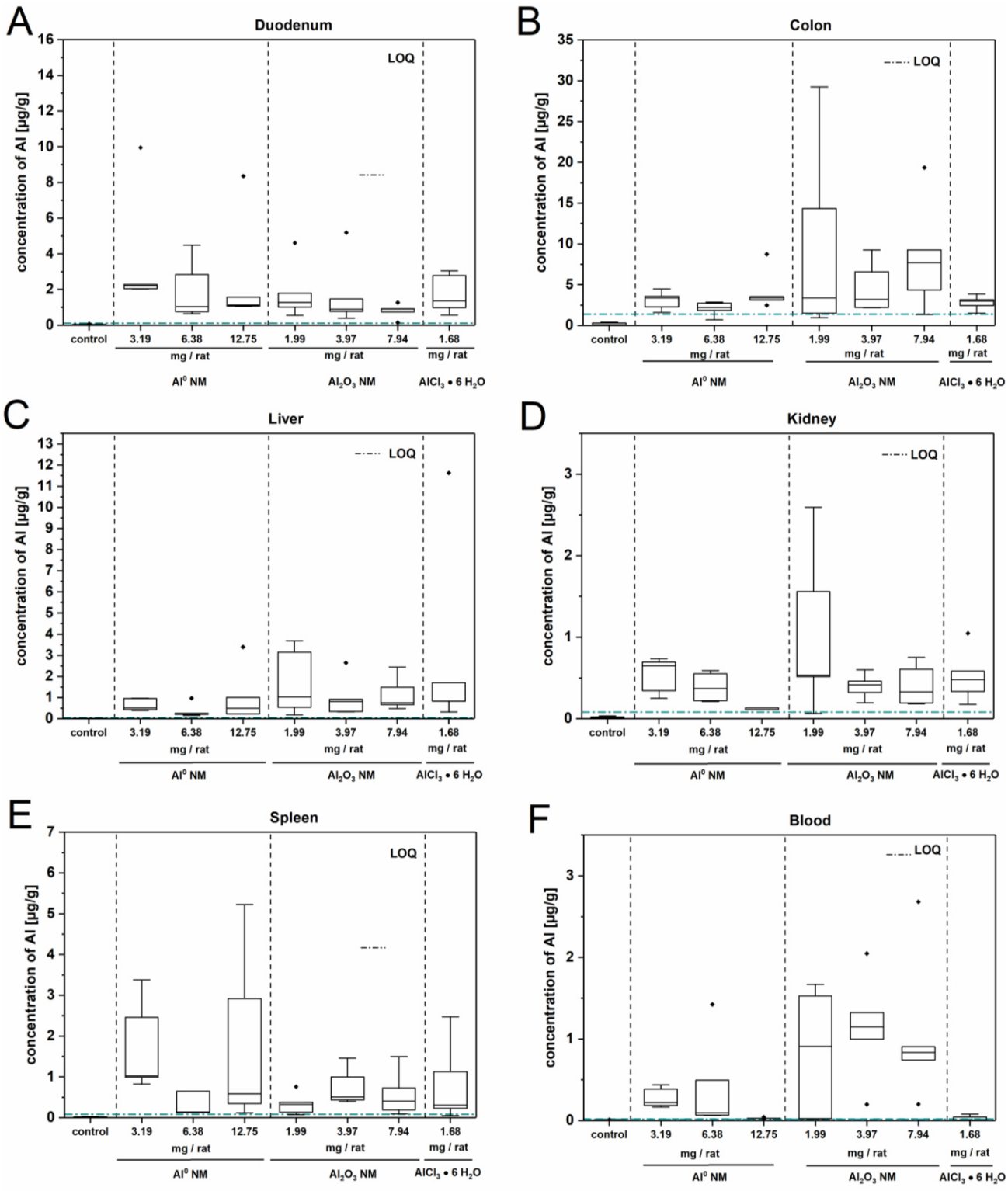

Supplementary Fig. S3: Boxplots showing the concentration of Al per organ. Data are given for all treatment groups with median and 1.5 IQR, including outliers. A: Al concentration in duodenum; B: Al concentration in colon; C: Al concentration in liver; D: Al concentration in kidney; E: Al concentration in spleen; F: Al concentration in blood.